THE UNIVERSITY OF CHICAGO

APPLICATION OF SYNTHETIC ANTIBODIES TO BIOLOGY: THE ENGINEERING OF ANTIBODY-BASED TOOLS AND THERAPEUTICS

A DISSERTATION SUBMITTED TO

THE FACULTY OF THE DIVISION OF THE BIOLOGICAL SCIENCES

AND THE PRITZKER SCHOOL OF MEDICINE

IN CANDIDACY FOR THE DEGREE OF

DOCTOR OF PHILOSOPHY

GRADUATE PROGRAM IN BIOCHEMISTRY AND MOLECULAR BIOPHYSICS

BY

TOMASZ SLEZAK

CHICAGO, ILLINOIS

JUNE 2023

I dedicate this thesis to my beloved parents,

Ela and Bronek

TABLE OF CONTENTS

LIST OF FIGURES

LIST OF TABLES

ABBREVIATIONS

ACE2	-	Angiotensin-converting enzyme 2
ADC	-	Antibody drug conjugate
APC	-	Antigen-presenting cells
ASF-1	-	Anti-silencing factor 1
BG	-	O^6-benzylguanine
BiTE	-	Bi-specific T-cell engager
BL	-	β-lactamase
BLF	-	β-lactamase fragment
BSA	-	Bovine serum albumin
CAR	-	Chimeric antigen receptors
CDR	-	Complementarity-determining region
ChIP	-	Chromatin immunoprecipitation
COVID-19	-	Coronavirus disease 2019
CryoEM	-	Cryo-Electron Microscopy
EBOV	-	Ebola virus
ELISA	-	Enzyme-Linked Immunoabsorbent Assays
Fab	-	Fragment antigen binding

Fab^{H}	-	Fab in human kappa scaffold
Fab^{S}	-	Fab in 4D5 scaffold
Fab^{LRT}	-	Fab in LRT scaffold
Fab^{L}	-	Fab in human lambda scaffold
Fab^{mH}	-	Fab in murine kappa scaffold
Fab^{mL}	-	Fab in murine lambda scaffold
FACS	-	Fluorescence activated cell sorter
GA1	-	Protein G-A1
GH	-	Growth hormone
GHR	-	Growth hormone receptor
Hc	-	Heavy chain
IBP	-	Immunoglobulin binding protein
IF	-	Immunofluorescence
IP	-	Immunoprecipitation
IgG	-	Immunoglobulin G
IHC	-	Immunohistochemistry
K_D	-	Binding constant
Lc	-	Light chain

LDH	-	Lactate dehydrogenase
MBP	-	Maltose binding protein
MT	-	Methyltransferase
NP	-	Nucleoprotein
NP_{CT}	-	Nucleoprotein C-terminal
POC	-	Point-of-care
pA	-	Protein A
PCR	-	Polymerase chain reaction
pG	-	Protein G
PhaNGS	-	Phage-antibody next-generation sequencing
pL	-	Protein L
RBD	-	Receptor binding domain
RU	-	Response unit
SA	-	Streptavidin
sAB	-	Synthetic antibody
SARS-CoV-2	-	severe acute respiratory syndrome coronavirus 2
scFv	-	Single-chain variable fragment
SPR	-	Surface plasmon resonance

S-protein	-	Spike protein
WHO	-	World health organization
VHH	-	Single variable domain of heavy chain
ZIKV	-	Zika virus

ACKNOWLEDGEMENTS

The following work would not have been possible without the help and support of many people throughout my time at the University of Chicago.

First, I want to express my profound appreciation to my Ph.D. mentor, Anthony Kossiakoff, for his guidance, support, and leadership. Throughout my Ph.D. journey, his constructive feedback, insightful suggestions, and willingness to challenge me to think critically have been incredibly valuable. I feel extremely fortunate to have had the opportunity to work under his guidance and learn from him. All of that has enabled me to approach my research with a broader perspective and deeper understanding, and I will never forget these lessons and will carry them with me throughout my career. Additionally, over the years, Tony has become not only my mentor but also a friend. I am grateful for all the conversations, advice, and shared laughs that will continue for years.

I want to thank the other thesis committee members: Robert Keenan, Stephen Meredith, and Joseph Piccirilli. I received tremendous feedback, insights, and expertise that have helped me succeed. I am very thankful for the exciting and encouraging conversations that accompanied our meetings, making them not stressful but a pleasurable experience.

This work would not be possible without a contribution from Elena Davydova and Kelly O'Leary, with whom I spent the most significant portion of my time at the University of Chicago. Elena was my supervisor when I started, providing me with much help and knowledge through the years. Kelly has been a great colleague and a friend with whom I could share results and discuss new ideas daily. We were always able to create a great atmosphere and share many laughs, even during more challenging moments in our Ph.D. journeys. We worked very closely on various

projects, and I want to thank him for all of his contributions to the work presented here and to all other projects we share. Over the years, Kelly has become one of my best friends, and I am very grateful for that. My thanks also go to the other members of Kossiakoff Lab. I want to highlight: Annika Sääf, Somnath Mukherjee, Carla Meints, Lucas Bailey, Ekaterina Filippova, Satchal Erramilli, and Vincent Lu for their training, help, and time spent together. I have made wonderful friends at the University of Chicago, who made my graduate experience so unique. Thanks to Aleksander Promiński, for all our time together, from the early morning gym to the afternoon swim at the promontory point. Jakub Kucharczyk always uses his sense of humor to create a great atmosphere. Manos Chatzopoulos, who was very important at the beginning of my time in Chicago, continues to be a great friend from a distance. Ahmed Rohaim for being my crystallography mentor and making our long hours in Argonne an extraordinary time. Hendrick Glauninger and Peter Chung for everyday friendship and support. Harry and Melissa Ayre for being fantastic friends and a "favorite couple" to hang out with. I feel very fortunate to meet so many special people; listing them all would be challenging. Still, I would also like to highlight: Sumit Bandekar, Wiola Nawrocka, Aleksandra Bebel, Andreas Kourouklis, Myles Minter, Brandon Rhodes, Brianna Mittelman, Agnieszka Borowik, Walter Alvarado, Michelle Bui, Steven Wasserman, Eric Rouviere, Michal Sawczyk, Katarzyna and Michał Kluszczyńscy. Moreover, this thesis would not be possible without access and help from the staff at GM/CA@APS Sector 23 at the Advanced Photon Source. I also want to thank Shani Charles and Lisa Anderson for their continued assistance with all requirements and paper works during my studies.

Finally, I want to share the most important thank you- to my family, to whom I dedicate this work. I would not be the person I am today without my parents, Elżbieta and Bronisław. Over the years, they provided me with encouragement and support even though following my dream

required living very far from each other. They share their love and continued support, and I always turn to them if I need life advice with every critical decision. To my brother, Łukasz, my best friend, who supports me and is always there for me, to my second family- Tony and Susan Kossiakoff. Over the years, they have become a significant part of my life, and I am grateful for that. To my fiancé, Sara, for your love, support, and daily help. I appreciate you and am excited for our future with the best partner possible. To my future in-laws, Laurie and Warren Twiehaus, for welcoming me to their family and for their support and encouragement.

ABSTRACT

Antibodies have the unique property of recognizing and binding specific antigens, making them valuable tools for studying biological processes and developing new disease treatments. The discovery of the technology that allowed for monoclonal antibody production has revolutionized the whole biological field. It has led to the creation of several methods used daily in every modern laboratory. The growing number of antibodies used in the clinic and laboratories require reagent personalization, which usually requires a time-consuming and ineffective chemical manipulation that can influence the antibody's performance. This thesis describes engineering an easy, high-throughput platform that allows for antibody personalization in a plug-and-play fashion. It discusses in detail the protein engineering approach that led to the platform's development, followed by the development of various applications. Finally, the thesis explains the generation of ultra-high affinity antibodies that recognize SARS-CoV-2 and their applications for virus neutralization and detection using the plug-and-play technology described above. The presented technology can potentially improve antibody-based research by the broader scientific community and can revolutionize future clinical approaches for many therapies.

CHAPTER 1: INTRODUCTION

1.1 Antibodies as tools for cell biology and biochemistry

Antibodies or immunoglobulins are proteins produced by B-cells in response to foreign antigens. There are five major classes of antibodies: IgA, IgD, IgG, IgE, and IgM, with IgG being the most common immunoglobulin in humans. Despite their architecture and function differences, all antibody classes possess similar general features. Their basic structure forms a Y shape molecule containing two heavy and two light chain domains, connected by the conserved cysteine residues (Williams and Barclay, 1988). Upon papain digest, the IgG separates into three functional components: two Fragment antigen bindings (Fab) and the fragment crystallizable (Fc). These components have distinct functions, with Fab responsible for the antigen binding, while the Fc fragment binds to specific cell receptors modulating immunological responses (Lazar et al., 2006). The hinge regions link the two Fabs to the Fc portion, providing flexibility and a wide range of conformations that IgG can utilize to bind its antigen (Poljak et al., 1973). Each Fab fragment contains a constant and variable portion of light and heavy chains. The complementarity-determining regions (CDRs) responsible for the antigen binding are located in the variable part (Figure 1.1). Each Fab contains six CDR loops, equally distributed between light and heavy chains (Figure 1.2) (Padlan, 1994), with the CDR-H3 having the most significant contribution to antigen binding. (Tsuchiya and Mizuguchi, 2016).

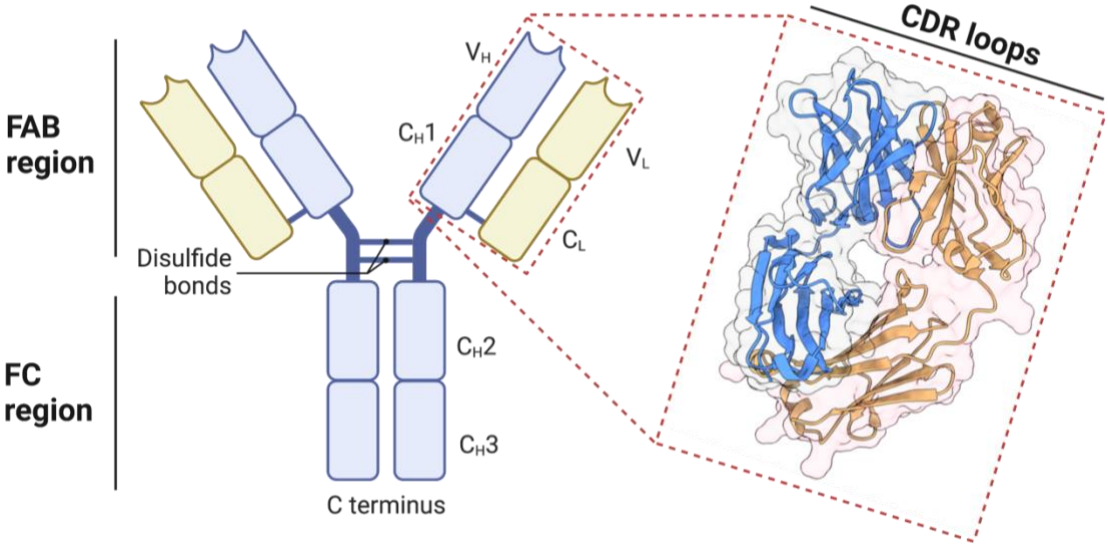

Figure 1.1 The structure of human IgG antibody. The IgG molecule contains two heavy and light chains linked by the disulfide bonds. The heavy chain contains one variable (VH) and three constant regions (CH1, CH2, CH3), while the light chain contains a single variable (VL) and constant domains (CL). Antibodies can be divided into two functional regions: Fab and Fc. Fab is responsible for the antigen recognition with the CDR loops located in the Variable part of each heavy and light chain. The Fc region interacts with specific cell receptor and thus mediates the immunological response. Heavy and light chains of the IgG are marked in blue and orange, respectively. Figure created using PDB: 6U8C.

Antibodies are an integral part of many techniques and applications used in biological research. These include: ELISA, immunoprecipitation (IP), chromatin immunoprecipitation (ChIP), or broadly used staining procedures, like western blot, immunofluorescence (IF), immunohistochemistry (IHC), and flow cytometry. These methods can identify protein complexes or the presence of a specific antigen on the cell surface or in cell homogenates, leading to many important discoveries over the years (Moritz, 2020). These types of approaches can also be utilized in medical diagnostics, and they are a standard method for detecting many diseases and infections. The portfolio of antibody-based applications is expanding, with next-generation technologies being developed in rapid fashion. Recent methods that profile the cell environment and identify

the proteins associated near cell receptors provide important insights into biological systems (Bar et al., 2018). For example, phage-antibody next-generation sequencing (PhaNGS) has the potential to revolutionize cancer diagnosis and targeting since it allows cell classification and profiling to distinguish between healthy and disease-state cell environments in a high-throughput manner (Pollock et al., 2018).

Further, antibody fragments (Fabs and nanobodies) are broadly used in structural biology to improve high-resolution structure determination. Their application effectively enhances the results in two primary structural techniques, X-ray crystallography and Cryo-Electron Microscopy (CryoEM). It is necessary to produce a good-quality crystal to determine the high-resolution protein structure by X-ray crystallography. Fabs can serve as crystallography chaperones and by inducing crystallization by providing robust lattice contacts. Structure determination of challenging targets like membrane proteins or protein-RNA complexes is difficult without the chaperones since the detergent-solubilized membrane proteins, or high flexibility can inhibit crystal formation (Koldobskaya et al., 2011; Rohaim et al., 2022; Uysal et al., 2009; Ye et al., 2008). Moreover, the structure of the Fab is well-defined. It can serve as a molecular replacement model to obtain the phasing information once the diffraction pattern of the crystal is acquired. In parallel, the recent resolution revolution in cryoEM has made it possible to solve high-resolution structures of macromolecules over 100 kDa. While the methods are constantly improved to accommodate smaller proteins, the size and symmetry are still major challenges for cryo-EM (Armache and Cheng, 2019). Fabs can overcome these limitations by adding mass, stabilizing the complex, and providing distinctive features that allow better image alignment and, thus, higher resolution of the achieved structure (Cater et al., 2021; Walsh et al., 2018; Wu et al., 2012).

Current research methods and day-to-day laboratory operations are only possible with reliable antibodies. Their important for basic and medical research purposes is substantial and expanding every day.

1.2 Antibody development techniques

Over the last 30 years, antibodies have largely replaced small molecules for therapeutic applications that involve stimulating or inhibiting cell surface membrane proteins. This is mainly because they are much more specific, thereby reducing off-target effects, and they possess longer half-lives in plasma than small molecules (Dostalek et al., 2013; Ovacik and Lin, 2018). Traditionally, to generate antibodies, immunization technologies were commonly used. Typically, these methods involve an animal immunization with a selected target (whole protein, polypeptide, or a single domain), followed by the serum collection from which the antibodies are purified (Kohler and Milstein, 1975). This method results in the production of a heterogeneous mixture of different antibodies called polyclonal antibodies. Such a combination could recognize multiple epitopes on the antigen, which is beneficial and effective when developing a potent immunological response against bacterial or viral infection (Galfre et al., 1977). However, the amino acid composition of polyclonal antibodies is usually unknown, which limits their reproducibility and efficiency. Several techniques exist to isolate a particular antibody (monoclonal antibody) to overcome the disadvantages of polyclonal antibodies. Multiple variations of the method exist; however, they all require the isolation of the antibody-producing B-cells from the immunized animals and their fusion with immortal myeloma cell lines to form hybridomas (Kohler and Milstein, 1975). Extended culturing of hybridoma cells can gradually degrade the properties of monoclonal antibodies due to a clonal drift (Lee and Palsson, 1994). Historically, the animal

immunization approach was a prevalent method for antibody production. However, the generated antibodies from animal sources are immunogenic and have limited use in the clinic (Clarke, 2010), they require additional molecular engineering and humanization that, in turn, reduces their effect in human patients (Ducancel and Muller, 2012).

The new generations of antibodies are being made using molecular display technologies, which usually include phage or yeast surface display (Boder and Wittrup, 2000; Bradbury et al., 2011; Viti et al., 2000). These methods enable the display of Fab fragments or single-chain variable fragment (scFv) and provide a direct relationship of the genotype to its phenotype since the variant's DNA incorporated in the microorganism genome directly corresponds to the amino acid sequence displayed on its surface (Barbas et al., 1991; McCafferty et al., 1990). These techniques allow for a library production containing 10^{10} variants and identification of antibodies having a particular function in a high-thruput manner (Fellouse et al., 2007).

1.3 Phage display as a superior method to generate customized reagents

While the animal immunization approach still exists, recombinant antibody display phage technology is taking over the generation of antibody-based reagents (Bradbury et al., 2011; Groff et al., 2020; Groff et al., 2015). Recombinant reagents are relatively inexpensive, and the user has much more control over their final characteristics. For instance, specific selection conditions can create binders to target conformational states or a particular epitope (Gao et al., 2009; Paduch and Kossiakoff, 2017). The importance of this approach is highlighted by the fact that nearly 35% of currently used antibodies are derived using phage display technology (Ecker et al., 2015; Omidfar and Daneshpour, 2015).

Phage and yeast display are the two primary surface display methodologies. Both techniques have their advantages and disadvantages. For instance, using yeast display allows for incorporating a fluorescence-activated cell sorter (FACS) during the sorting procedure, which can characterize the affinity, expression, and specificity of the displayed antibody. Still, the achievable library size is much smaller than the library generated using phage display (Boder and Wittrup, 2000). The most used in phage surface display is filamentous phage M13. Its popularity comes from several benefits since M13 is stable, non-lytic, and allows for the incorporation of a large foreign DNA. Additionally, phage M13 is easy to modify and has a short propagation cycle, while its production results in a phage filament secretion without the disturbance of the bacterial cells (Binz et al., 2005; Sidhu et al., 2000). These advantages resulted in phage display becoming a leading in vitro protein engineering technique used for various applications, including, for example, studying the direct evolution of enzymes (O'Neil and Hoess, 1995), identification of peptide ligands (Cwirla et al., 1990), epitope mapping (Bottger and Bottger, 2009), or antibody generation (Bradbury and Marks, 2004; Sidhu and Fellouse, 2006). The efforts for phage display development were awarded a 2018 Nobel Prize in Chemistry to George Smith and Gregory Winter (Smith, 2019; Winter, 2019).

Over the years, various proteins have been displayed on the surface of the phage particles (Bailey et al., 2014; Bass et al., 1990; Schiffer et al., 2002). However, our lab is focused on antibodies and their derivatives. Antibody generation with phage display techniques are well established for myriad types of soluble (Hornsby et al., 2015; Lee et al., 2007), and membrane proteins (Arrigoni et al., 2022; Feng et al., 2022). Especially successful were libraries displaying Fab (Fellouse et al., 2007; Lee et al., 2004; Miller et al., 2012), scFv (Krauss et al., 2003) or nanobody (Guilliams et al., 2013). We have developed a pipeline for the rapid production of Fab-

based affinity reagents using phage display. The Fab library is based on the Herceptin Fab scaffold, which has been engineered for stability and expression (Eigenbrot et al., 1993; Miersch et al., 2015; Slezak et al., 2020).

As described in section 1.1, the Fab contains six CDR loops responsible for the binding to the antigen, with each of the chains containing three CDRs (Figure 1.2). The strategy for library generation involved the introduction of the highest randomization into the CDR-L3 and CDR-H3. CDR-L3 and H3 have the most significant diversity from other loops and provide most of the interaction with the target. The library allows for the introduction of all amino acids except cysteine, but the design favors tyrosine, serine, glycine, tryptophan, and phenylalanine residues over the others (Figure 1.2C). The library construction strategy did not involve the randomization of CDR-L1 and L2. At the same time, the diversity in CDR-H1 and H2 is significantly reduced and incorporate mostly serine and tyrosine residues since their antigen recognition is less significant. The length of CDR-H1 and H2 is constant, while the size of the H3 and L3 loops is also subject to change. While the length of CDR-L3 does not vary much (6-8 residues), the pallet of CDR-H3 loop length is much broader, containing from 6 to 19 amino acids (Fellouse et al., 2004; Miller et al., 2012).

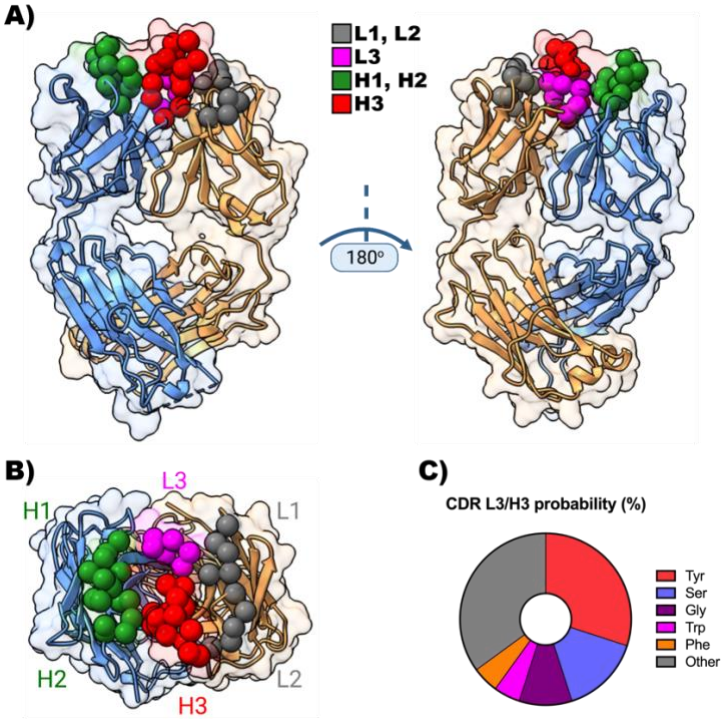

Figure 1.2 The design of Fab-based phage library. (**A**) The Fab structure. The Fab contains six CDR loops equally distributed on heavy (blue) and light (orange) chains. The library design involves limited randomization of CDR-H1 and CDR-H2 (green spheres), including mostly serine and tyrosine residues, while CDR-L1 and CDR-L2 (grey spheres) are not varied. Further, the library contains the most extensive diversity in CDR-L3 (magenta spheres) and CDR-H3 (red spheres), where 19 amino acids are allowed (excluding cysteine residue). (**B**) Top view on CDRs location within the Fab fragment of the antibody. (**C**) The CDR-L3 and H3 composition. The library design favors certain amino acids, with their probability of displaying 30% for tyrosine, 15% for serine, 10% for glycine, and 5% for phenylalanine and tryptophan. In comparison, each remaining residue has a 2.5% probability of being incorporated into the CDR. Figure created using PDB: 6U8C.

The phage display biopanning is a relatively uncomplicated procedure that involves four steps. First, the antigen is introduced to the phage library to allow for Fab binding. Usually, the antigen is immobilized to the plate or magnetic/agarose beads. In some specific circumstances, the whole cells can be subjected to selection (Alfaleh et al., 2017). However, this method increases the number of non-specific binders and thus deters the success of the procedure. The next step

involves a set of extensive washes that remove a non-specific and low-affinity phage particle. At the same time, higher affinity binders are carried out to the elution step, achieved by low pH. Lastly, the released phage is amplified in *E. coli* and used in the subsequent selection round. Typically, high-affinity antibodies can be selected after four or five rounds of selection (Figure 1.3A). Additional selection pressure between each round involves a reduction of target concentration and negative selection of the phage pool against empty magnetic beads to eliminate non-specific binders being carried throughout the procedure. After the selection, the individual phage particles are amplified, and their specificity is validated using phage ELISA. Positive clones are sequenced and cloned into expressing vectors to allow their further validation and characterization (Figure 1.3B).

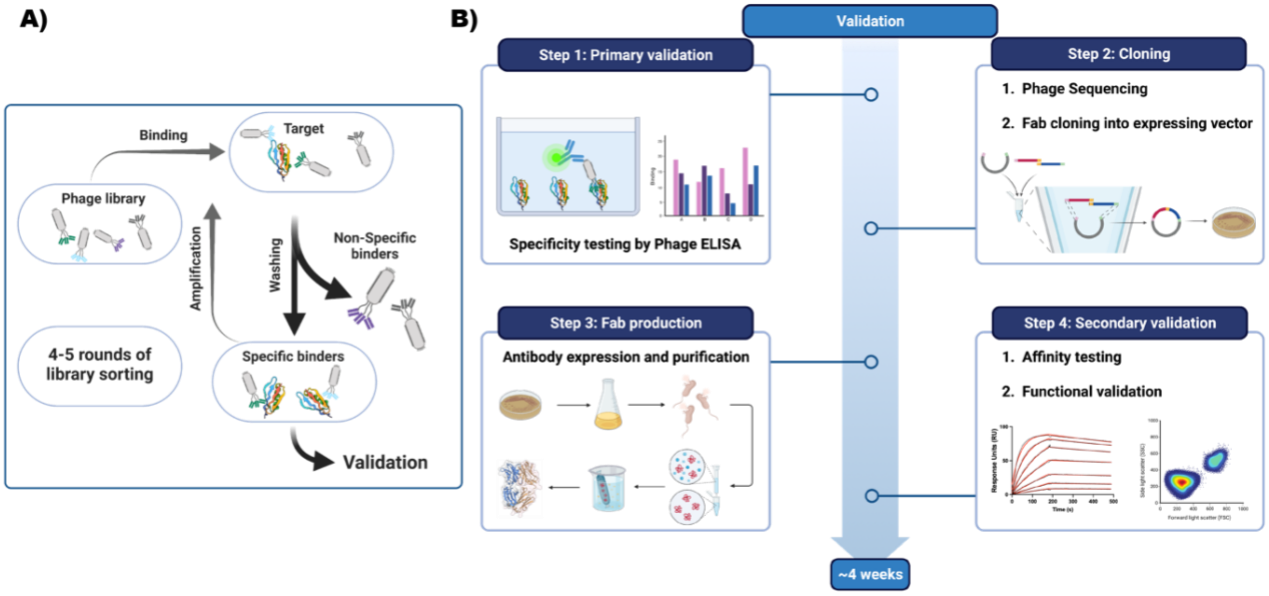

Figure 1.3 Model of phage display biopanning. (**A**) Phage display protocol includes four steps. First, the phage binds to the immobilized antigen. Then rigorous washes remove non-specific binders. Further, the phage is eluted, amplified, and used in a subsequent round. Usually, 4-5 rounds of phage display biopanning are performed, and the specific binders are further validated and characterized. (**B**) Overview of selected antibodies validation. After successful selection, phage particles displaying Fabs are subjected to a primary validation that usually includes a phage ELISA confirming their affinity and specificity against the antigen.

Figure 1.3 continued. Clones showing good binding are sequenced, and individual antibodies are cloned into the expressing vector (bacterial or mammalian). The Fabs are expressed and purified to allow for secondary validation, such as the biophysical and functional characterization (binding to the cells or inhibitory/stimulatory activity, etc.).

The ability to control and modify the selection conditions is one of the most significant advantages of using display technologies over animal immunization for antibody development. A careful selection strategy can produce antibodies with customized functions (Paduch et al., 2013; Rizk et al., 2011). For instance, supplementing the substrate or binding partner during the selection protocol can result in the generation of antibodies that recognize the particular conformation state of the target. Antibodies recognizing protein complexes or possessing other anticipated characteristics can be obtained by adding the competitor during the selection procedure. This results in the phage pool being depleted from the binders recognizing the not desired target (Paduch et al., 2013). The ability to functionalize the properties of antibodies can be critical while developing affinity molecules for detecting infection or a disease state of the cell. Animal immunization does not provide the ability to control antibody production conditions. Therefore, the phage display technique is a superior method of antibody generation for therapeutics.

1.4 Membrane proteins as a major therapeutic target

Due to their crucial roles in many cellular processes, membrane proteins are critical pharmacological targets for research, diagnostics, and therapeutic applications. They are encoded by over 30% of open reading frames in sequenced mammalian genomes. (Almen et al., 2009; Wallin and von Heijne, 1998). Specific membrane proteins, called Cluster of Differentiation (CD) markers, can define specific cell types and thus allow distinguishing between healthy and cancer

cells (Barnkob et al., 2014). Moreover, the expression level of membrane protein receptors is often significantly increased in diseased state cells (Slamon et al., 1989). Therefore, approximately 60% of drugs today target membrane protein to reach their therapeutic goal (Overington et al., 2006). Most of these therapies use small molecules present on the cell surface proteins, especially GPCRs and ion channels (Santos et al., 2017). Still, the development of new small molecules drastically slows down because of their toxicity and low target selectivity (Dodd et al., 2018), while the importance of antibody-based therapeutics is drastically increasing (Lu et al., 2020).

Generating functional antibodies against membrane proteins is challenging since success is highly dependent on the quality of the antigen and its native conformational state. Membrane proteins need to be removed from their native lipid membranes using detergents or other solubilizing agents, which decreases the success of an antibody generation campaign. Thus, the new phage display method incorporates nanodiscs to stabilize membrane proteins in their native-like environment during the antibody screening (Dominik and Kossiakoff, 2015).

1.5 Advantages of antibody-based treatment over the currently common small molecule approach

Generally, therapeutics are divided between small molecules and biologicals. These two categories are based on the size of the drug as well as its manufacturing process. While small molecules are typically smaller than 1 kDa and chemically derived, the biologicals are larger and extracted from biological systems. Many molecules are in the biologicals category, but antibodies are an undisputed leader. Small molecules are the most commonly used therapeutics worldwide. The development of synthetic chemistry techniques revolutionized medicine and allowed for a high-thruput production and testing of many new small molecules in a relatively short time. These

drugs are relatively cheap to produce and easy to administer for patients since they can be easily crystallized and formed into convenient pills or capsules. These have been driving forces for its market success. However, the long list of limitations has slowed its expansion in recent years, while antibody-based drugs are becoming more significant. The specificity of small molecules is low, generating considerable off-targeting and increased toxicity.

In contrast, biologics are much more precise. Antibodies possess longer half-lives in plasma than small molecules (Dostalek et al., 2013; Ovacik and Lin, 2018). However, drug administration requires specialized equipment and is much more complicated. The patient's safety overcomes the overall cost of the treatment, and the FDA has approved nearly 60 antibody-based products for treatments, most of which utilize membrane proteins as targets (Rodgers and Chou, 2016).

1.6 Thesis outline

My thesis work aims to engineer an accessible plug-and-play technology to improve antibody-based research and applications. The general idea is to generate a set of synthetic immunoglobulin-binding proteins with a selective binding characteristic that would allow for temporary cargo attachment to the antibody (Figure 1.4). It would allow for antibody personalization in a high throughput manner without requiring individual modification of multiple antibodies. The cargo would not be permanently attached to the antibody, and its lifetime would depend on the lifetime of the platform binding. That could be particularly beneficial for developing therapeutics that could lead to toxicity or immunogenicity upon more prolonged exposure.

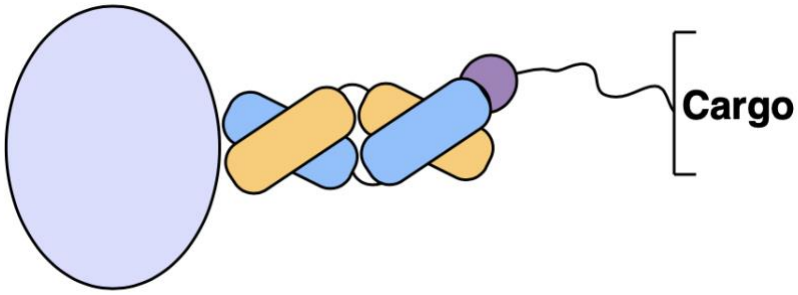

Figure 1.4 Plug-and-play antibody personalization platform. Engineered immunoglobulin binding protein would allow cargo attachment to the antibodies without modification. The system does not limit the cargo size and allows linker adjustment for results optimization.

In chapter 2, I describe in detail the protein engineering approach I took to generate a synthetic antibody scaffold and a cohort of modified protein Gs with different characteristics. Several phage libraries were constructed and utilized in a campaign of subsequent phage display biopanning. I provide a complete biophysical characterization of engineered protein Gs, including the detailed analysis of their specificity obtained from the three independent crystal structures. Next, I demonstrate possible applications for the plug-and-play system, including, for example, a universal purification resin, formation of bi-specific antibodies, detection assay, or simultaneous co-binding detection to two distinct targets on the cell surface.

Chapter 3 describes the adaptation of a plug-and-play complementation assay for detecting SARS-CoV-2. This work introduced in chapter 3 was done during the pandemic under the lockdown condition, showing that the previously developed plug-and-play detection assay can be quickly adapted for detecting other threats. I explain how the assay was further optimized for the reliable and shelf-stable point-of-care. Finally, I show how the highly controlled phage display can generate a superior, ultra-high affinity antibody to neutralize SARS-CoV-2. This chapter confirms the usefulness and plasticity of the plug-and-play system described in chapter 2.

In chapter 4, I provide a complete summary of the collaborative efforts to generate antibody-based reagents for various applications. I specify the targets that were used for the antibody development and the outcome of the selection.

CHAPTER 2: ENGINEERING PROTEIN G (PG) MODULES TO FACILITATE "PLUG AND PLAY" APLLICATIONS IN CELL BIOLOGY

Majority of the chapter has been published: (Slezak et al., 2020)

2.1 Summary

A platform that would allow direct cargo delivery to a cell of interest with low off-target effects is highly desirable in myriad cell biology applications. Affinity-based reagents such as antibodies are ideal candidates for such an approach; however, cargo attachment is cumbersome and often not amenable to high throughput applications. I have developed a novel platform to introduce multiple functionalities into a class of Fab-based affinity reagents in a "plug and play" fashion. This platform exploits the orthogonal pairs of different variants of a Fab scaffold and an engineered domain of an immunoglobulin binding protein, protein G. The protein G- Fab scaffold pairs are characterized by the ultra-tight binding and slow dissociation, allowing long lifetime of the complexes. Protein G is a small protein that can be easily manipulated, enabling the attachment of various functional components with adjustable spacing. Additionally, the specificity of protein G variants towards different engineered Fab scaffolds allows for the simultaneous cargo delivery to individual targets. To demonstrate the utility of this platform, I applied it to a variety of applications, such as a detection proximity assay based on the β-lactamase (BL) split enzyme system, Bi-specific T-cell engager (BiTE) cell killing, simultaneous binding detection of two antibodies, and many more. The advantage of the system is in its simplicity, yet has broad applications in multiple biological contexts.

2.2 Introduction

2.2.1 Current ways to customize antibodies and its applications

Affinity reagents such as antibodies are powerful tools in research, diagnostic and therapeutic fields. Their customization and labeling are highly desired in many biological applications; however, the process can be expensive and time-consuming with relatively low efficiency. For instance, Antibody Drug Conjugates (ADC) are among the most used antibody-based cancer therapeutics. They consist of an antibody linked to some type of cytotoxic cargo. Additionally, the attachment of fluorophores or enzymes are commonly used methods to visualize and detect antibodies binding their antigens. The two standard methods used for antibody labeling include (1) nonspecific acylation of lysine residues through esters and (2) alkylation of cysteine thiols with maleimides (Agarwal and Bertozzi, 2015). However, these approaches contain several limitations. Targeting the nonspecific lysine residues often result in a non-homogenous product since multiple labeling sites are available (Wang et al., 2005). Alternatively, introducing cysteine residues allows for the controlled location of the cargo in more disciplined stoichiometry, it can compromise the antibody production and purity. Recently, two additional methods for antibody labeling are becoming more popular. The first takes advantage of naturally existing glycosylation of IgGs (O'Shannessy et al., 1984), the second involves the incorporation of unnatural amino acids (Axup et al., 2012). The most significant advantage of using glycosylation sites is their locations are unsually distal from the CDRs- the antigen binding site. However, this post-translational modification is generally a heterogenous process, resulting in a population of different glycans, making labeling difficult and often insufficient. Instead, the incorporation of unnatural amino acids results are an effective method to incorporate multiple labeling locations, but the process is not straightforward and the production yield of the IgGs is usually compromised (Tian et al., 2014).

All these methods are low throughput and require multiple purifications steps to remove an excess of the labeling agent, which prolongs the process and decreases the final yield of the product. This often requires the individual labeling and modification of many antibodies, a time-consuming and expensive process, especially since the following-up validation often reveals the limiting functionality of previously selected and labeled antibodies. Developing an easy, plug-and-play system that allows facile antibody labeling would benefit researchers in many areas of biological research. A selective Immunoglobulin Binding Protein (IBP) that is straightforward to produce and label could eliminate this bottleneck of antibody-based research.

2.2.2 Immunoglobulin Binding Proteins

Immunoglobulin Binding Proteins were first discovered and identified to function as a bacterial weapon against host immunological responses. These proteins are characterized by the ability to bind IgGs and prevent the immunological response. Several different IBPs were isolated from different bacterial species, each having a unique binding characteristic. Over the years, using IBPs has become a gold standard method for industrial antibody purification. The main IBPs commonly used include Protein A from *Staphylococcus* (Forsgren and Sjoquist, 1966), protein L from *Peptostreptococcus Magnus* (Nilson et al., 1992), and Protein G from *Streptococcus (Bjorck and Kronvall, 1984)*. These proteins bind to very distinct epitopes on the IgG. Protein L binds exclusively to the Light chain (Lc) portion of the Fab with a high affinity (nM range), but its binding interface is in proximity to the CDRs (Graille et al., 2001) (Figure 2.1). Alternatively, protein G and A bind to both IgG fragments (Fab and Fc) with a different affinity. Each bind in a similar location between C_H2 and C_H3 of the Fc portion, with comparable affinity falling within a low nM range. However, their binding location on the Fab portion and the kinetics of this

interaction are very different. Protein A recognizes the variable part of a Fab's Heavy chain in proximity to CDR, while protein G simultaneously binds to the constant parts of a Fab's Hc and Lc (Derrick and Wigley, 1992) (Figure 2.1). However, the affinity of the Fab-protein G interaction is very low (μM). Even though proteins A and L are excellent antibody purification reagents, their binding location in proximity to the CDRs limits their potential in cell biology applications since it could interfere with antigen recognition.

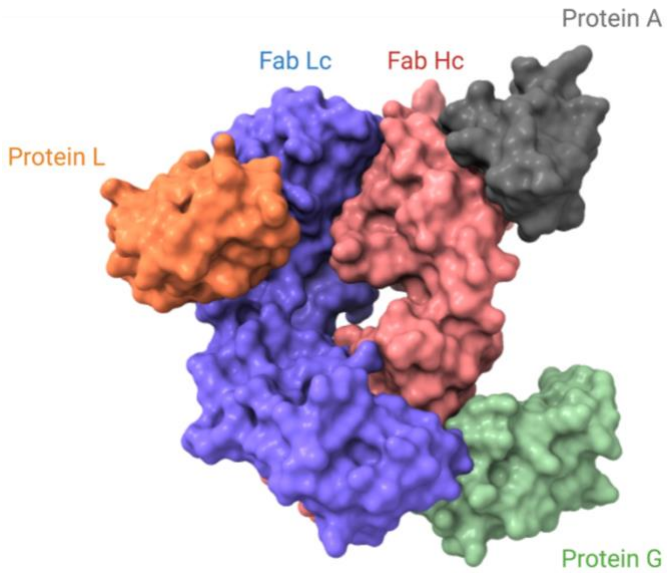

Figure 2.1 Immunoglobulin binding proteins. Binding epitopes of immunoglobulin binding proteins are displayed on the Fab fragment. Protein A binds to the variable part of the heavy chain of the antibody, while protein L binds to the variable part of the light chain. Protein G binds to the constant part, and the interface includes both the heavy and light chain of the Fab. Figure created using PDB: 4HKZ and 6U8C.

2.2.3 Protein G-A1 engineering

Protein G binding to the Fab in the distal location to the CDRs (Derrick and Wigley, 1992) creates the opportunity to use it in various applications. However, the low affinity (μM) to the Fab portion of the antibody drastically limits its potential. Taken this, Bailey et al. performed the affinity maturation campaign against the Fab in 4D5 scaffold (Fab^{S}). The choice of the Fab scaffold

came from Fab^S presence in our phage display library. It contains E123S substitution in the light chain compared to the wild-type Human Kappa Fab (Fab^H). Protein G interacts with Fab through two points of contact with a Fab. The first interaction involves residues 15-24 from protein G, which forms an antiparallel β-strand with Fab Heavy chain (Hc). Secondly, residues 37-43 interact with the constant part of the Fab Light Chain (Lc) (Derrick and Wigley, 1992).

Protein G was displayed on the surface of the M13 phage, and the soft randomization of these two areas of interaction between protein G and Fab was performed. The approach biases the protein G library towards the wild-type sequences but allows the introduction of substitutions upon applied selection pressure during a phage display biopanning. As a result, an affinity maturated GA1 variant of protein G was selected. This variant had several substitutions in both areas, resulting in 50 nM affinity to Fab^S (Bailey et al., 2014). While this improvement was significant, allowing GA1 to be used as an antibody purification reagent, the fast dissociation that characterizes GA1-Fab^S interaction limits its capabilities for cell-based assays.

2.3 Results and Discussion

2.3.1 Fab scaffold engineering to improve the Fab -protein G-A1 affinity

The effort to engineer a high affinity protein G, resulted in a significant improvement in binding to Fab^S; however the kinetics of this binding is characterized by a very fast dissociation that is a limiting factor in many applications (Bailey et al., 2014) (Figure 2.4A). To further improve the affinity and dissociation rate, I decided to generate a new variant of the Fab scaffold that would have superior interaction properties with protein G-A1 (GA1). To do so, a phage display library was built, focusing on residues 123-127 of the Fab light chain, since it forms the principal

interaction with the area of protein G that was the least randomized during the initial GA1 engineering (Figure 2.2). Additionally, I hypothesized that there is room for further optimizing the interaction, since GA1 does not interact with a naturally existing Human Fab Kappa (Fab^{H}), that has only 1 amino acid difference from Fab^{S} at position 123 (Figure 2.2C). Two libraries with different levels of diversity in each position were generated- the first library was designed using a hard randomization strategy, where every amino acid type was introduced in each of the five randomized positions. The second library contained leucine at position 125, since this amino acid is conserved across the species (Figure 2.2C). These procedures resulted in generation of libraries with a theoretical diversity of 1.7×10^{7}.

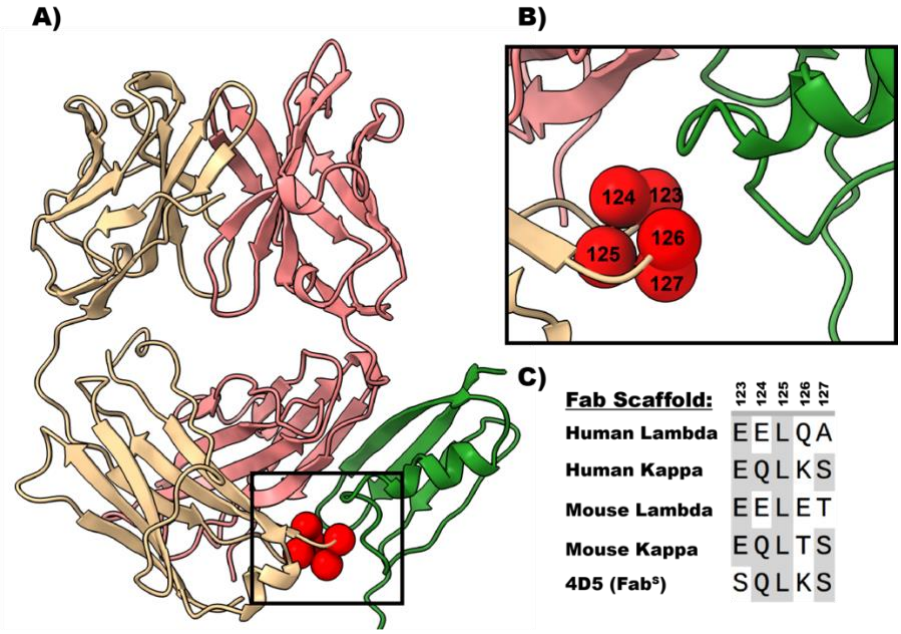

Figure 2.2 Interface between constant part of Fab Light Chain and Protein G. (**A**) Model of protein G binding to Fab. Main interaction comes from an antiparallel β-strand configuration of Fab Hc and protein G. Additionally, protein G interacts with Fab Lc via a α-helical cap. Spares represent randomized residues in the constant part of Fab Light Chain. Fab Heavy Chain is colored in red, while Light chain is colored as yellow. (**B**) The interaction between Fab Light Chain and Protein G is limited to 5 amino acids. Naturally existing Fab scaffolds contain conserved glutamic acid at position 123 and leucine at position 125. Interestingly, GA1 was previously engineered against Fab^{S}, and does not recognize any of the naturally existing Fab scaffolds due to a negative charge at position 123.

Figure 2.2 continued. (**C**) Sequence alignment of constant part of the light chain (position 123-127) in different Fab scaffolds. The sequence alignment of Fab area recognized by protein G shows the opportunity for affinity improvement.

I performed a phage display selection, where GA1 was used as a target for the Fab light chain library. Five rounds of selection were performed by systematically reducing the GA1 concentration from 200 nM in the first round to 1 nM in round 5. To validate the specificity of the selected Fabs, phage ELISA was performed on 96 clones, resulting in 6 unique Fab scaffold variants. Remarkably all the clones contained a conserved Leucine at position 125 and a K126R substitution. Interestingly, one of the variant scaffold (Fab^{LRT}) contained a serendipitous two amino acid deletion. These deletions were not part of an original library design, and I speculate that they occurred because of an error during the randomizing DNA oligonucleotides synthesis (Figure 2.3). The two amino acid deletions did not affect the Fab stability or expression, yet improved the binding significantly.

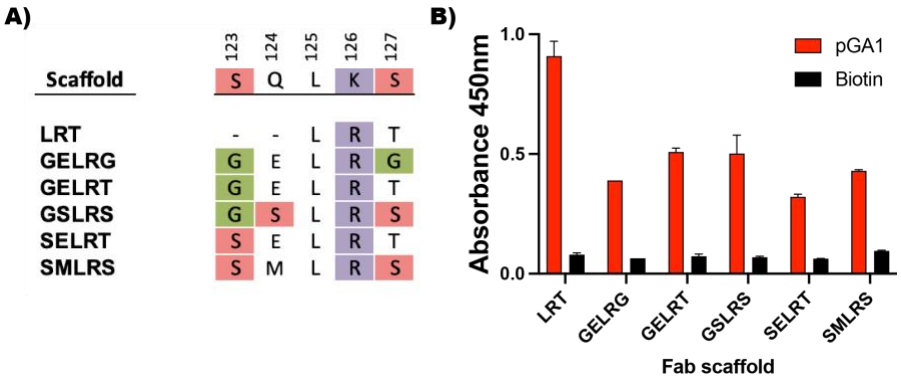

Figure 2.3 New Fab scaffolds characterization. (**A**) Sequences of unique Fabs scaffolds generated with GA1 as a target. Six unique Fabs scaffolds were identified. All the scaffolds contained a conserved Leucine and Arginine at position 125 and 126, respectively. Additionally, one of the variants contained two deletions that were not initially a part of the designed library and appear due to a serendipity and error while primers were synthetized. Template sequence that was randomized during phage library generation is displayed on the top. Selected amino acids are color-coded as follows: serine (S) – red, glycine (G) – green, tyrosine (Y) – yellow, tryptophan (W) – blue, positively charged amino acids (R, K, H) – violet, other amino acids – white. (**B**) Single-point phage ELISA of the new Fab scaffolds selected by phage display. Clones with strong signal with GA1 were chosen for further sequencing and characterization. All Fabs show specific binding to GA1 compared to the Biotin control.

Biophysical characterization of new Fab scaffolds by surface plasmon resonance (SPR) showed 5 to 10-fold improvement of affinity to GA1 for all the scaffolds. However, Fab^{LRT}, showed a 500-fold (K_D ~0.1 pM) increase in affinity compared to original Fab^{S} kinetics (Figure 2.4) with a significantly improved dissociation rate. Next, I wanted to estimate the significance of the Fab^{LRT} conservative mutations K126K and S127T in relation to the two amino acid deletion at position 123 and 124. I constructed two variants: 1) ΔΔL**K**T, where Arginine was replaced with the wild type Lysine, and 2) **SQ**LRT, containing wild type residues at position 123 and 124 instead of deletions, followed by LRT. SPR analysis showed that both variants have improved affinity over the Fab^{S} scaffold (K_D of 12 and 8 nM, respectively), but they were far below the Fab^{LRT} –

GA1 interaction (K_D – 0.1 nM). These data suggest direct and significant involvement of the Arginine and two amino acids deletion in the enhanced interaction with GA1.

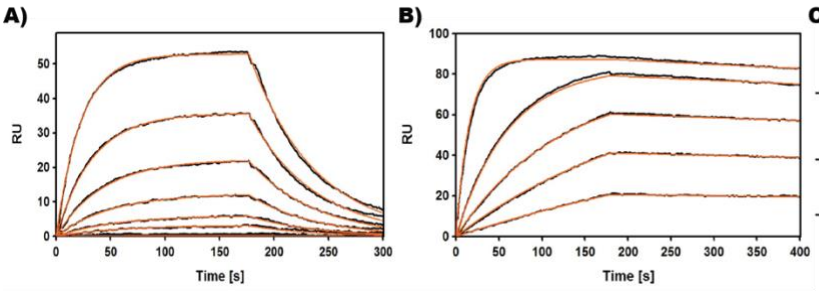

Scaffold	K_{on} (M^{-1} s^{-1})	K_{off} (s^{-1})	K_D (nM)	χ^2 (RU^2)
Fab^S	3.2×10^5	1.6×10^{-2}	50	0.41
Fab^{LRT}	2.6×10^6	2.4×10^{-4}	0.1	0.67

Figure 2.4 Characterization of Fab^{LRT} scaffold by SPR. (**A**) SPR sensogram showing fast on-fast off binding kinetics between Fab^S and the GA1. The concentration of Fab was serially diluted 2-fold, starting at 100 nM. (**B**) SPR sensogram showing the affinity improvement of Fab^{LRT} and GA1 with a slow dissociation rate. The concentration of Fab was serially diluted 2-fold, starting at 12 nM. (**C**) SPR kinetics for GA1 binding to Fab^S and Fab^{LRT}.

2.3.2 Crystal structure of Fab^{LRT}-Protein G-A1

The affinity improvement of the new Fab scaffold with the serendipitous two deletions was unexpected and fortuitous for myriad applications. To gain insights how the deletions enhance the binding affinity between the Fab and GA1, I endeavored to determine the crystal structure of the Protein G-A1 and Fab^{LRT} complex. I set up high-throughput crystallization campaign using multiple crystal screens, and after several days initial crystal "hits" were observed, and further optimized. Multiple datasets better than 3Å resolution were collected, but they were characterized by multiple problems: mosaicity, twinning and an overall poor quality that made the data impossible to use. After multiple attempts over several months of optimization, better looking crystals were obtained using crystal seeding technique (Luft and DeTitta, 1999). The final conditions were 0.1 M magnesium chloride, 0.1 M sodium acetate pH 5.0, and 20% (w/v) PEG 4000 (Figure 2.5C). The resulting crystals diffracted to 2.61Å resolution. The complex crystallized in space group $P3_221$ with two Fab^{LRT}- GA1 complexes in the asymmetric unit.

The Fab^{LRT}- GA1 interface is formed through two sets of contacts that bury ~560Å^2 in the interface with Hc and ~160Å^2 with Lc. The larger interaction is through the formation of an antiparallel β-strand configuration that includes H-bond formation between the residues 16-22 of GA1 $\beta 2$ and residues 221-227 of Fab Hc. Similar H-bonding was previously reported in the structure of a wild-type protein G- Fab complex (Derrick and Wigley, 1992). The second important contact comes from α-helical cap of GA1 and Fab residues 137-140 of the Hc and 123-127 in the Lc, which includes the distinctive ΔΔLRT motif (Figure 2.1). Remarkably, the LRT motif interacts with the residues of GA1, that were involved in the GA1 engineering from a wild-type PG (^{40}YVHE^{43}). Two deletions in the Fab^{LRT} induce a conformational change of the loop that position the guanidium group of Arginine 126 to pack against the aromatic ring of Y40 of GA1 resulting in the formation of a cation-π interaction (Figure 2.6). Additionally, the R126 forms an H-bond with the carbonyl of Y40. The GA1's lack of binding to naturally existing Fabs can be explained by the E43 exposure to the solvent into the cavity created by the two deletions in the Fab^{LRT}. Naturally existing Fab scaffolds contain a negative charge in this space, while the synthetic Fab^{S} scaffold that was used as a target during GA1 affinity maturation contains a serine (Figure 2.2C). Furthermore, V41 of GA1 forms hydrophobic interactions with F139 of Fab Hc. Additionally, H42 of GA1 is buried at the Hc Fab interface, where it forms an H-bond to the main chain nitrogen of the V129.

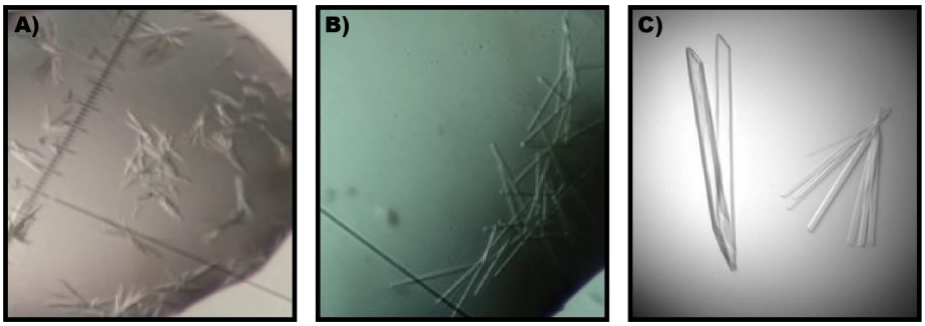

Figure 2.5 Crystals of Fab^{LRT}- GA1 complex. (**A**) First optimized crystals that were taken to APS for data collection. (**B**) Crystals after further optimization with the seeding technique shows the improvement of their morphology. (**C**) Final Fab^{LRT}- GA1 complex crystals that were used to collect 2.61Å dataset that was used to solve the structure.

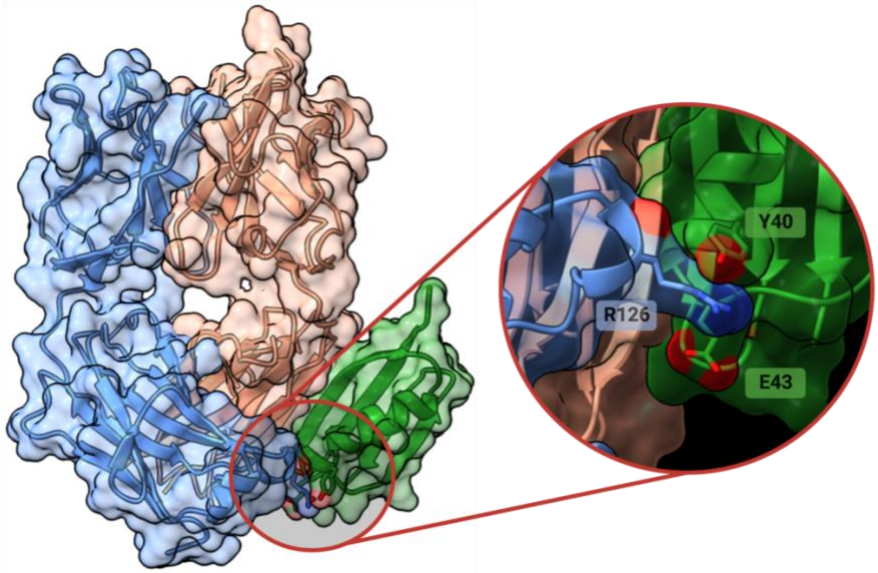

Figure 2.6 The structure of GA1-Fab^{LRT}

The interface of Fab^{LRT} with GA1 showing the significant rearrangement of the Fab Light chain induced by two amino acid deletion, allowing for the key R126 interaction with protein G. The guanidinium portion of the Fab^{LRT} R126 side chain forms a cation-π interaction with the ring of Y40 from GA1. R126 forms an additional H-bond with Y40 main chain carbonyl. Molecules are colored as follows: Fab Hc- red, Fab Lc- blue, GA1- green.

2.3.3 Development of new Protein-G variants with Fab scaffold-based selectivity

The unique characteristics of GA1 and its orthogonal Fab^{LRT} scaffold form a distinct pair that does not bind to their wild-type homologs. This provides the opportunity to expand this concept to make other specific orthogonal pairs that could be used in parallel in plug and play

applications. Thus, to expand the portfolio, I decided to proceed with a similar tandem phage display approach to generate a new set of Protein-G variants with distinct specificities. I approached undertaking this with two primary goals: 1) Engineering a universal Protein-G variant that would broadly recognize naturally existing Fab scaffolds. A variant would be helpful for Fab purification and many applications for general users who want to avoid introducing synthetic Fab scaffolds, i.e., Fab^{LRT}. 2) Generation of the orthogonal set of G-Fab that would allow for simultaneous usage with the Fab^{LRT}-GA1 platform. The requirement for such a molecule would be a high-affinity interaction with Fab^{H} and no binding to Fab^{LRT}.

To generate PGs that would fill these criteria, I designed phage display libraries focusing on the C-terminal cap of the α-helix responsible for the interaction with the constant part of the Fab light chain. Using Kunkel mutagenesis, I built six phage libraries containing a hard randomization strategy in a different position of the PG α-helix (Figure 2.7B). 4 libraries preserved histidine at position 42 since it has previously been shown to improve the pH dependence of the engineered PG (Bailey et al., 2014). To allow for loop conformational change, I also decided to introduce randomization in positions bordering the α-helix that was previously shown to interact with the Fab Lc (Figure 2.7B). To obtain new PGs, I carried out a set of phage display selection campaigns using the biotinylated Fab with a set of different scaffold as the targets. The first phage display campaign aimed to create a pan PG, that is, to bind to all scaffolds. To do so, five rounds of selection were performed with the strategy that involved swapping different Fab scaffolds in between the selection rounds starting with Fab^{H}, followed by Fab^{L} (Human Lambda), Fab^{LRT}, and Fab^{S} in the respective rounds. The selection process is finished by Fab^{H} in the final round. To generate a high-affinity interaction, the antigen target concentration was gradually decreased, starting from 1 μM during the first round and ending with 1 nM in round 5. To validate the

specificity of the selected PGs, a phage ELISA was performed on 96 clones, which led to the identification of seven universal PG variants.

Interestingly, most universal PGs conserved the wild-type PG amino acid composition at positions 42 and 43. (Figure 2.7D). However, the previously introduced interaction improvement by the β-strand and Fab Hc, and the introduced substitutions in the helical cap resulted in meaningful affinity improvement compared to wild-type PG. Next, I aimed to generate a Fab^{H}-specific PG. To do so, five rounds of selection were performed with 2 μM of unbiotinylated Fab^{LRT} as a competitor in every step of biopanning. This was to deplete the library from all possible PG variants that bind to Fab^{LRT}. Fab^{H} was used as the target antigen, systematically reducing the concentration from 1 μM to 1 nM in the final round. The phage ELISA identified positive clones that were then sequenced, resulting in 5 PG variants. These were then characterized by a high affinity binding to Fab^{H} without the measurable interaction with Fab^{LRT} (Figure 2.7C). Sequence alignment of these variants shows a high diversity introduced in each position, with the dominating methionine at position 40 (Figure 2.7E).

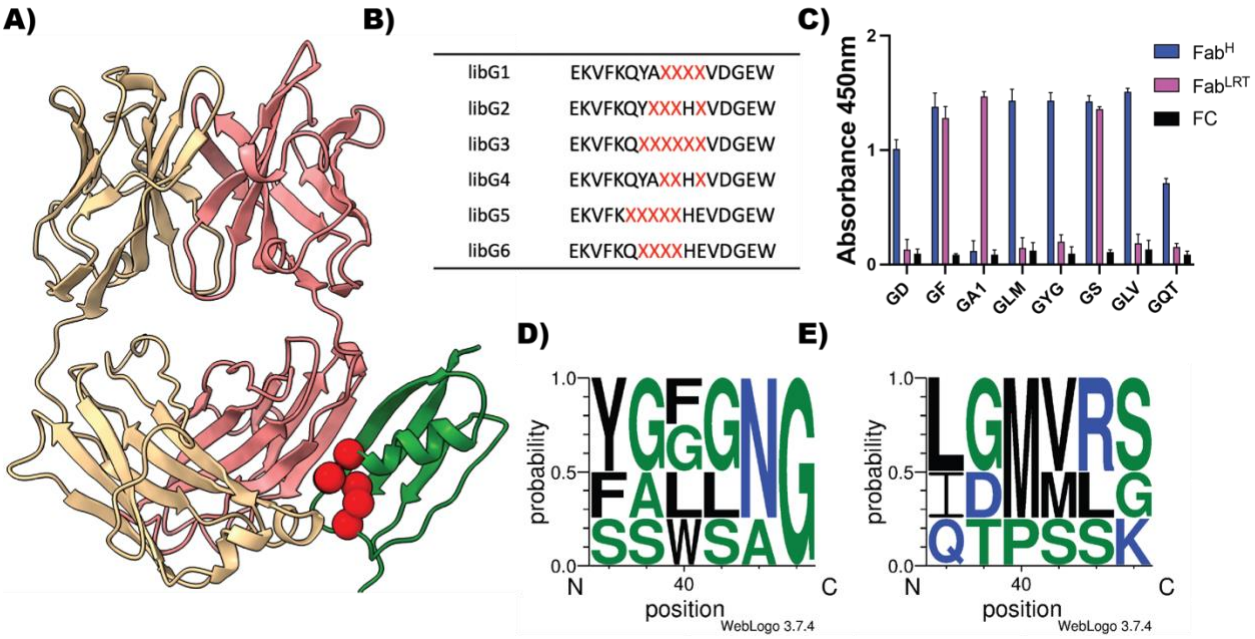

Figure 2.7 New Protein G engineering. (**A**) Model of protein G binding to Fab. Spheres represent randomized residues in protein G helical cap interacting with Fab light chain. (**B**) Generated phage libraries. Hard randomization (NNK) of selected residues is represented by "X." (**C**) ELISA of selected protein G variants against Fab^{H}, Fab^{LRT}, and FC. Results show the high specificity towards specific Fab scaffolds that allows the formation of orthogonal pairs that would not cross-react. For example, GA1-Fab^{LRT} and D -Fab^{H}. Proteins GF and GS are universal high-affinity Fab binders. Notably, the interaction with the Fc portion of the IgG has been engineered out. (**D**) Weblogo represents amino acid sequences of newly developed protein Gs that pose universal binding properties (binds all existing Fab scaffolds). (**E**) Weblogo represents protein Gs selectively binding only Fab^{H} and Fab^{L} but does not bind to Fab^{LRT}.

Biophysical characterization of new PGs by SPR showed a significant improvement in affinity and specificity compared to wild-type PG (Table 2.1, Table 2.2). The generation of multiple universal PGs was confirmed by testing the binding with the most populated Fab scaffolds – Human Kappa, Human Lambda, Mouse Kappa, and Mouse Lambda (Fab^{H}, Fab^{L}, Fab^{mH}, and Fab^{mL}, respectively). The best candidate, Protein-GF, possessed a very high affinity towards all tested Fab scaffolds – Fab^{H} (KD- 1.9 nM), Fab^{L} (KD- 21 nM), Fab^{mH} (KD- 3.2 nM), Fab^{mL} (KD- 37 nM), and Fab^{LRT} (KD- 0.9 nM) (Figure 2.8). Additionally, the results revealed the successful generation of the orthogonal set of G-Fab that would allow for simultaneous usage with the Fab^{LRT}-

GA1 platform. Several generated PGs are characterized by a high affinity and specificity towards Fab^{H}, with the best candidates (GD, GLM) having affinities of 6.4 and 8.9 nM, respectively (Figure 2.9A). The high specificity of the system was tested by injecting 100 nM of Fab^{LRT} over the GD and GLM; however, no detectable binding was observed (Figure 2.9C). Both GD and GLM recognized Fab^{L}. However, the affinity was ~3-fold lower than Fab^{H} (Figure 2.9B), which is consistent with the decreased affinity observed for GF and Fab^{L} (Figure 2.8F).

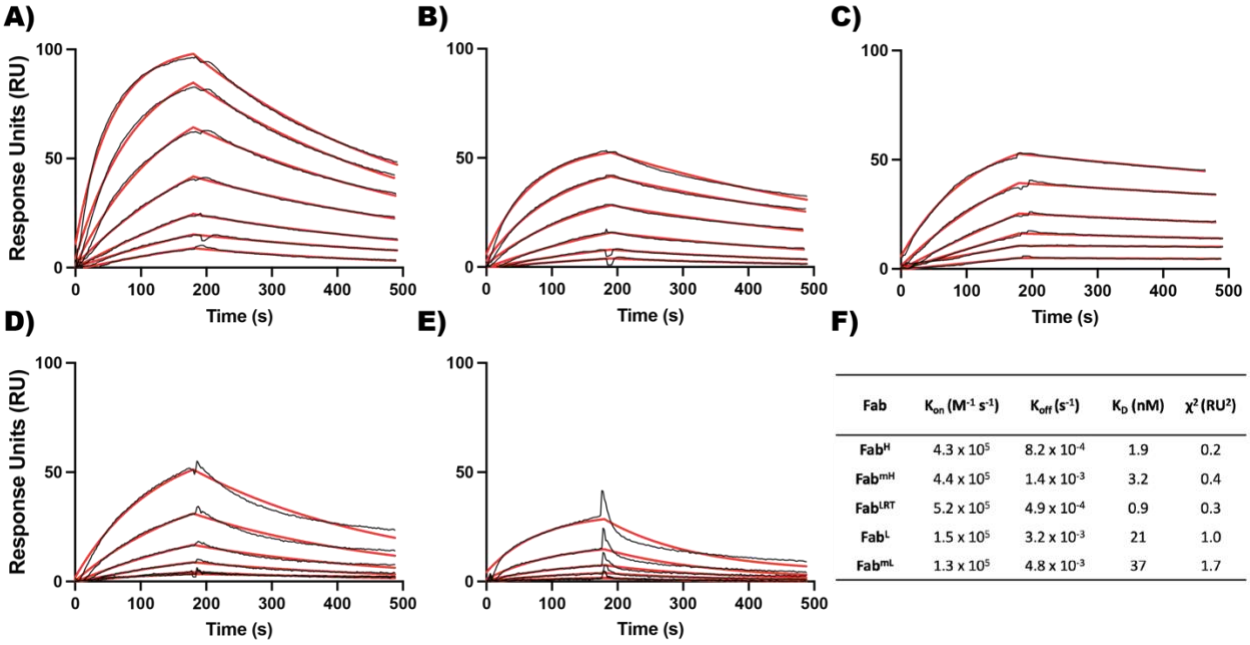

Fab	K_{on} (M^{-1} s^{-1})	K_{off} (s^{-1})	K_D (nM)	χ^2 (RU^2)
Fab^{H}	4.3×10^5	8.2×10^{-4}	1.9	0.2
Fab^{mH}	4.4×10^5	1.4×10^{-3}	3.2	0.4
Fab^{LRT}	5.2×10^5	4.9×10^{-4}	0.9	0.3
Fab^{L}	1.5×10^5	3.2×10^{-3}	21	1.0
Fab^{mL}	1.3×10^5	4.8×10^{-3}	37	1.7

Figure 2.8 Characterization of GF- a universal Fab binder. (**A**) SPR sensogram showing the interaction with Fab^{H}. (**B**) SPR sensogram showing the intraction with Fab^{mH}. (**C**) SPR sensogram showing the interaction with Fab^{LRT}. (**D**) SPR sensogram showing the interaction with Fab^{L}. (**E**) SPR sensogram showing the interaction with Fab^{mL}. (**F**) Kinetic binding parameters. For the kinetic experiment, fabs were serially diluted two-fold, starting at 50 nM for all Fabs, and 25 nM for Fab^{LRT}.

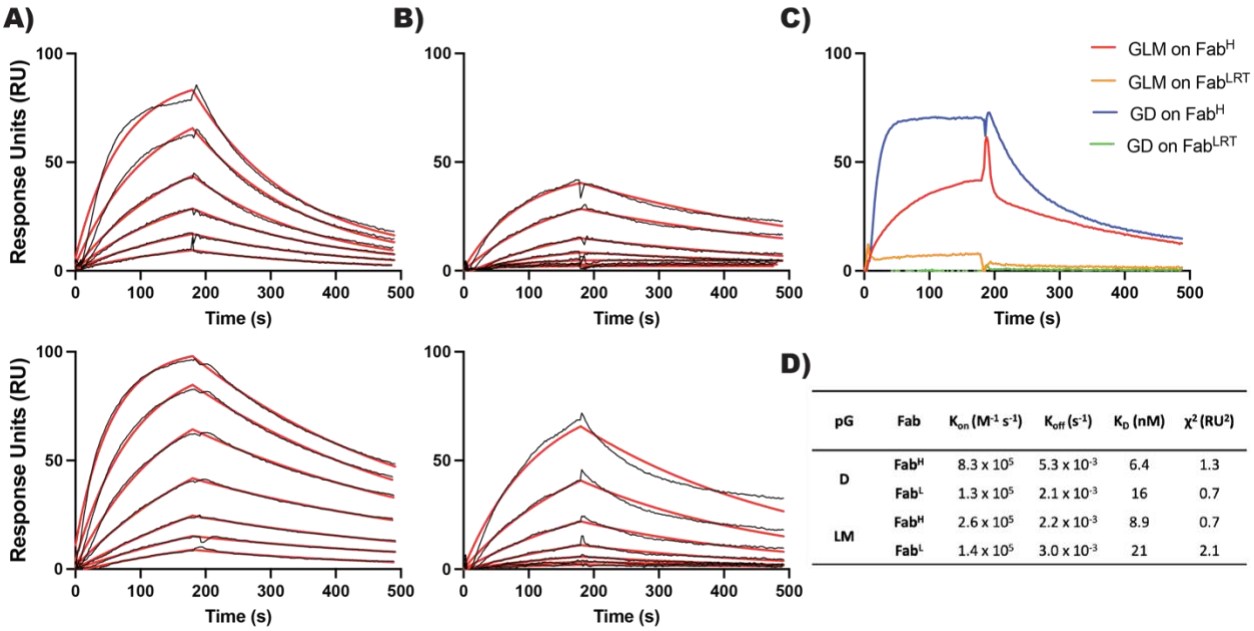

pG	Fab	K_{on} (M^{-1} s^{-1})	K_{off} (s^{-1})	K_D (nM)	χ^2 (RU^2)
D	Fab^{H}	8.3 x 10^5	5.3 x 10^{-3}	6.4	1.3
	Fab^{L}	1.3 x 10^5	2.1 x 10^{-3}	16	0.7
LM	Fab^{H}	2.6 x 10^5	2.2 x 10^{-3}	8.9	0.7
	Fab^{L}	1.4 x 10^5	3.0 x 10^{-3}	21	2.1

Figure 2.9 Characterization of GD and GLM. (**A**) SPR sensogram showing the interaction of GD (top) and GLM (bottom) with Fab^{H}. (**B**) SPR sensogram showing the interaction of GD (top) and GLM (bottom) with Fab^{L}. (**C**) A single injection of Fab^{H} and Fab^{LRT}. 25 nM of Fab^{H} and 100 nM of Fab^{LRT} were injected, and no binding to Fab^{LRT} was observed. (**D**) Kinetic parameters of binding. For the kinetic experiment, Fabs were serially diluted two-fold, starting at 100 nM.

Protein G	Amino acid sequence in position 38-43	K_{on} (M^{-1} s^{-1})	K_{off} (s^{-1})	K_D (nM)
GF	YAFGNG	4.3×10^5	8.2×10^{-4}	1.9
GD	IDMVSS	8.3×10^5	5.3×10^{-3}	6.4
GLM	LGMMRS	2.6×10^5	2.2×10^{-3}	8.9
GS	SGLLAG	2.8×10^5	1.6×10^{-3}	5.8
GLV	LGMVRG	2.9×10^5	4.8×10^{-3}	16.5
GYG	YGTANG	3.6×10^5	2.6×10^{-3}	7.2
GQT	QTPSLK	2.5×10^5	3.2×10^{-3}	13.0
GW	FGWSNG	2.7×10^5	1.2×10^{-3}	4.3
GY	YSGGNG	3.7×10^5	1.4×10^{-3}	3.9
GFH	FAHGNA	2.0×10^5	2.1×10^{-3}	10.4
GFS	FGNSNG	2.3×10^5	1.9×10^{-3}	8.3

Table 2.1 Kinetic binding parameters of different PGs binding to Fab^H determined by SPR

Protein G	Amino acid sequence in position 38-43	K_{on} (M^{-1} s^{-1})	K_{off} (s^{-1})	K_D (nM)
GF	YAFGNG	5.2×10^5	4.9×10^{-4}	0.9
GA1	YAYVHE	2.6×10^6	2.4×10^{-4}	0.1
GS	SGLLAG	3.7×10^5	2.4×10^{-3}	6.6
GW	FGWSNG	3.2×10^5	1.4×10^{-3}	4.2
GY	YSGGNG	5.2×10^5	1.6×10^{-3}	3.2

Table 2.2 Kinetic binding parameters of different PGs binding to Fab^{LRT} determined by SPR

2.3.4 Structural insight into specificity differences between the protein GF and GD

The crystal structure of protein GF and Fab^{H} was determined to gain structural insight into GF's universal Fab binding features. The crystals were set up with the histone chaperone Anti-silencing factor 1 (ASF1) and Fab E12 that was previously generated against ASF1 (Bailey et al., 2018). The Fab was grafted into the Fab^{H} scaffold before complex formation and incubated with GF in 1:1 molar concentration. I set up a high-throughput crystallization campaign using the hanging drop vapor diffusion technique (Benvenuti and Mangani, 2007) After 24 hours, the initial hits were observed and further optimized. Taking the previously described success, the seeding technique (Luft and DeTitta, 1999) was applied during optimization. Crystals with different morphology were obtained. However, the best diffracting data sets (2.4Å- 2.6Å resolution) were generated from large needle-shaped crystals while using vector data collection (Dauter, 1999) (Figure 2.10). The complex crystallized in space group $P22_12_1$ with one molecule per asymmetric unit. As previously described, Protein G binds to the Fab through an antiparallel β-strand interaction with the heavy chain and the helical cap interactions with the light chain. Since our protein engineering strategy did not modify this surface, the β-strand contact is mostly by H-bonding and was identical to the previously analyzed GA1-Fab^{LRT} structure (See chapter 2.3.2). The main interest of this structure was the PG's helical cap interaction with Fab Lc since the helical cap was broadly randomized in our PG phage library. The Fab^{H}- GF interface is formed through two contacts that bury ~530$Å^2$ for the interaction with Hc and ~198$Å^2$ with Lc. The GF-Fab^{H} structure analysis reveals minor binding of F40 from protein GF to the Fab light chain in the previously described area (Slezak et al., 2020). Most of the GF interaction comes from the contact with the Fab heavy chain, which includes an H-bond formed between Y38 from GF and Fab P124. Further, a set of interactions is formed between Y38, G41, and N42 from GF with S125, F127, and

V212 from the Fab heavy chain (Figure 2.11B). These findings explain the universal binding to all tested Fab scaffolds by the GF since the heavy chain sequence is conserved between the Fabs framework.

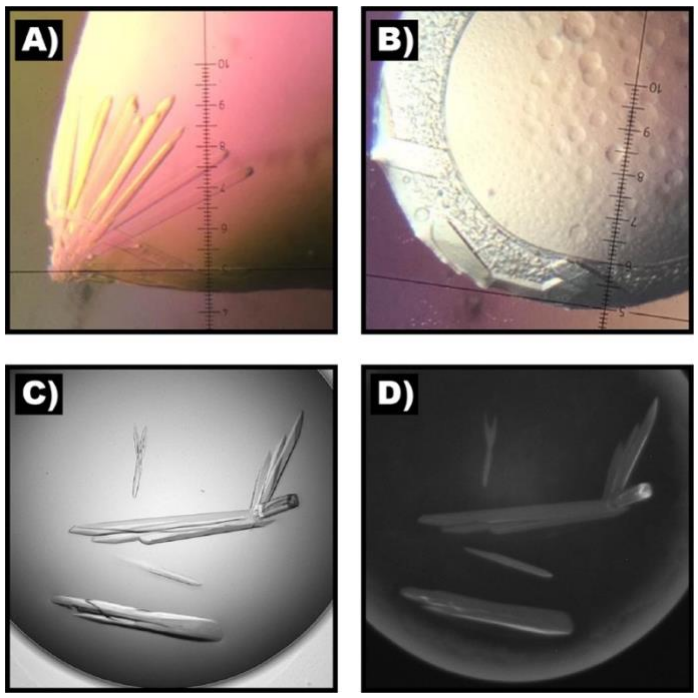

Figure 2.10 Crystals of the ASF1-E12 Fab^{H}-GF complex. Crystals with a different morphology were obtained. (**A**) Needle shaped crystals after optimization. (**B**) Rectangle shaped crystals after optimization. (**C**) Needle shaped crystals after optimization using the seeding technique. (**D**) Verification of protein crystals with a UV light microscopy.

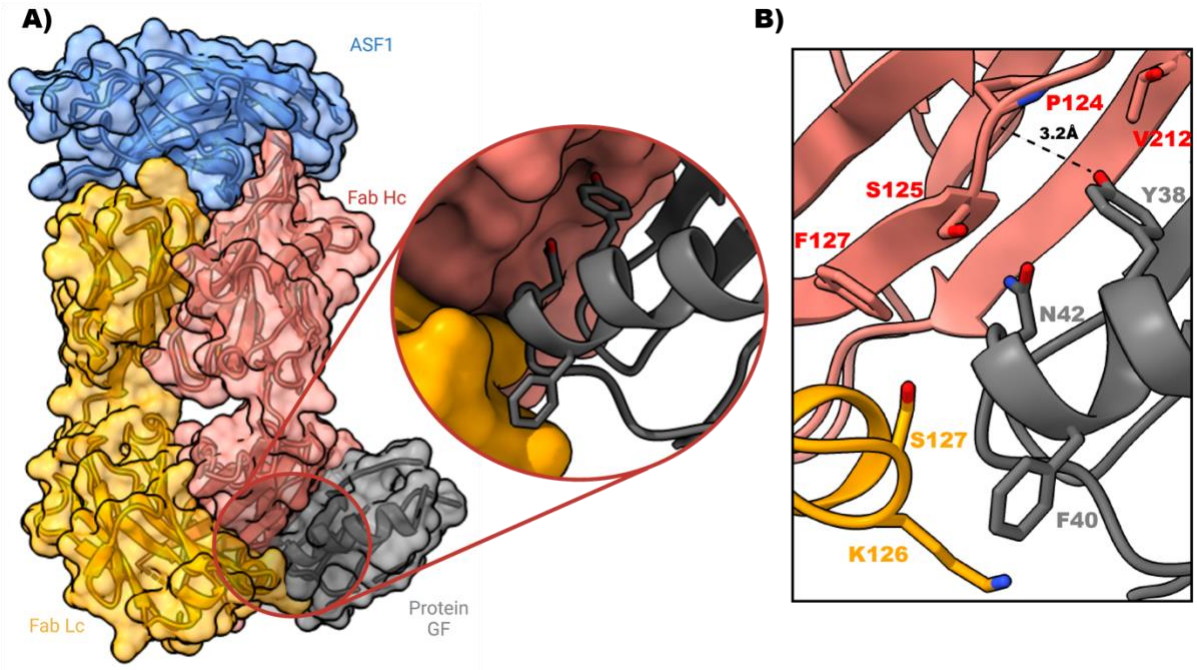

Figure 2.11 The structure of the ASF1-E12 Fab^{H}-GF complex. (**A**) General view of the structure. (**B**) The interface between Protein GF and Fab^{H}. Universal binding of GF comes from the extensive interactions of Y38, G41, and N42 with the Fab Hc. Y38 forms a hydrogen bond with a main carbonyl of P124 from the Fab Hc. F40 placed itself between K126 and S127, forming the only interaction of GF with the Fab Lc. Molecules are colored as follows: ASF1- blue, Fab Hc- red, Fab Lc- orange, GF- gray.

Next, the crystal structure of Fab^{H}-GD was determined to better understand the interesting properties of the second pool of engineered PGs, which recognize naturally existing Fab scaffolds, but do not bind to Fab^{LRT}. The crystals were set up with the same complex of Fab^{H} (E12) and the ASF1 protein, as described for the GF structure. The complex formed, and several crystals with different morphology were obtained (Figure 2.12). The complex crystallized in space group $I4_122$ with one molecule per asymmetric unit. The Fab^{H}- GD interface is formed through two contacts that bury ~596Å^2 for its interaction with Hc and ~185Å^2 with Lc (Figure 2.13). The specificity of GD appears to come from the set of hydrogen bonds formed by D39, S43, and D45 from the GD with Fab^{H} Lc. The side chain of S127 from Fab^{H} forms hydrogen bonds with D39 from GD. Additionally, K126 forms a salt bridge with the side chain of D45 and a hydrogen bond to the main

chain carbonyl of S43 from GD (Figure 2.14A). These interactions are disrupted by the significant loop rearrangement caused by the two amino acid deletions in Fab^{LRT}. Additional interactions of I38, D39, and M40 from GD are created with Fab Hc. M40 inserts in the hydrophobic pocket formed by P124, S125, V126, and V212. Furthermore, the interactions are formed between I38 and D39 with S125 and F127 from Fab Hc, respectively (Figure 2.14B).

Using the obtained structures with both orthogonal pairs: GA1-Fab^{LRT} and GD-Fab^{H}, I decided to model the interactions of GA1-Fab^{H} and GD-Fab^{LRT} to better understand the molecular basis for their specificity. The absence of binding of Fab^{H} with GA1 can be explained by the charge clash of E123 from Fab LC and E43 from GA1 (Figure 2.15A), while the significant loop rearrangement in Fab^{LRT} creates the clash of T127 with D39 from the GD (Figure 2.15B).

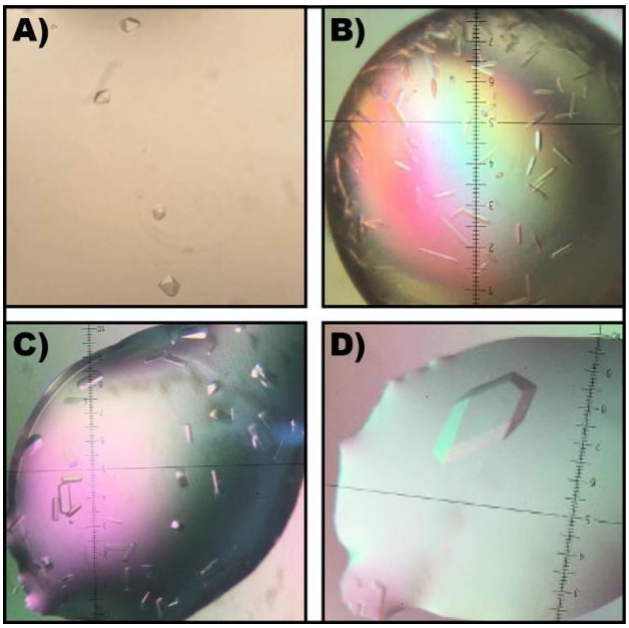

Figure 2.12 Crystals of the ASF1-E12 Fab^{H}-GD complex. (**A**) Small diamond-like crystals observed in the initial screen. (**B**) Rod-like crystals obtained after optimization. (**C**) Rod-like crystals after optimization using the seeding technique. (**D**) Large diamond-like crystals after optimization.

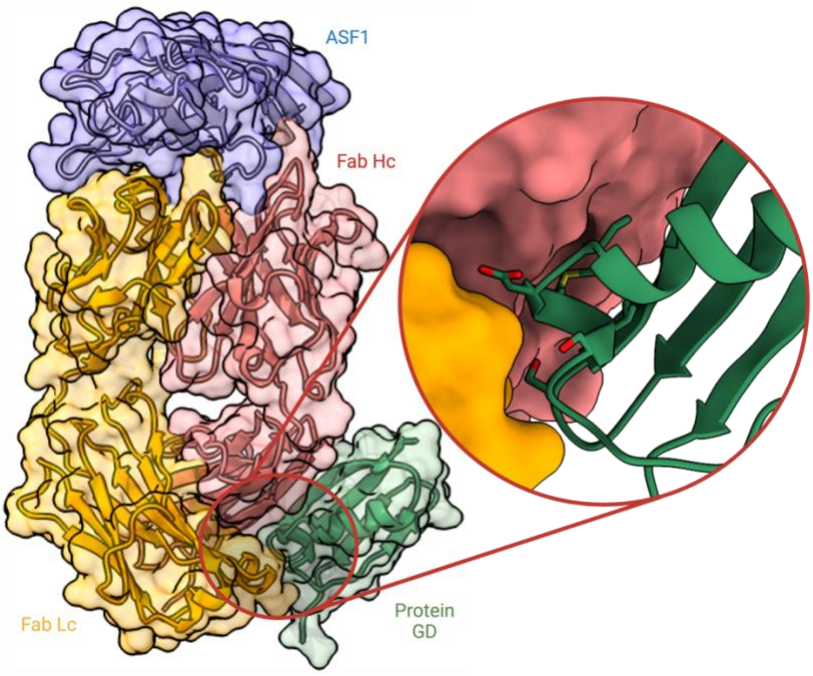

Figure 2.13 The structure of the ASF1-E12 Fab^{H}-GD complex. General view of the structure. The interface of Fab^{H} with GD shows an extensive interaction with both heavy and light chain of the Fab. Molecules are colored as follows: ASF1- blue, Fab Hc- red, Fab Lc- orange, GD- green.

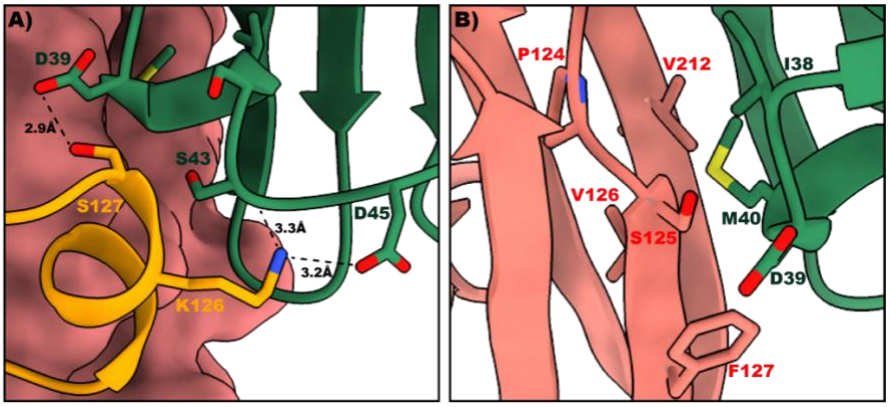

Figure 2.14 Interface between Protein GD and Fab^{H}. (**A**) GD interaction with Fab Lc. The specificity of GD is driven by the set of H-bonds formed by D39, S43, and D45, which is disturbed by the significant loop rearrangement caused by the two amino acid deletions in Fab^{LRT}. Side chains of S127 from Fab^{H} form hydrogen bonds with D39 from GD. Additionally, K126 forms two hydrogen bonds with a side chain of D45 and a main chain carbonyl of S43 from GD. (**B**) GD interaction with Fab Hc. I38, D39, and M40 are engaged in several hydrophobic interactions with Fab Hc. M40 is placed in the hydrophobic pocket formed by P124, S125, V126, and V212 from the Fab Hc. I38 and D39 interact with S125 and F127 from Fab Hc, respectively. Molecules are colored as follows: Fab Hc- red, Fab Lc- orange, GD- green.

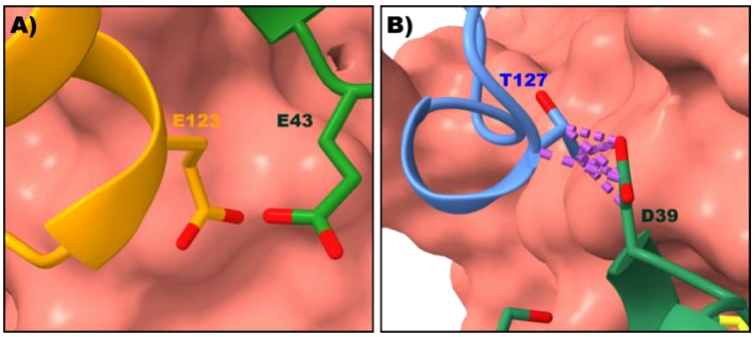

Figure 2.15 Structural basis of an orthogonal specificity between GA1-Fab^{LRT} and GD-Fab^{H}. (**A**) Model of GA1-Fab^{H}. The charge clash of E123 from Fab^{H} and E43 from GA1 is responsible for no interaction between these molecules. (**B**) Model of GD-Fab^{LRT}. Light chain loop rearrangement caused by two amino acids deletion in Fab^{LRT} causes a clash between T127 and D39 from the GD. Molecules are colored as follows: Fab Hc- red, Fab^{H} Lc- orange, Fab^{LRT} Lc- blue, GA1, and GD- green.

2.3.5. Engineering of Protein G-Fc

The molecular understanding of the GA1 interaction with Fab created an opportunity to engineer a protein G variant that would specifically recognize an Fc without binding to the Fab portion of the IgG. Protein GA1 is only functional in the context of synthetic Fab scaffolds such as Fab^{S} or Fab^{LRT}, and it does not bind to naturally existing Fabs due to a charge clash of the glutamic acids from both FabH and GA1 (Figure 2.15A). The glutamic acid is conserved in all naturally existing Fab scaffolds (Figure 2.2C). The wild-type protein G has a high-affinity interaction with the Fc portion of the IgG (Derrick and Wigley, 1992), but it has been engineered out during the initial generation of GA1 (Bailey et al., 2014). Based on the previously published structure of the wild-type protein G in complex with the Fc domain of human IgG (Sauer-Eriksson et al., 1995), I selected seven residues in GA1 that were mutated in order to reintroduce the binding to the Fc portion of the IgG (Figure 2.16A). Two separate variants were created, where an additional residue in the helical cap was mutated. The biophysical characterization by SPR showed

a successful generation of G-Fc, which possesses a low nM affinity to the Fc domain (3.8 nM) with a prolonged dissociation rate (Figure 2.16B). A 200 nM injection of FabH tested the high specificity of the G-Fc, but no detectable binding was observed (Figure 2.16C). The second variant, G-Fc2, was characterized by lower affinity to the Fc domain (33.7 nM), with a much faster dissociation rate (Figure 2.16D), which can be beneficial in applications where it is unfeasible to have a long-lasting linkage of the cargo to the IgG.

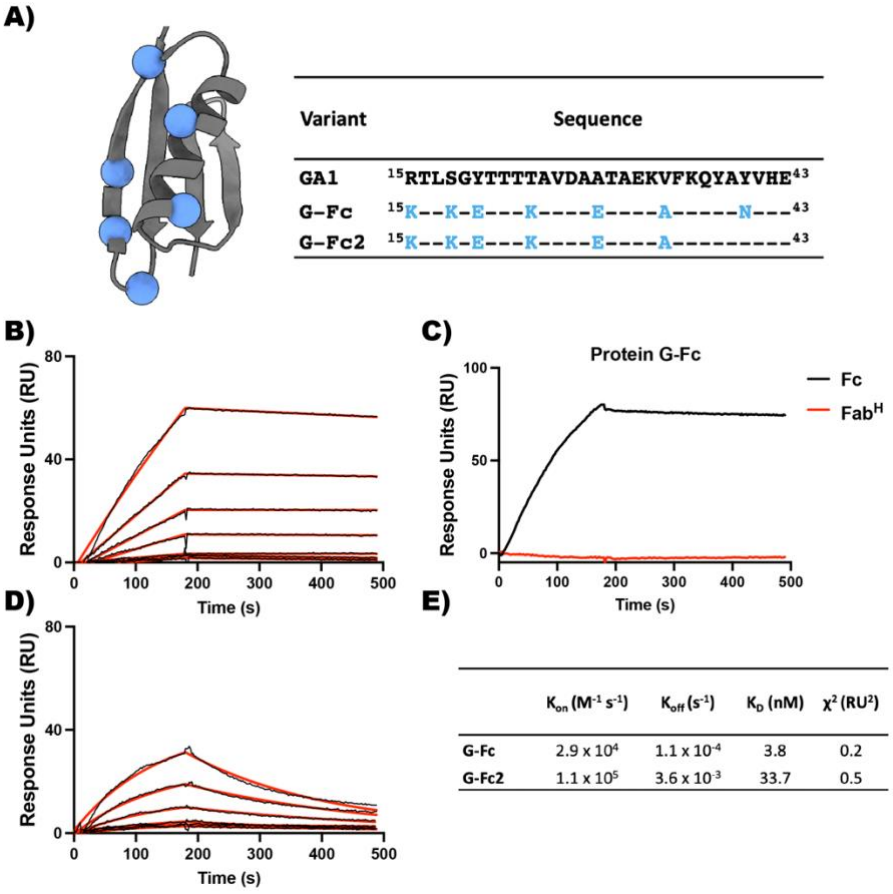

Figure 2.16. Engineering of Protein G-Fc. (**A**) Residues mutated to generate a Protein G-Fc are represented as blue spheres. (**B**) SPR sensogram showing the interaction of G-Fc with human Fc. (**C**) A single injection of Fc and Fab^H on G-Fc. 200 nM of Fc and 200 nM of Fab^H were injected, and no binding to Fab^H was observed. (**D**) SPR sensogram showing the interaction of G-Fc2 with human Fc. (**E**) Kinetic parameters of binding. For the kinetic experiment, analytes were serially diluted two-fold, starting at 100 nM.

2.3.6. Applications of a plug-and-play Fab-Protein G platform

2.3.6.1 A universal affinity chromatography resin for antibody purification

The wild-type protein G (PG) has been broadly used for antibody purification due to its high affinity towards the Fc portion of the antibody. However, it is not a suitable reagent for Fab purification since this affinity is in the μM range. Thus, a typical Fab purification strategy involves incubating with the protein A (pA) resin, and despite being a very successful tool for antibody purification, pA has distinct disadvantages. Binding selectively to Fab Hc (see section 2.2.2) can compromise the purity of the final product and thus, require an additional cation-ion exchange to remove single-chain degradation products. Additionally, protein A is not generally recommended for the purification of antibodies from murine due to a very low affinity and efficiency (Fishman and Berg, 2019). In contrast, protein G resin is a perfect substitute since it binds to the Fab's heavy and light chains. Since the GF has an improved affinity and universal binding characteristics independent of the Fab scaffold, I created a GF agarose resin for Fab purification. The GF resin was successfully applied to purify multiple Fab scaffolds, including Fab^{H}, Fab^{LRT}, and full-length IgGs (Figure 2.17). The in-house produced resin is characterized by a very high capacity (20mg of Fab/mL) with a long lifespan (>1.5 years) and stability that allows for resin cleaning and regeneration with the low pH treatment. Industrial procedures to clean such resins include a base treatment. This leads to GF deamination and decreased resin efficiency, which was previously observed for wild-type protein G (Gulich et al., 2002). The alternative resin with a deamination-free variant, GS, has been generated to circumvent this issue. The GS variant was characterized by similar and universal high affinity towards all tested Fab scaffolds (Table 2.1, 2.2).

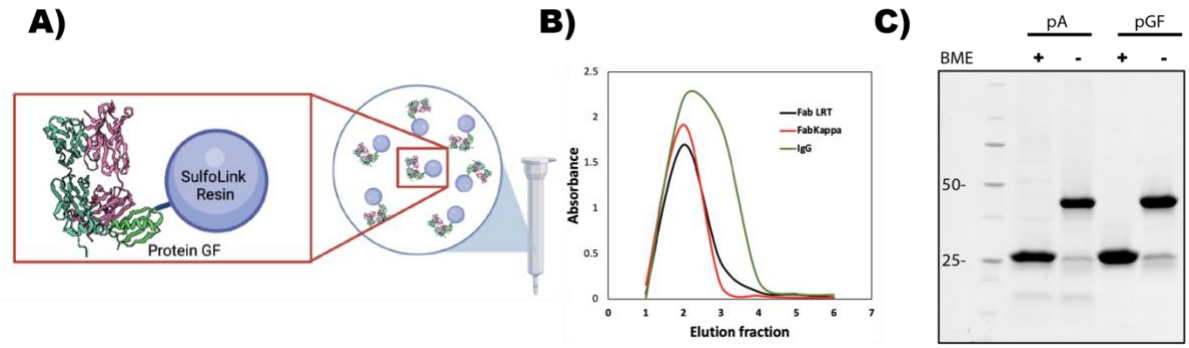

Figure 2.17 In-house generation of affinity chromatography resin for universal Fab purification. (**A**) Schematic showing the covalent immobilization of SUMO-GF with SulfoLink Coupling Resin. The resin is a high capacity (20mg of Fab/mL), has a long lifespan (>1.5 years), and is reusable due to its tolerance to low pH regeneration. (**B**) A single step with a SUMO-GF coupled resin purified elution profiles of full-length IgG, Fab^{H}, and Fab^{LRT}. (**C**) SDS-PAGE gel post-purification. The purity of the product is superior to the commonly used Protein-A resin due to its single-chain binding profile.

2.3.6.2 β-lactamase complementation-based assay for protein detection

Having the set of tools in hand, I decided to develop a protein complementation assay (PCA) as a further application for the plug-and-play GA1-Fab^{LRT} platform. I used a well-established proximity-driven reactivation of the TEM1 β-lactamase (BL) split enzyme system (Galarneau et al., 2002). The assay was designed to evaluate protein-protein interactions and thus two separate fragments of the BL enzyme were attached to the two different targets that are to be evaluated for the proximity. The concept is, if they are in proximity, then the BL fragments (BLF) can associate to form an active enzyme that can be evaluated by introducing a BL substrate. The system requires that the individual BL fragments be genetically fused to the potential interaction partner, which is a bottleneck of the standard format. To overcome the issues, I developed a plug-and-play system that uses the high affinity of GA1 and Fab^{LRT}. The strategy was to express and purify two GA1 fusions with one or the other of the two complementary BLF: N-terminal fragment- residues 26-196 and C-terminal fragment- residues 198-220. The two GA1 fusions with

complementary BLFs become associated separately with two Fabs in the Fab^{LRT} scaffold, that recognize a non-overlapping epitope on a target. Upon addition of the antigen, simultaneous antigen-binding of these Fabs occurs and results in BL refolding and activation (Figure 2.18A). This can be detected by the increase in fluorescence signal upon addition of a fluorogenic BL substrate.

To optimize the system and explore the different options, I constructed and produced four fusions of combinations of the N-terminal (BLF1) and C-terminal (BLF2) fragments of BL connected to GA1 by a Gly–Ser linker of about 30 residues. Next, I demonstrated the functionality of GA1-BLF fusion constructs by testing their reconstitution at 1 μM concentration with the complementation partner in the absence of antigen. All possible pairs were tested, with the best pair: 1 and 4 (BLF1 fused to the C-term of GA1 and BLF2 fused to the N-term of GA1) showed the lowest spontaneous activity at 1 μM concentration (Figure 2.18B). This pair was then used to establish the background level at concentrations between 2 μM and 15 nM. This showed that BL activity in the absence of antigen was triggered at concentrations above 500 nM. Thus, I chose a concentration of 250 nM (Figure 2.18C) that was well below this threshold as the baseline for the antigen-detection conditions, since it was the highest concentration that displayed minimal background activity in the absence of antigen. As a proof of concept for the assay development, I chose the previously described ASF1 as an antigen. Work performed by previous members of the lab resulted in two Fabs (11E and 12E), which bind to orthogonal epitopes on ASF1 (Schaefer et al., 2016). Crystal structures of these Fabs with ASF1 established their binding sites on the opposite site of the antigen (Bailey et al., 2018). A model of superimposed crystal structures of the ASF1:12E:11E complex with GA1 bound to each Fab was used to design the optimal length of the linker. It indicated the need for a ~100-150 Å distance accommodated between the termini of the

two GA1 proteins (Figure 2.18A). The dilemma however was to not generate too long linker length that could diminish the local concentration effect and there is a need for a built-in excess to take into consideration inherent flexibility of the Fab and universality of the system. Taken this, I generated a 30 amino acid Gly-Ser $(GGGGS)^6$ as a reasonable compromise between the above requirements. Indeed, in pilot experiments where each of the pairs of complementary BLF–GA1 fusions were pre-mixed separately with 11E or 12E $Fabs^{LRT}$, an increase (~10-fold) in the fluorescent signal was observed upon addition of an equimolar amount of Asf1 (Figure 2.18D). Notably, all BLF-GA1 worked, but I established before that the 1-4 pair generated the best signal-to-noise ratio and thus our efforts were further concentrated on this pair.

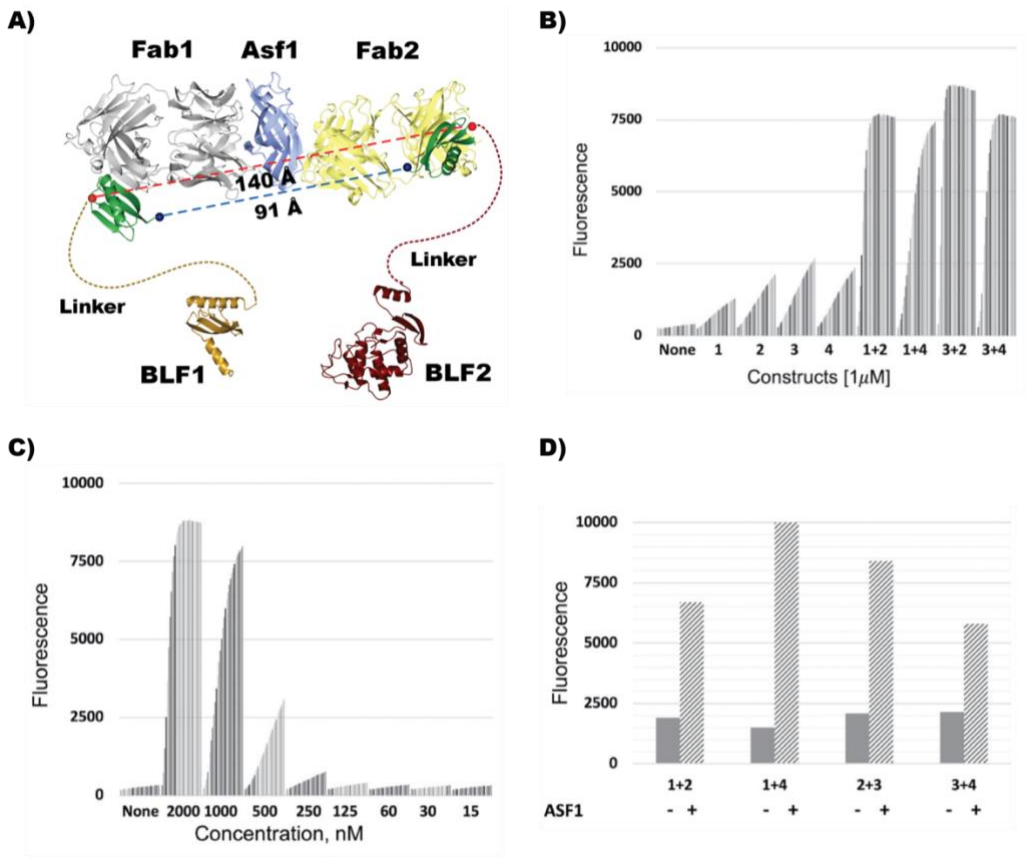

Figure 2.18 Optimization of β-lactamase complementation-based assay. (**A**) Model of β-lactamase complementation-based assay for protein detection. The potential fusion points between the Fabs and the linker-BL fragments. The structure of the ASF1 with Fab1 and Fab2 complex shows that the Fabs bind to the opposite faces of the ASF1. In those positions, it is possible to measure the direct distances between the N- and C-terminal fusion points the BL fragments on GA1 bound to its respective Fab. The direct distances range from ~90 to 140 Å. A 30-residue linker was thought to have enough reach that it would be effective in all possible combinations. Molecules are colored as follows: Fab 1- silver, Fab 2 - yellow, ASF1- blue, GA1- green, BLF1- gold, BLF2- red. (**B**) Different BL fragments were mixed at 1 μM concentration. Fluorescent readings were taken every 2 mins over 20 time points. No activity was observed when the individual fusion components were mixed without their complementary pair. Activity was seen at this high concentration when the component pairs were mixed. Although at the last time points activities are similar, the 1 + 4 pair, shows a distinct difference from the others over the time course. (**C**) Background activity for the complementation pair 1-4 (GA1-BLF1(1) and BLF2-GA1(4)) when mixed at varying concentrations. Readings were taken at 2 min intervals over a 1h incubation. Data show that the signal is at background at 250 nM concentration of the pair. (**D**) Asf1 antigen detection using different BFL combinations. Fabs 11E and 12E were mixed with BLF fragments at 250 nM concentration. Then, 250 nM of Asf1 was added. (−) is the signal prior to Asf1 addition, (+) after addition of antigen. BL activity was measured after 20 mins incubation at room temperature.

This non-wash system was further tested by applying it for antigen detection of two viral proteins with the unknown structural organization. The first was the 98 residues C-terminal domain of the Zaire strain of Ebola virus nucleoprotein (EBOV NP), and the second was the 261 N-terminal methyltransferase domain of the Zika virus bifunctional NS5 enzyme (MT ZIKV). I generated the pool of Fabs that recognize two distinct epitopes on NP. Most of the selected epitopes recognized one epitope (from the group, MJ20 was selected for further use), while one Fab (MJ6) was found to bind on the non-overlapping epitope. The complementation-based assay requires antibodies that bind to its target with a relatively high affinity. Thus, I analyzed the binding kinetics of the selected Fabs against NP. Both are characterized by a high affinity of 3.4 nM (MJ20) and 0.7 nM (MJ6), with a slow dissociation rate (Figure 2.19A). Furthermore, consecutive injections of both Fabs on SPR showed that Fabs recognize a non-overlapping epitope on NP (Figure 2.19B). The same criteria were applied to select antibodies that could detect ZIKV MT. Epitope binning experiment identified two candidates- Z2C4 and Z2G6 (Figure 2.19D). Their binding kinetics (0.7 and 1.7 nM, respectively) are desirable for our detection assay (Figure 2.19C). The Fabs were then grafted into the Fab^{LRT} scaffold and tested in the plug-and-play β-lactamase complementation-based assay for protein detection.

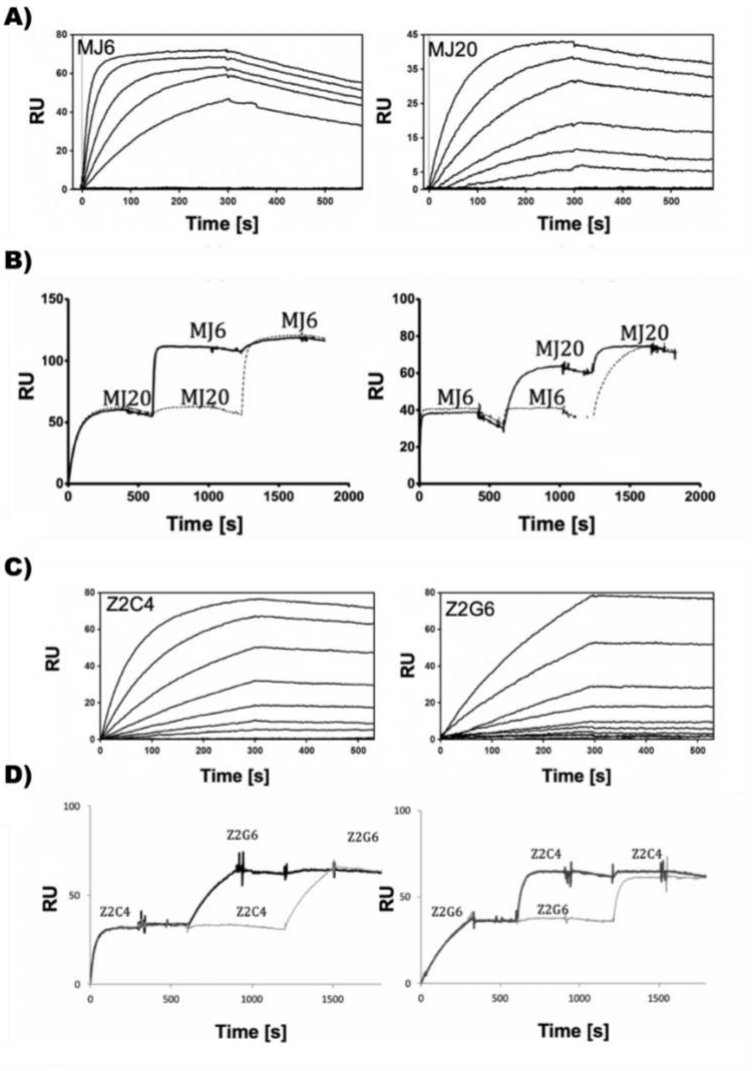

Figure 2.19 Binding epitopes of EBOV and ZIKV Antibodies. (**A**) SPR senograms used for kinetic analysis of MJ6 and MJ20 binding to EBOV NPCT. Initial concentrations (MJ6–50 nM; MJ20–100 nM) Fabs were serially diluted two-fold starting at 100 nM (MJ20) or 50 nM (MJ6). (**B**) Epitope binning experiment of MJ6 and MJ20 against EBOV NPCT showing the Fabs have non-overlapping epitopes. Fab MJ20 (or MJ6) was injected as an analyte first, followed by a second injection of the other Fab. Substantial increase in RUs upon the second injection indicates the two Fabs bind simultaneously. (**C**) SPR sensogram for Z2C4 and Z2G6 binding to ZIKV MT. Fabs were serially diluted two-fold starting at 100 nM. (**D**) Epitope binning experiment of Z2C4 and Z2G6 showing the Fabs have non-overlapping epitopes.

The previously mentioned, detection of ASF1 had the advantage of having structural information that allows for the precise GA1-BLFs design. Unfortunately, both antigens I sought to detect (EBOV NP and ZIKV MT) did not have the structural information of the epitope-paratope interface for the selected Fabs. I hoped that a 30 amino acid spacer between GA1 and BLFs would be universal and allow the fragment's reconstitution. Fabs were premixed with GA1-BLFs in 250 nM concentration and applied as previously described for ASF1. As a result, the detectable signal starting at 15 nM of NPCT with a linear increase was observed. A reduction of the signal at the high NP concentration was observed due to antigen excess that breaks down the stoichiometry of the system (Figure 2.20A). Further, the detection of ZIKV MT was achieved with a detectable signal starting at 30 nM of MT, with the highest signal observed at 250 nM (Figure 2.20B). These results show the β-lactamase complementation-based assay potential with a detection limit that falls within the range of laboratory-performed detection assays.

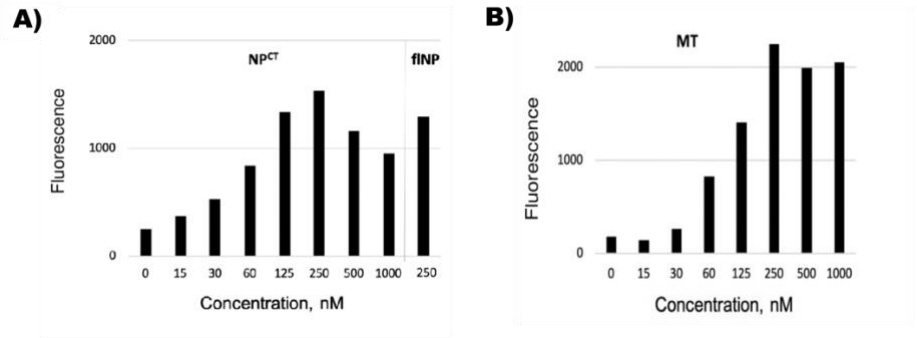

Figure 2.20 Ebola Zaire NP and Zika MT detection. (**A**) Detection of EBOV NP (C-terminus) at different concentration indicate the detectable signal starting at 15 nM and peaking at 250 nM. The full-length NP was also successfully detected using the MJ6 and MJ20 Fab pair. (**B**) Detection of ZIKV MT. Detectable signal was observed starting at 30 nM. All experiments were incubated for 20 minutes at RT and the results were normalized by a subtraction of background fluorescence (200 units).

2.3.6.3 Bi-specific T-cell engager immuno-reagent

In recent years Bi-specific T-cell engagers (BiTEs) have become an important immuno-therapeutic assembly (Chames and Baty, 2009). These molecules are engineered to engage an activated T-cell through one binding arm and to attach it to a cell surface target on an antigen-presenting cancer cell (APC) through its second arm (Brinkmann and Kontermann, 2017), which leads to T-cell dependent cell death of the cancer cell (Figure 2.20A). Several formats of BiTEs have been engineered and successfully applied (Huehls et al., 2015; Mack et al., 1995). The most prevalent formats to induce engagement between the two cells are: 1) bispecific antibody where one arm recognizes the T-cell and the other the APC, and 2) two cell directed single-chain Fvs attached by a flexible linker. Each of these approaches contains strengths and weaknesses, but neither has an adaptability provided by GA1-Fab^{LRT} plug-and-play format (Figure 2.21A). The concept of the bi-Fab design based on a GA1-Fab^{LRT} contains a Fab^{H}-GA1 fusion with adjustable linker that recognize one of the antigens and the second Fab in Fab^{LRT} format aiming for another target (Figure 2.21B, 2.21C). A number of constructs with different linker lengths (tested constructs had from 3 to 73 aa linkers) between GA1 and the C-terminus of the Lc of the Fab^{H} with a specificity directed at one of the target antigens. The usage of Fab^{H} in a direct fusion with GA1 is essential to prevent the "self" association within the same module, since GA1 does not recognize Fab^{H}, as discussed above (Figure 2.15A). The proof of concept described below is that a Fab(1)^{H}-linker-GA1 fusion that binds to antigen target 1 can be combined with a Fab(2)^{LRT} that binds antigen target 2 (Figure 2.21C). As a result, a noncovalent entity is being formed, containing two antibodies that recognize different antigen targets. I refer to these modules as plug-and-play "bi-Fab" BiTEs. This system allows for a high throughput cloning of any desired Fab CDRs into the Fab scaffold, resulting in an easy preparation and testing of potential therapeutic candidates.

The GA1-Fab^{H} fusions can be efficiently produced in *Escherichia coli* periplasm and premixed with Fab^{LRT} prior to experimental testing.

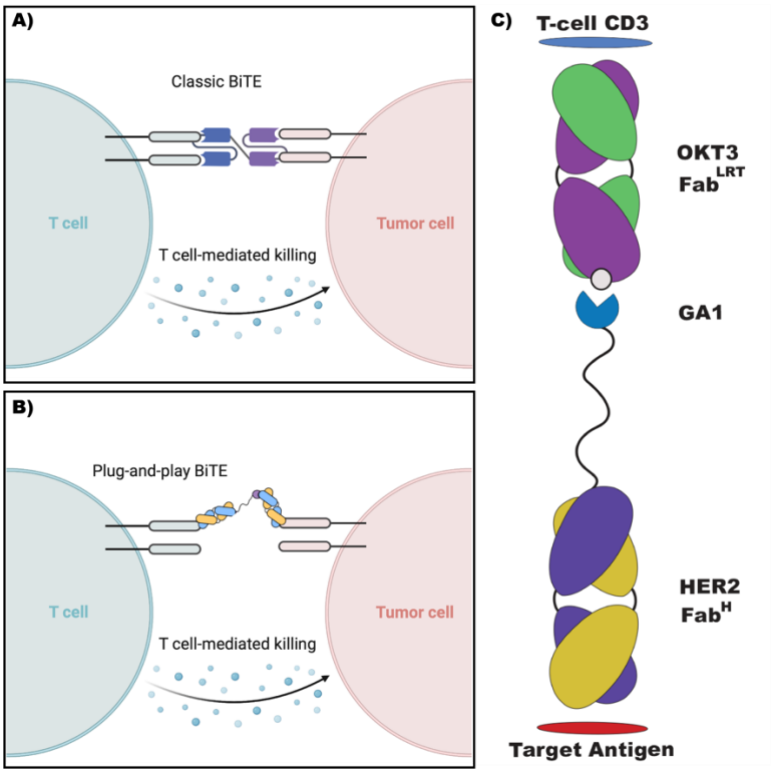

Figure 2.21 Bi-specific T-cell engager. (**A**) Classical BiTE model. Design contains bispecific antibody where one arm recognizes the T-cell and the other the APC, leading to T-cell activation and tumor cell death. (**B**) GA1-Fab^{LRT} plug-and-play "bi-Fab" BiTEs model. (**C**) BiTE construct. Fab^{H} recognizes HER2 extracellular domain on the antigen-presenting cells (APC). The Fab is attached by an adjustable Gly-Ser linker to GA1 via a direct fusion to the C-term of its light chain. Fab^{LRT} components binds to CD3 of the T-cell receptor. This Fab contains the CDRs of either of the CD3 binders, OKT3 or UCHT1.

To test the GA1-Fab^{LRT} plug-and-play bi-Fab module in a biological application, I chose to construct a module that would induce the engagement between a cell that had an overexpressed cell surface cancer marker through one arm and a cytotoxic T-cell through the other. Therefore, the first Fab (Fab^{H}) was targeting Her2, a highly over-expressed marker on the surface of many

breast cancer cell lines. The second Fab (in Fab^{LRT} scaffold), was targeting and activating a CD3 component of the T-cell receptor complex (Gebel et al., 1989; Landegren et al., 1984). I hypothesized that the linkage between T-cells and tumor cells created by GA1-Fab^{LRT} bi-Fab would induce robust immunological-synapse formation and would activate T-cells to secrete cytokines and cytotoxic granules resulting in tumor cell killing. To target Her2, I introduced CDRs from the trastuzumab IgG antibody (Carter et al., 1992) to GA1-Fab^{H} fusion. Further, the CDRs from widely used CD3 antibodies, OKT3 or UCHT1 (Burns et al., 1982) were grafted onto Fab^{LRT} scaffold and produced in the *Escherichia coli* periplasm.

I performed a redirected tumor-cell killing assay to determine the efficiency and functionality of our bi-Fab module. The assay has three readouts: (1) the activity of a cytoplasmic enzyme, lactate dehydrogenase (LDH), released into the medium upon cell lysis, (2) interleukin IL2 and (3) interferon γ production by T-helper cells. I used isolated human PBMCs, as a source of T-cells, and Her2-positive SKBR3 human breast-cancer cells as the APC. Addition of 50 nM bi-Fabs in several different active combinations to PMBC-SKBR3 co-cultures, resulted in robust cell killing (up to 70%), and prominent IL2/ IFNγ release (Figure 2.22). Remarkably, these results surpassed the results produced by the positive-control bi-specific antibody, representing hOKT3 Fab- hHer2 scFv genetic fusion (Figure 2.22 lane 9). Next, I switched the format and fused anti-CDR Fab to GA1, while Her2 Fab was introduced as a Fab^{LRT} component, which resulted in the comparable results. This experiment established that the activity of bi-Fab is independent of the Fab component organization. System activity was abolished upon introduction of the CD3 Fab^{LRT} mutant that had eliminated CD3 binding. No activity was observed when the separate components (Fab^{H}, Fab^{LRT}, GA1) were added, which demonstrated that the functional bi-Fab assembly is dependent upon the genetic fusion of GA1 to Fab^{H} (Figure 2.22). Presented results illustrate the

bi-Fab potential that should be especially useful for a high throughput screening of many antibodies in various combination, streamlining the production of bispecific antibodies.

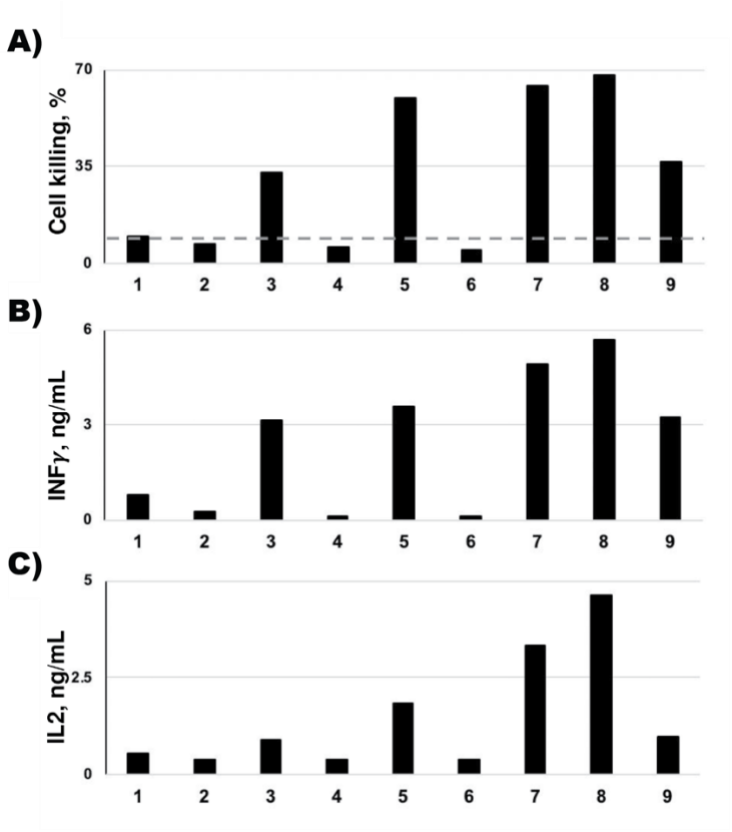

Figure 2.22 Results of a plug-and-play GA1-Fab^{LRT} bi-Fab. The effects of the bi-Fab (Fab^{H}(Her2)GA1 / Fab^{LRT}(OKT3/UTCH1)) on PBMC/SKBR3 (10:1) co-cultures. Experiment was setup as follows: 20K SKBR3 cells were attached to the plate overnight, followed by addition of 200K of PBMCs premixed with 50 nM of the BiTE. Cell killing effect was measured after 24 hr by LDH activity (**A**) and cytokine release upon T cell activation (**B**, **C**). As a control, all the individual components of the BiTE reagents (lanes 1 and 2) and with mutant CD3 Fab^{LRT}, deficient in CD3 binding (lanes 4 and 6) were tested and showed practically no effect on LDH or cytokine levels (dashed line). The CD3 activation and cell killing was observed only when both active components of the BiTE were present (lanes 3, 4, 7, and 8) and with genetically linked bi-specific molecule used as a positive control (lane 9). Results of representative experiments out of three (or more) are shown. Contents of lanes: 1 (GA1+ Fab^{H}(Her2) + Fab^{LRT}(OKT3); 2 (GA1+ Fab^{H}(Her2) + Fab^{LRT}(UTCH1), 3 (Fab^{H}(Her2) + GA1 + Fab^{LRT}(OKT3); 4 (Fab^{H}(Her2) + GA1 + mutFab^{LRT}(OKT3)); 5 (Fab^{H}(Her2) + GA1 + Fab^{LRT}(UTCH1); 6 (Fab^{H}(Her2) + GA1+ mutFab^{LRT}(UTCH1); 7 (Fab^{H}(OKT3) + GA1+ Fab^{LRT}(Her2); 8 Fab^{H}(UTCH1) + GA1+ Fab^{LRT}(Her2); 9 classical BiTE control: Fab^{H}(OKT3) fused to Her2 scFV.

2.3.6.4 Modular CAR-T technology

Genetically engineered T lymphocytes that express chimeric antigen receptors (CAR) are a new cell therapy modality that has demonstrated extraordinary success in hematological malignancies. However, most patients develop acute toxicities that can be highly severe or lethal (Bonifant et al., 2016; Neelapu et al., 2018), and a significant number of patients do not achieve durable response or relapse due to mechanisms like antigenic escape or tumor heterogeneity (Majzner and Mackall, 2018; Park et al., 2018). This identifies the bottleneck of the system and the need for additional effort to optimize it. Taking advantage of the GA1-Fab^{LRT} module and the successful development of bi-Fabs, I engineered a novel CAR-T system I call GA1CAR. In the construction, I fused the protein GA1 upstream of a second-generation CAR-T lentivirus construct containing a CD8 hinge, a CD28 transmembrane domain, a 41BB co-stimulatory domain, and a CD3ζ domain (Figure 2.23) and used this construct to create GA1 T cells (GA1CAR). Incorporating the GA1-Fab^{LRT} system into CAR-T generation allows for the exchange of the T cell cytotoxicity towards different antigens presented on the surface of cancer cells upon using complementary Fabs for the target. Additionally, even though the affinity of GA1-Fab^{LRT} is superior and is characterized by an ultra-slow dissociation constant, it is not a covalent linkage. It will result in Fab dissociation over a time course, which should limit the system's cytotoxicity.

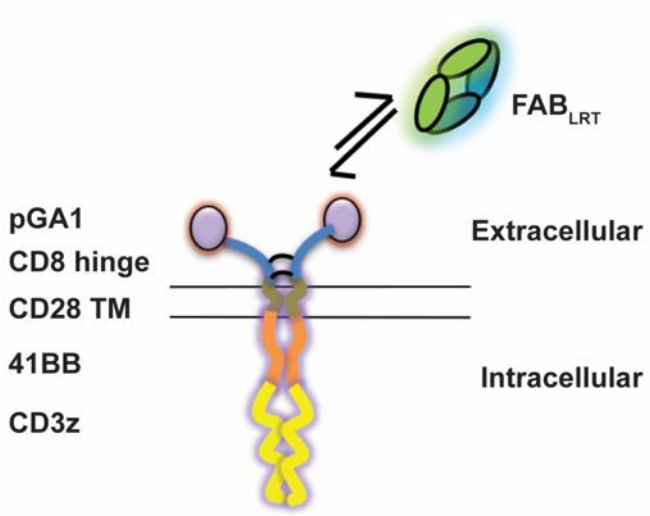

Figure 2.23 Model of GA1CAR. Schematic of GA1CAR design containing GA1, CD8 hinge, CD28 TM, 41BB, and CD3ζ domains. System contains exchangeable targeting feature due to a GA1-Fab^{LRT} platform.

The members of the Kossiakoff Laboratory are still validating this technology; however, the initial *in vitro* and *in vivo* results are promising. The manuscript is currently in preparation by Arauz et al. To further explore the advantages of the GA1-Fab^{LRT} in the GA1CAR system, I tested using different Fab scaffolds to serve as emergency "stop switches". The GA1CAR concept and activity are based on two sets of interactions provided by the Fab being administrated. The first interaction that controls the system's efficiency is the affinity of the employed Fab to its target on the cancer cell surface (K_D 1). The second one is connected to the Fab scaffold and GA1 located on the surface of GA1CAR (K_D 2) (Figure 2.24A). I hypothesized that the usage of Fab scaffolds with lower affinity to GA1 would modulate the CAR-T activity, and the use of an isotype Fab scaffold (Fab that does not recognize any human proteins) with a higher affinity to GA1 should replace the initial Fab and deactivate CAR-T (Figure 2.24B). This will allow for a more controlled CAR-T application and a possible "turn off" system. Current usage of the classical CAR-T system

struggle with the potential toxicity effect without a proper way to turn it off once the CAR-T is being administrated to the patient (Brudno and Kochenderfer, 2016).

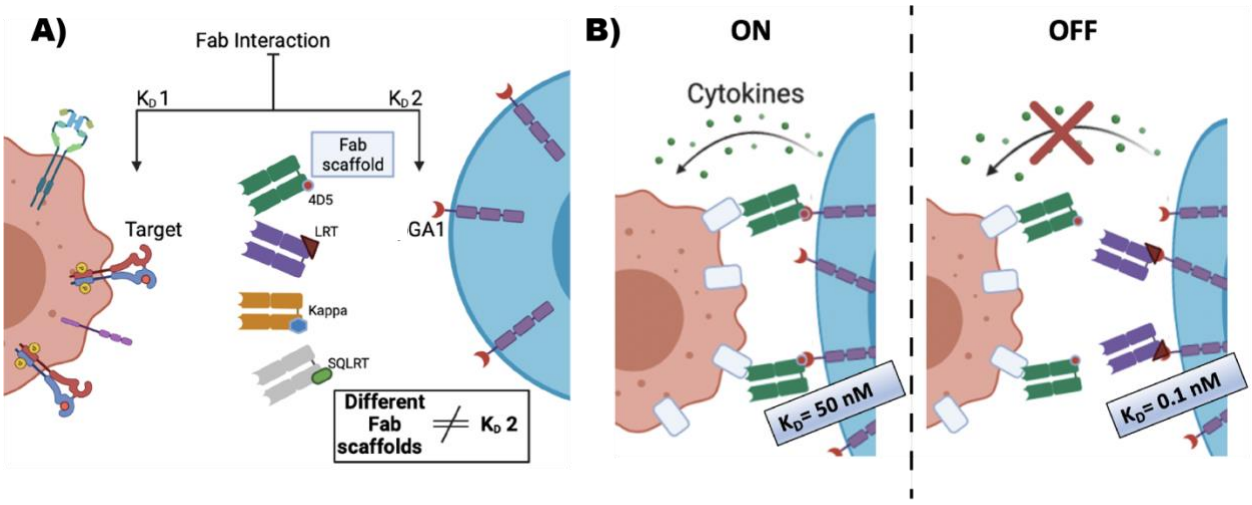

Figure 2.24 Model of CAR-T emergency stop switch. (**A**) GA1CAR-T efficiency depends on two sets of interactions, the affinity of the used Fab to its target on the cancer cell surface (K_D 1) and its Fab scaffold towards GA1 on the surface of CAR-T (K_D 2). The panel of engineered Fab scaffolds with a different affinity to GA1 allows for more controlled CAR-T usage. (**B**) CAR-T emergency stop switch. Isotype Fab in the scaffold with a higher affinity to GA1 can compete and deactivate the CAR-T.

To test the GA1CAR emergency stop switch, I performed a similar experiment previously described for the plug-and-play bi-Fab (see section 2.3.6.3). I used the same Fab targeting Her2, that was grafted into two Fab scaffolds: Fab^{SQLRT} (SQLRT) and Fab^{S} (4D5), which have different binding kinetics to GA1 (8 and 50 nM, respectively) (see section 2.3.1). The isotype Fab, which does not recognize human proteins and has a low off-targeting, was needed to serve as an emergency switch. Previously generated antibodies against SARS-CoV-2 were a good candidate for this purpose since they are characterized by their high affinity and specificity (Slezak and Kossiakoff, 2021). The Fab was grafted in Fab^{LRT} (0.1 nM affinity towards GA1) to detach

GA1CAR from cancer cells and hence interrupt the cell killing, or Fab^{H} (No affinity to GA1) to serve as a negative control (Figure 2.24). SKBR3 cells were incubated overnight, followed by the addition of GA1CAR cells and 100 nM Fab in either the Fab^{SQLRT} or Fab^{S} scaffold. After increments of one, two, four, or eight hours, the safety switch was applied by adding five μL of 20 μM Isotype Fab^{LRT} directly to the well for the Isotype Fab final concentration of 1 μM. The same Isotype Fab in the Fab^{H} scaffold was added as a negative control. After 24h of co-culturing, the cells were spun down, and the medium was analyzed for two readouts: (1) Cell killing measured by the LDH activity and (2) interferon γ release by T-helper cells. The addition of GA1CAR with both variants of Fabs (Fab^{SQLRT} and Fab^{S}) resulted in robust cell killing (~70%) and T cell activation. As expected, the addition of Isotype Fab^{LRT} provided an efficient separation of GA1CAR from the target cell and hence stopped the cell-killing activity of the T cells (Figure 2.24A). However, I did not observe a reduction in interferon γ release, suggesting that the T cells are detached, but not deactivated (Figure 2.25B). A similar experiment was performed to test the GA1CAR fatigue, and the expression of an early T cell activation marker, CD69, was tested using flow cytometry. Co-culture of SKBR3 cells with GA1CAR/Her2 Fab in Fab^{S} resulted in a significant CD69 expression. However, it was significantly reduced upon administration of Isotype Fab in Fab^{SQLRT}. Next, I reactivated GA1CAR using Her2 in Fab^{LRT}, which resulted in the CD69 expression level comparable to untreated, but activated GA1CAR (Figure 2.26).

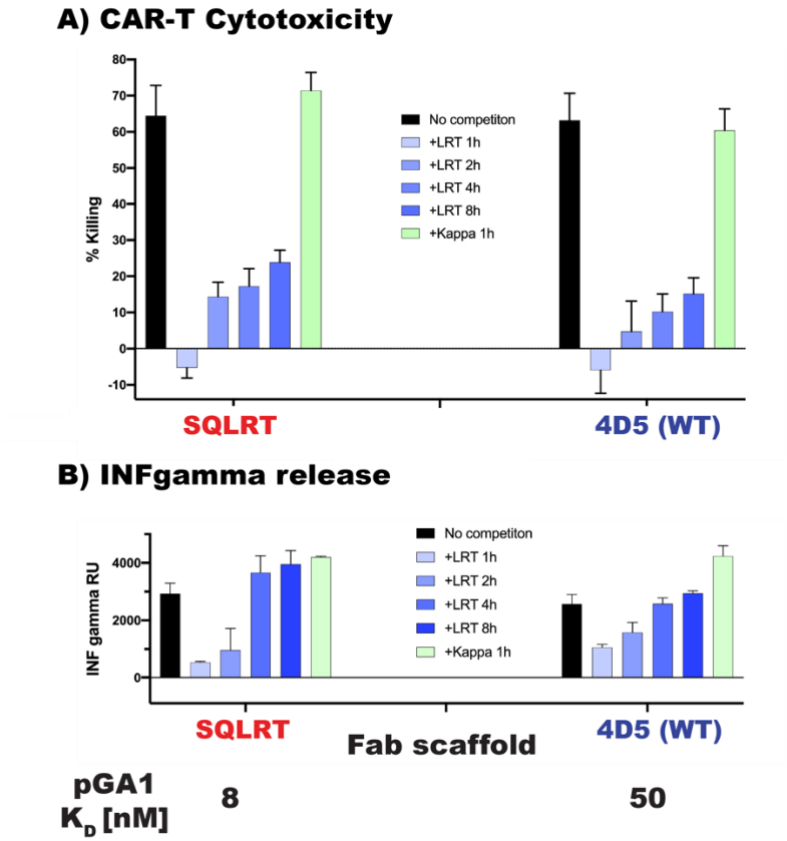

Figure 2.25 CAR-T emergency stop switch. SKBR3 cells were attached to the plate overnight, followed by the next day's addition of the GA1CAR and 100 nM of HER2 Fab in either SQLRT or 4D5 scaffolds. After 24 hours, the cell-killing effect was measured by LDH activity (**A**) and cytokine release (**B**) upon T-cell activation. To test the effect of the emergency stop switch, 1 μM of the Isotype Fab (α- SARS-CoV-2 RBD protein) in the Fab^{LRT} scaffold was added after one, two, four, or eight hours. The same Isotype Fab in the Fab^{H} scaffold was added as a negative control. I observed a reduction of cell killing upon CAR-T detachment from the HER2 Fabs in both SQLRT and 4D5 scaffolds (blue bars) compared to no emergency switch-off (black bar) or control (green bar). However, I did not see a reduction in interferon-gamma release post four hours. The emergency switch efficiency was higher for lower affinity scaffold HER2 Fab (4D5). The experiment was done in triplicate, and the error bars represent the SD value from the mean.

Figure 2.26 CAR-T exhaustion. To test the GA1CAR fatigue, SKBR3 cells were incubated overnight, followed by the plate, CAR-T, and HER2 Fabs addition. The expression of an early T cell activation marker, CD69, was tested using flow cytometry. Unstimulated CAR-T showed no CD69 expression (1), while 24h incubation with CAR-T and HER2 Fab^{S} resulted in a significant CD69 expression (2). Emergency stop switch after one (3) and two hours (4) shows reduced CD69 expression compared to not stopped reaction (2). Her2 in the Fab^{LRT} scaffold was able to reactivate previous CAR-T that was treated with the safety switch (6) to the CD69 expression level comparable to not stopped CAR-T (5).

2.3.6.5 Secondary reagents for antibody binding detection by flow cytometry.

To further develop the protein G platform for another important application for cell biology, I chose to apply it as a secondary detection reagent for flow cytometry. I attached a self-labeling SNAP-tag to PGs to allow for easy and high throughput labeling with different fluorophores, resulting in a very efficient and quick fluorophore attachment. Initially, I used GA1-SNAP labeled with Alexa 647 to detect a conformational specific anti-MBP 7O Fab in the Fab^{LRT} scaffold, binding to a HEK cell line that was engineered to display Maltose Binding Protein (MBP) (Mukherjee et al., 2018). This model system allows for additional experimental control since the conformational change of MBP upon maltose binding results in the elimination of the 7O Fab binding. The high affinity between GA1-Fab^{LRT} allows for simply premixing all reagents prior to the staining protocol. This eliminates an additional washing step and shortening the procedure time. This facilitated detecting a high Alexa 647 signal in a flow cytometry experiment, which was

fully eliminated by spiking in 1 mM maltose. No signal was observed when previously generated isotype Fab^{LRT} against Ebola virus nucleoprotein was used in the experiment (Figure 2.27). Furthermore, the comparison between the commonly used Anti-Human F(ab')2 and GA1 as a secondary reagent exhibit a similar positive signal while using both methods. However, the GA1 had a much lower background signal in the negative controls (Figure 2.28).

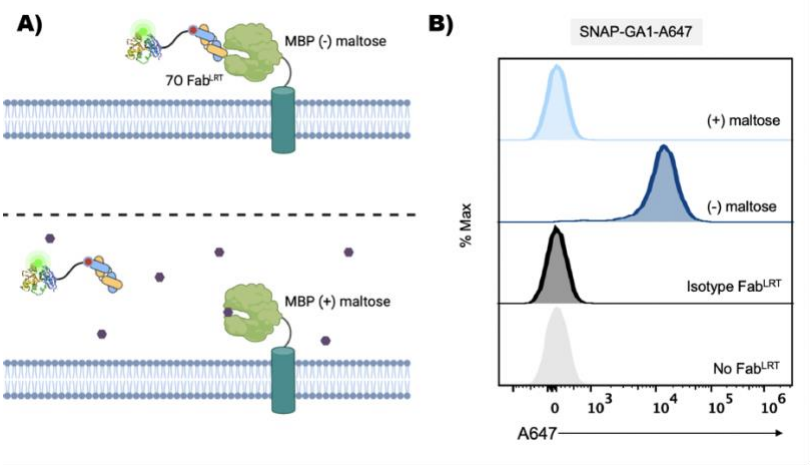

Figure 2.27 Labeled SNAP-protein G as a tool for antibody binding detection by flow cytometry. (**A**) Experimental model. A conformation specific anti-MBP 7O Fab^{LRT} was used to detect the extracellular MBP stably engineered on the surface of the HEK cell line. Conformational change of MBP upon maltose addition eliminates the anti-MBP 7O Fab^{LRT} binding. SNAP-GA1 labeled with Alexa 647 is used for the detection in flow cytometry and is premixed with fab before the cell staining. (**B**) Flow cytometry histogram of anti-MBP 7O Fab^{LRT} binding to HEK cell line stably expressing extracellular MBP without the presence of the maltose. The system exhibits a strong signal with a shallow background. Fab binding is abolished upon maltose addition. As a negative control, the SNAP-GA1 alone and the isotype Fab against Ebola nucleoprotein were used. No detectable signal was observed. The Fab is premixed with SNAP-GA1 before cell staining, significantly shortening the staining protocol.

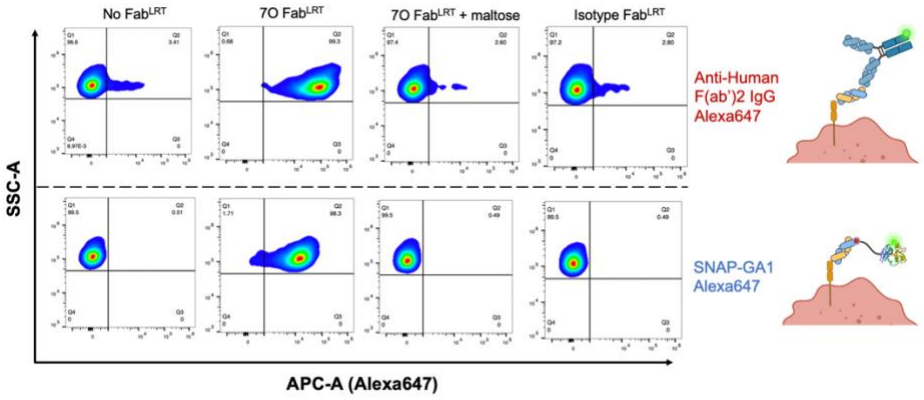

Figure 2.28 Specificity comparison between SNAP-GA1 and commercially available secondary antibody. Flow cytometry comparison of cell surface Fab binding using commercially available Anti-Human F(ab')2 and house-made SNAP-GA1, each labeled with Alexa647. A HEK cell line stably expressing extracellular MBP was used to compare secondary detection of the conformation specific anti-MBP 7O Fab^{LRT}. SNAP-GA1 exhibits a strong signal in the detection of 7O Fab^{LRT} and shows a meager background in the negative controls of no Fab^{LRT}, 7O Fab^{LRT} + maltose, and isotype Fab^{LRT}. Fab can be premixed with SNAP-GA1 before cell staining, significantly shortening the staining protocol.

Next, I asked if orthogonal pairs of protein Gs and Fab scaffold would allow for the co-binding detection of two antibodies that recognize different cell surface targets (Figure 2.29A). SNAP-GA1 and SNAP-GLM were labeled with Alexa 647 and Alexa 488 via SNAP-tag, respectively. As a proof-of-concept, I choose the SKBR3 cell line and two model cell surface receptors, HER2 and EGFR. Before cell staining, SNAP-GA1-A647 and SNAP-GLM-A488 were premixed with anti-EGFR Fab^{LRT} and anti-HER2 Fab^{H}, respectively. The binding of anti-EGFR and anti-HER2 were detected with SNAP-GA1-A647 and SNAP-GLM-A488. At the same time, no co-staining was observed when the control isotype Fabs against Ebola nucleoprotein and MBP in analogous Fab scaffolds were used (Figure 2.29B). Efficient detection of simultaneous binding of EGFR and HER2 fabs was achieved when co-staining was tested (Figure 2.29C). Not surprisingly, the fusion of double SNAP-tag to GA1 significantly improved signal to noise ratio of the system (Figure 2.29D).

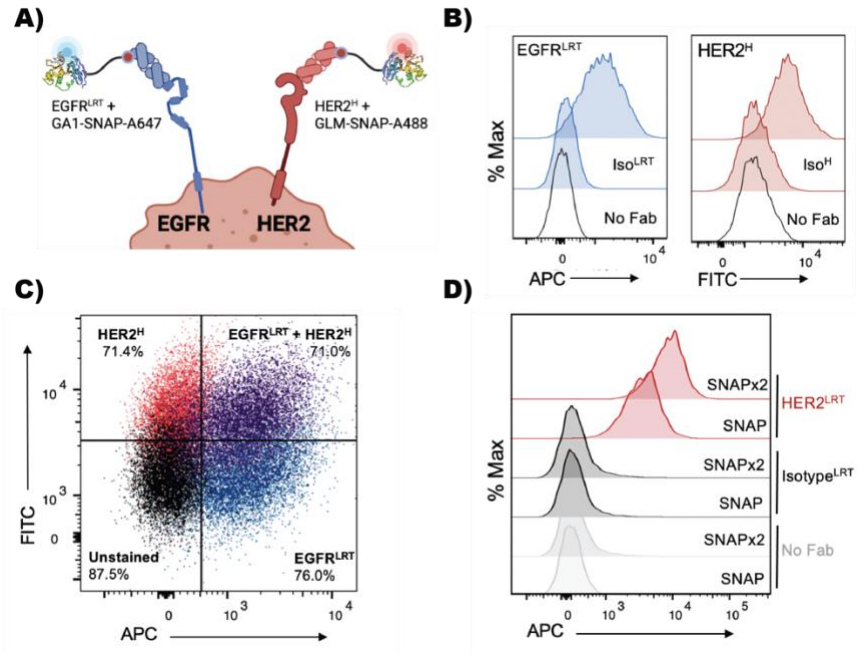

Figure 2.29 Flow cytometry simultaneous binding detection of two different Fabs by the orthogonal pairing of GA1-Fab^{LRT} and GLM-Fab^{H}. (**A**) Model of secondary co-detection using the orthogonal pairing of GA1-Fab^{LRT} and GLM-Fab^{H}. SNAP-GA1 and SNAP-GLM fusions are labeled with benzylguanine- (BG) Alexa 647 and Alexa 488, respectively, and then incubated with Fab^{LRT} and Fab^{H} molecules before addition to cells. Protein GA1 and GLM scaffold specificity allow for the simultaneous detection of the other fab binding on the cell surface. (**B**) Flow cytometry analysis of SKBR3 cell surface receptors. EGFR was detected by an anti-EGFR Fab^{LRT} using SNAP-GA1-A647 as a secondary detection agent (*left*). HER2 was detected by an anti-HER2 Fab^{H} using SNAP-GLM-A488 as a secondary detection agent (*right*). (**C**) Density plot analysis of simultaneous detection of anti-EGFR Fab^{LRT} and anti-HER2 Fab^{H} via flow cytometry using SNAP-GA1-A647 and SNAP-GLM-A488, respectively, as secondary detection agents. The high degree of specificity for each GA1-Fab^{LRT}and GLM-Fab^{H} interaction allows all Fab and secondary detection components to be mixed in one tube before adding to cells. The low background and depleted off-target recognition are demonstrated using Fab^{LRT} and Fab^{H} isotype controls. (**D**) Double SNAP fusion significantly increased the detected signal.

2.3.6.6 Plug-and-play IgG

Using the synthetic library for Fab generation often results in numerous potential hits, which is one of the most significant advantages of the technology. However, it requires time-consuming validation to determine the leading candidate for further development. The cloning and

production of each antibody into a full-length IgG are expensive and have low throughput. On the other hand, producing Fab fragments is an easy, fast, and high-throughput procedure, allowing for the manufacture of many antibodies for initial validation and testing. To speed up and expand the portfolio of validation done with Fab fragment, I decided to engineer a plug-and-play IgG using our protein G platform. This technology is created by linking protein G molecules to IgG Fc fragment to mimic the full-length IgG (Figure 2.30A). Using the replaceable Fab^{LRT}, many Fabs could be tested for their efficiency and functionality to narrow down the potential candidates that would then be produced in full IgG format (Figure 2.30B). I used the ELISA assay to validate the efficiency of plug-and-play IgG. I tested the binding affinity of 7O Fab described earlier (section 2.3.4.5) and the effect on Fab binding to MBP upon the addition of maltose. Not surprisingly, the avidity effect improved the affinity and decreased the effect of maltose when 7O Fab^{LRT} was used in plug-and-play IgG (Figure 2.30C).

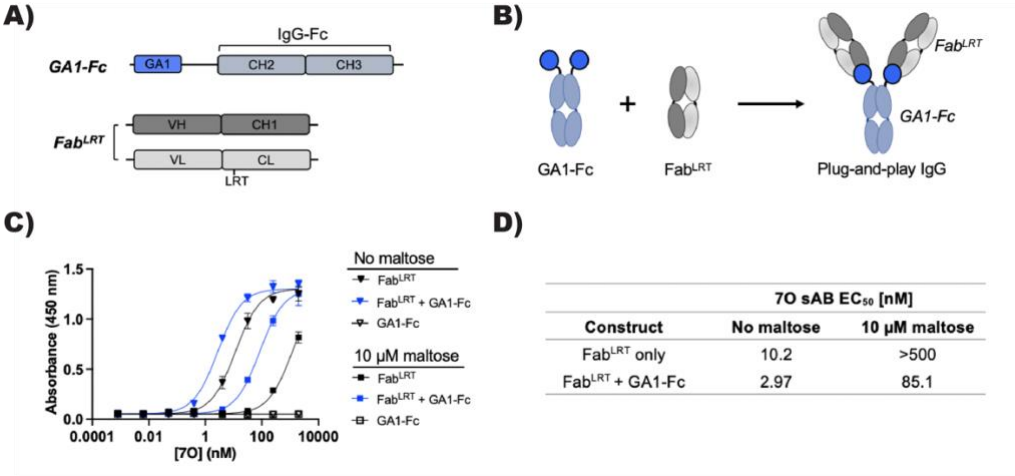

Figure 2.30 GA1-Fc fusion enables modular assembly of bivalent IgG-like sABs. (**A**) Map of constructs used to enable IgG-like assembly between Fab^{LRT} and GA1-Fc fusion. (**B**) Schematic of plug-and-play IgG assembly. (**C**) ELISA EC_{50} analysis of sAB 7O binding to immobilized MBP in the absence of maltose or with 10 µM maltose. In both cases, the IgG-like sAB format improves the 7O EC_{50} value substantially. (**D**) Table of 7O EC_{50} values.

Next, I asked if I could generate a set of plug-and-play IgGs that would facilitate the orthogonal pairs of GA1-Fab^{LRT} and GLM-Fab^{H}, allowing for the co-binding detection of two antibodies. Such technology could be beneficial for detecting low abundant cell surface targets, where the avidity effect could increase the detected signal. To do so, I linked GLM to murine Fc fragment, creating the set of reagents that could be detected using anti-Human Fc or anti-Murine Fc secondary antibody. I performed a similar co-binding experiment using the HCC1954 cell line and two model cell surface receptors, HER2 and EGFR. Anti-Her2 Fab was grafted into Fab^{H}, while a Fab^{LRT} scaffold was introduced into ant-EGFR Fab prior to mixing with GLM-Fc or GA1-Fc, respectively. The binding of anti-Her2 Fab^{H} + GLM-Fc and anti-EGFR Fab^{LRT} + GA1-Fc were detected using anti-murine-Fc-A647 or anti-human-Fc-A488, respectively (Figure 2.31A). As a result, efficient detection of simultaneous binding of EGFR and HER2 plug-and-play IgGs was recorded when co-staining was tested. The controls of Isotype Fabs in each configuration did not produce detectable binding, establishing the system's efficiency (Figure 2.31B).

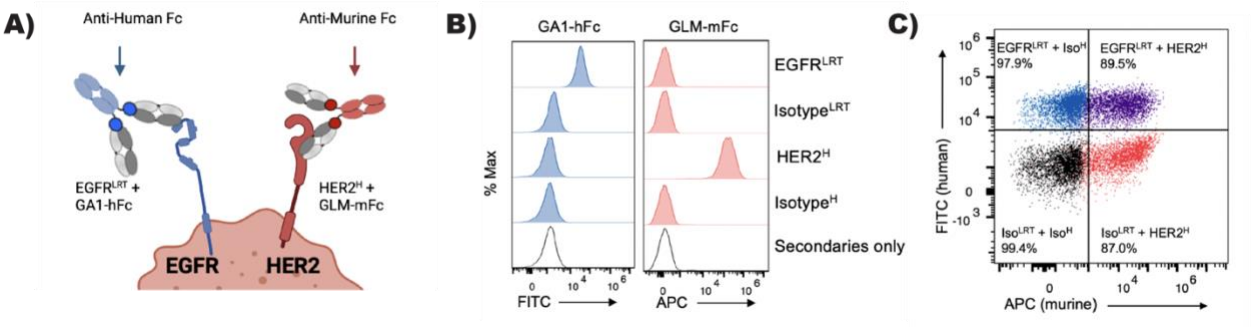

Figure 2.31 Orthogonal pG-Fc fusions enable simultaneous detection of two different sABs binding to the cell surface. (**A**) Model for secondary detection by anti-Fc secondary antibodies that recognize either human IgG1 Fc or murine IgG2a Fc. (**B**) HCC1954 cells were stained with IgG-like sABs targeting EGFR (Fab^{LRT} format) or HER2 (Fab^{H} format). *Left panel*, anti-human-Fc-A488 (FITC) recognizes only the combination of GA1-hFc + EGFR^{LRT}. *Right panel*, anti-murine-Fc-A647 (APC) recognizes only the combination of GLM-mFc + HER2^{H}. (**C**) Simultaneous staining of EGFR and HER2 using the IgG-like assemblies shown in (B).

2.4 Conclusions

I described the engineering of a platform that allows for the coupling of antibodies in multi-valent and multi-specific formats using Protein G. The technology is based on the ability of Protein G to associate with the Fab portion of the IgG in a distal region from the Fab's antigen binding site. I engineered a pair of novel synthetic molecules, GA1-Fab^{LRT}, with a superior binding property and an affinity of 100 pM. Then, I generated a cohort of Protein Gs that have a high affinity to Fab^{H} but do not recognize Fab^{LRT}. Additionally, I engineered a universal Protein G that could be used as a broad antibody purification reagent. The specificity of both variants was examined by structural work, revealing that they have a different hydrogen bond coordination between Fab and Protein G. The Protein G-Fab plug-and-play system was developed to address the limitations of traditional antibody-based reagents. The system was designed to use affinity reagents like Lego blocks to generate the desired outcome using ultra-high affinity protein Gs with their orthogonal Fab scaffolds. The first step was to create a universal, high-efficiency Fab purification resin. The described protein GF was a perfect solution, and the purification resin was sufficient to purify human and mouse kappa Fabs and full-length IgG. The purity of the product was superior compared to the Fab purified using protein A resin, and it did not require the additional ion exchange step. The system was further investigated to detect antigens using the protein G fusions to the split enzyme. The overall success demonstrated that the system had flexibility and potential for broad utilization as a detection assay of antigens with unknown structural information and orientation of the epitopes. The system was tested in a real-life scenario to detect Ebola and Zika viruses. The overall success of the GA1-Fab^{LRT} complementation assay demonstrated the high potential and ability for a quick adaptation to detect new world threats, as shown during the SARS-CoV-2 pandemic (see chapter 3). The system was also used to develop a bi-Fab BiTE construct and CAR-T technology in a plug-and-play format. BiTEs and CAR-Ts aim

to tie and bring together two distinctive cell types, a cytotoxic T-cell and a tumor cell, to initiate the T-cell killing machinery. However, these constructs are designed with specific antigen pairs in mind, which limits their utility. The Protein G-Fab plug-and-play system overcomes this limitation by creating a tool kit that uses affinity reagents mixed to generate the desired outcome. The system offers advantages over traditional antibody-based reagents, such as optimizing specificity and scaffolding by relatively uncomplicated methods. Overall, the Protein G-Fab plug-and-play system offers a flexible, efficient, and rapid approach to developing affinity reagents for various applications. The system has a high potential to revolutionize antibody-based reagents and their applications in biotechnology.

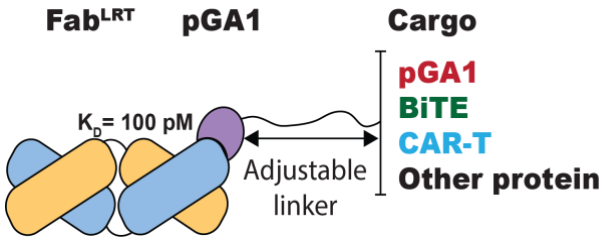

Figure 2.32 Plug-and-play GA1-Fab^{LRT} platform. Model of GA1-Fab^{LRT} platform with some potential applications. Due to a high-affinity GA1-Fab^{LRT} pair, the Fab can be connected to various cargo linked to GA1. Many potential cargos were tested for their efficient coupling to GA1. Tested examples include: another Fab or scFv to generate a bi-specific assembly, another protein, tags, chemical moieties, or even GA1 to mimic the IgG characteristics. The linker length of the construct can be easily modified and optimized.

CHAPTER 3: ENGINEERING ULTRA-HIGH AFFINITY SYNTHETIC ANTIBODIES FOR SARS-COV-2 NEUTRALIZATION AND DETECTION.

*Majority of the chapter has been published: (Slezak and Kossiakoff, 2021)

3.1. Summary

The COVID-19 pandemic caused by the severe acute respiratory syndrome coronavirus 2 has become a global health and economic threat. The principal shortcomings are inadequate infrastructure and the incapability to detect and impede the virus before it spreads through society. The global catastrophe caused by similar events will likely happen in the future. Thus, the development of an easily adaptive technology that could increase our ability to stop the virus at the early stage is highly desirable.

In this chapter, I describe the generation of a cohort of ultra-high affinity Fabs that recognize SARS-CoV-2 and can be used as a potent inhibitor of viral entry into human cells. Additionally, these Fabs were used, as described in chapter 2, a β-lactamase complementation-based assay that was optimized into a point of care (POC) assay for SARS-CoV-2 detection.

3.2. Introduction

3.2.1. SARS-CoV-2 and the molecular mechanism of the viral infection.

The Coronavirus Disease 2019 (COVID-19) is a highly contagious, novel severe acute respiratory syndrome coronavirus 2 (SARS-CoV-2) (Zhu et al., 2020). In 2020, it led to a global pandemic that continues to present a health and economic catastrophe. SARS-CoV-2 is a member

of the β coronavirus family, which contains seven known viruses that infect humans. Four of these coronaviruses cause the common cold and are generally non-lethal. On the other hand, the remaining three, namely SARS-CoV, MERS-CoV, and SARS-CoV-2, are capable of causing severe symptoms with a high fatality rate (even up to 37% for the MERS-CoV) (Wang et al., 2020). SARS-CoV-2 is an enveloped virus with a single-stranded RNA genome that encodes 9860 amino acids. The genome encodes for both structural and nonstructural proteins. The structural proteins contain only four molecules: proteins S, E, M, and N. In contrast, the number of nonstructural proteins is not fixed, as some of the proteins can be translated in different forms due to post-translational modifications or alternative splicing. The main nonstructural proteins include 3-chymotrypsin-like protease, papain-like protease, and RNA-dependent RNA polymerase (Bai et al., 2022).

The basic architecture of SARS-CoV-2 contains an abundance of the highly glycosylated Spike protein scattered across the virus's surface. The spike protein is an essential component responsible for binding to the host cell receptor angiotensin-converting enzyme 2 (ACE2), followed by the membrane fusion facilitated by the conformational changes of the spike protein leading to the viral entry into the host cell (Earp et al., 2005; Letko et al., 2020). The spike protein forms a 700 kDa, trimeric complex, that is extensively glycosylated to avoid the recognition from the host immune system (Watanabe et al., 2020). The prefusion conformation of a spike protein contains two distinct states differing by the degree of availability of the receptor binding domain (RBD) that binds to the ACE2 receptor. The two states described are known as the "down" and "up" conformation. The down conformation denotes the state where the receptor is inaccessible. In contrast, the up conformation corresponds to the state where the receptor is exposed and thus accessible for interaction with ACE2 (Wrapp et al., 2020; Yan et al., 2020) (Figure 3.1). Because

of the essential function of the spike protein for viral entry, it is a commonly used target for therapeutic generation, such as neutralizing antibodies and vaccines. Therefore, I generated ultra-high affinity antibodies targeting Spike protein's RBD domain. The binding epitope of engineered Fabs overlap with the ACE2 binding site on the RBD and thus provides adequate protection from viral entry into the host cell.

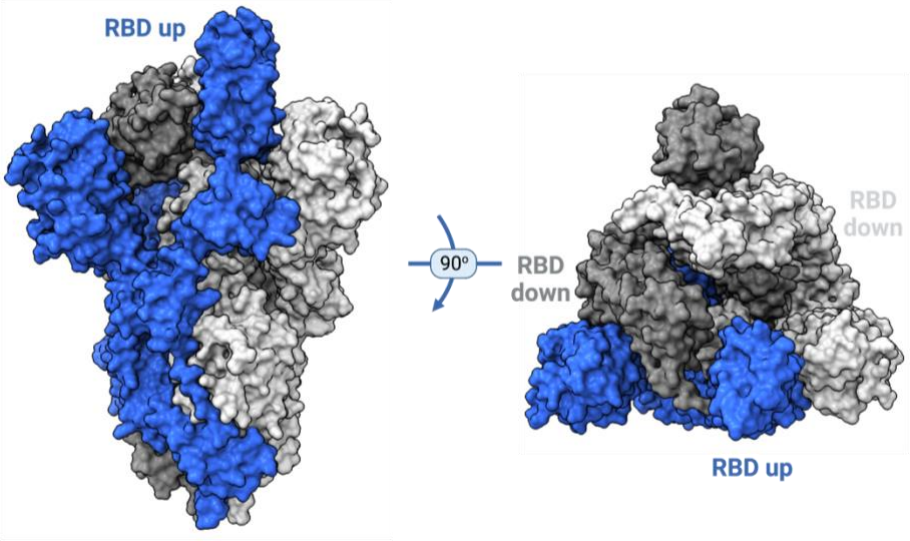

Figure 3.1 SARS-CoV-2 Spike protein. The cryoEM structure of a trimeric Spike protein from SARS-CoV-2 in a side and a top view. Prefusion S protein contains a single RBD domain in the up conformation, while the remaining two are in the down conformation. Spike protein binds to the human ACE2 receptor with opened RBD domain. Figure created from pdb: 6VSB.

3.2.2 SARS-CoV-2 detection

The lack of methods and reagents at the pandemic's start muted the proper response and a high-thruput identification of infected individuals. Initially, SARS-CoV-2 detection was carried out exclusively in laboratories using nucleic acid-based assays that require the application of polymerase chain reaction (PCR) (Udugama et al., 2020). Despite their high reliability, these methods have a slow turnaround time and could be more practical for large-scale testing. The rapid

spread of new infections like SARS-CoV-2 throughout populations made it nearly impossible to respond effectively in real-time when detecting requires well-established facility and trained personnel. Moreover, many asymptomatic cases fail effective diagnosis and isolation of contagious patients. Thus, there was an urgent need to develop easy and reliable point-of-care approaches to detect low levels of viral proteins without requiring sophisticated facilities and instrumentation. The POC is characterized by the technology the patient can easily approach and would provide quantitative or semi-quantitative results in a short time (up to 30 minutes) (Luppa et al., 2011). This type of testing allows for an efficient and regular population screening, which leads to the isolation of infected individuals and the reduction of the viral spread.

The majority of POC assays utilize ELISA formats for detection readouts. However, the detection assay described in this study employs a split-enzyme complementation readout, which provides significantly higher signal-to-noise discrimination than conventional ELISA methods. This complementation assay employs a split enzyme based on the reconstitution of two fragments of β-lactamase to produce a fluorogenic signal. It is a variant of a traditional sandwich assay. The N and C-terminal fragments of β-lactamase are separately attached to different Fabs that recognize distinct epitopes and can, therefore, simultaneously bind to the RBD target. Moreover, the complementation constructs containing the enzyme fragments are designed to be modular, allowing for the easy interchange of Fabs generated for other virus targets in a plug-and-play fashion. For example, by simply adding appropriate Fabs for the target of interest, the same system was used for Ebola and Zika antigens detection, as described in chapter 2. As a result, the assay can be quickly adapted, requiring only the generation of Fabs for the desired target antigen. Additionally, our POC detection assay has several other features, including the ability to be packaged in a kit that can be stored and rapidly activated without sacrificing sensitivity.

3.3. Results and Discussion

3.3.1. Generation of synthetic antibodies recognizing SARS-CoV-2 RBD.

Our motivation when initiating this project was to develop a group of high-performance antibodies that could be used for sensitive viral detection and neutralization to be further transformed into a potential therapeutic. Such molecules have to be characterized by several benchmarks. To be a suitable neutralization reagent, the epitope had to be shared with the ACE2 binding site on the SARS-CoV-2 receptor binding domain (RBD). The affinity must be greater than the RBD-ACE2 interaction with a prolonged dissociation rate. Moreover, as described in chapter 2, a split-enzyme detection assay requires a set of antibodies that recognize RBD through the independent epitopes. The phage display mutagenesis campaign was done using RBD expressed in mammalian cells to preserve its high glycosylation. As described previously, our pipeline requires a biotinylated target to facilitate immobilization onto streptavidin-coated paramagnetic beads.

Taking the high level of RBD glycosylation, I used EZ-Link Hydrazide Biotins (Thermo) to biotinylate through its carbohydrate groups. To obtain high-affinity binders, the five rounds of selection with a high-diversity library were performed. The target concentration was systematically reduced, starting from 500 nM in the first round to 1 nM in the last. To achieve the strict requirement of a slow dissociation rate, the additional selection pressure with longer washes during the biopanning was applied. After the third and fourth rounds, the phage particle enrichment was evaluated. Enrichment compares the number of target-specific particles to the background isolated after a consecutive round (Paduch et al., 2013). I could observe a significant enrichment in phage particles in both the third and fourth rounds (Figure 3.2A), indicating that the selection was successful. To validate the specificity of the selected antibodies, a phage ELISA was

performed on 192 clones resulting in 5 unique binders named RBD1- RBD5. All Fabs showed a very high affinity, with RBD1 being the best candidate (Figure 3.2B).

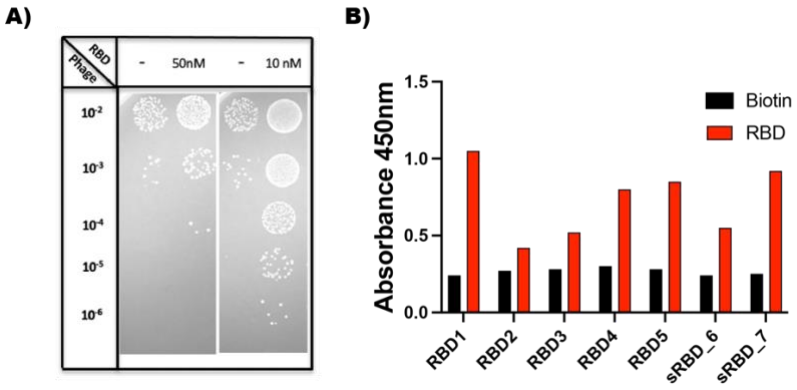

Figure 3.2 Phage specificity characterization. (**A**) Enrichment of phage clones after the RBD selection. Positive enrichment in a number of phage particles eluted from the third and fourth rounds can be observed. The number of RBD-specific phage particles is more significant than those eluted from the empty paramagnetic beads (-). (**B**) Single-point phage ELISA of the RBD binders selected by phage display. Clones with strong signals against RBD were chosen for further sequencing and characterization. All Fabs showed specific binding to RBD compared to the Biotin control.

A crucial component of a protein complementation assay introduced in chapter 2 is a high-affinity antibody couple that recognizes non-overlapping epitopes. The extensive glycosylation of a small-size RBD reduces potential epitopes and for simultaneous binding of two Fabs. I performed an epitope masking selection to address this challenging task and have high-affinity RBD1 Fabs. To ensure second epitope binders, I added 1 μM RBD1 Fab as a competitor in every selection round (Paduch et al., 2013). Five rounds of the library screening were performed, with the antigen concentration gradually reduced from 200 nM in the first round to 1 nM in round five. Identical to the previous selection, the additional longer washes were introduced into the protocol to ensure a

low dissociation constant of the selected Fabs. The phage ELISA indicated the positive clones that were then sequenced. Third resulted in two new Fabs: sRBD6 and sRBD7 (Figure 3.2B) and the previously selected RBD5, implying that this Fab had an independent epitope than RBD1 Fab (Figure 3.2). Based on the ELISA data, I choose sRBD7 to proceed alongside RBD1 for the complementation assay development.

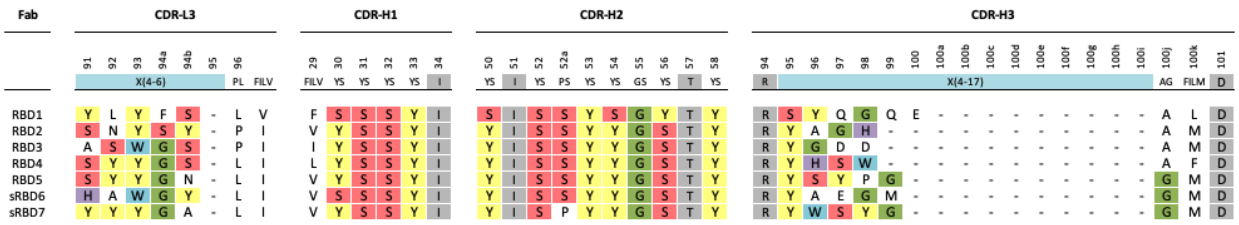

Figure 3.3 Sequences of unique Fabs generated against SARS-CoV-2 RBD. Seven unique Fabs were identified. Abnormally, all selected antibodies were characterized by a very short CDR-H3. Amino acids randomization in CDR-L3, H1, H2, and H3 of Library E are shown on the top. Selected amino acids are color-coded as follows: serine (S) – red, glycine (G) – green, tyrosine (Y) – yellow, tryptophan (W) – blue, positively charged amino acids (R, K, H) – violet, other amino acids – white, conserved amino acids – grey.

I then used SPR to confirm a high affinity of the RBD1 and sRBD7. A similar K_D of ~3 nM characterizes the binding affinities of both Fabs. However, the kinetics of the interactions were very different. The dissociation rate for sRBD7 is an order of magnitude slower than RBD1 (Figure 3.4). Since the success of the detection assay relies on the non-overlapping epitopes, I performed an epitope binning experiment by SPR. Epitope binning is an experiment where the immediate injection of the second Fab follows the injection of another Fab over the immobilized target.

Taking the high sensitivity of the SPR, the increase of response units (RU) upon the injection of the second Fab indicates binding to separate epitopes on the target. The experiment confirmed that RBD1 and sRBD7 bind to two distinct epitopes on the RBD since I could observe an increase of RU corresponding to the size of the Fab when sRBD7 is injected after saturating the target with the RBD1 Fab (Figure 3.4D).

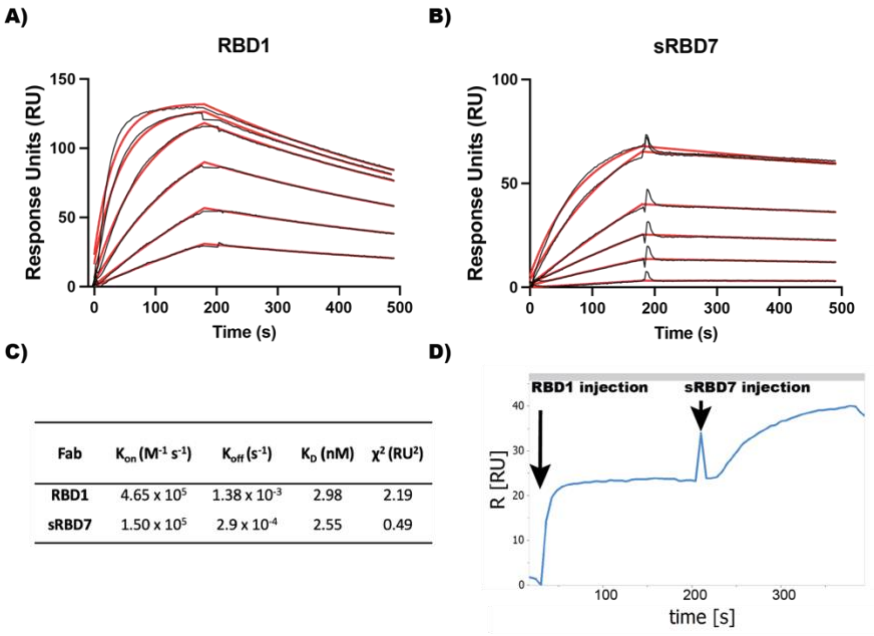

Fab	K_{on} (M^{-1} s^{-1})	K_{off} (s^{-1})	K_D (nM)	χ^2 (RU^2)
RBD1	4.65×10^5	1.38×10^{-3}	2.98	2.19
sRBD7	1.50×10^5	2.9×10^{-4}	2.55	0.49

Figure 3.4 Characterization of Fab binding against RBD. (**A**) SPR sensogram showing the fast on-fast off kinetics between RBD1 and RBD. (**B**) SPR sensogram showing slower association and slower dissociation between RBD7 and RBD. (**C**) Kinetic parameters of binding. The concentration of Fab was serially diluted two-fold for each run starting at 200 nM. (**D**) Epitope binning of RBD1 and sRBD7. The increase of RU upon sRBD7 injection indicates binding to two separate epitopes on the SARS-CoV-2 RBD.

3.3.2. Affinity maturation of RBD1 Fab.

The RBD1 Fab possesses a high affinity with reasonable kinetics; however, the complementation and neutralization assays require a superior dissociation rate. Thus, I initiated an affinity maturation to improve the RBD1 further. The library E (Fellouse et al., 2007) used to generate the initial antibodies has a relatively low diversity in CDR-H1 and CDR-H2. The lack of structural insight and direct evidence of these CDRs engagement with the antigen made the choice of CDR-H1 somewhat subjective. However, most of the Fab-antigen structures obtained in the Kossiakoff Lab show that the heavy chain CDRs have a higher propensity to be involved with antigen binding than light chain CDRs. Based on this, I designed and constructed a phage display library that introduces greater variety in CDR-H1 using a combination of "tailored" and "hard" randomization strategies incorporated into all six CDR-H1 positions. Two RBD1 phage sublibraries were generated, wherein in the first library, all possible amino acids were incorporated. The second library was biased to hydrophobic and aromatic amino acids. Since the RBD1 possess high affinity, the biopanning campaign contained three rounds, with the RBD concentration decreasing accordingly, from 10 nM in the first round to 20 pM in the third round. Additional selection pressure with four consecutive 30-minute washing steps was incorporated to ensure the improvement of the off-rate. Phage enrichment was evaluated after each round and is pattern showed the success of the campaign (Figure 3.5A). After the last round, 96 colonies were sequenced and tested in phage ELISA, resulting in 19 unique Fabs: mRBD1.1- mRBD1.19 (Figure 3.5B).

Sequence alignment showed very limited randomization in the 1, 5, and sixth positions of the CDR-H1, suggesting the importance of RBD recognition. The high diversity at positions 2, 3, and 4, with the preference for Histidine at position 2, was observed (Figure 3.5C). I used SPR to

confirm the dissociation rate improvement of the mRBD1 Fabs. The analysis showed 10 to 100-fold affinity enhancement due to slower dissociation than RBD1. The most promising variant, mRBD1.5, had both association and dissociation rates improved by two orders of magnitude resulting in an overall K_D of 42 pM (Figure 3.6, Table 3.1).

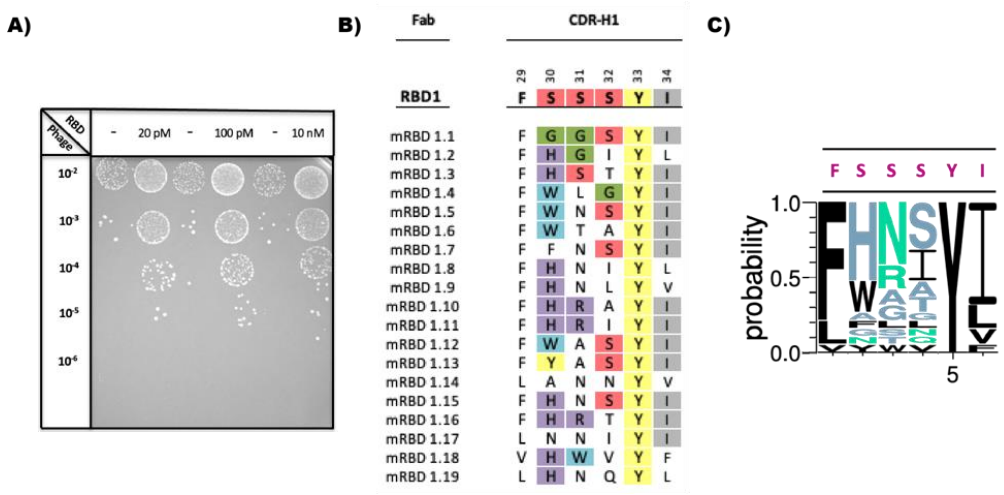

Figure 3.5 RBD1 affinity maturation evaluation. (**A**) Enrichment of phage clones after the RBD1 affinity maturation. Positive enrichment was observed in all rounds of affinity maturation, indicating the improvement of the RBD1 affinity. (**B**) Sequences of unique Fabs generated after the RBD1 affinity maturation. Selected amino acids are color-coded as follows: serine (S) – red, glycine (G) – green, tyrosine (Y) – yellow, tryptophan (W) – blue, positively charged amino acids (R, K, H) – blue, other amino acids – white, conserved amino acids – grey. (**C**) WebLogo plot showing the sequence variants of the affinity-matured CDR-H1 variants. The original sequence is presented in red.

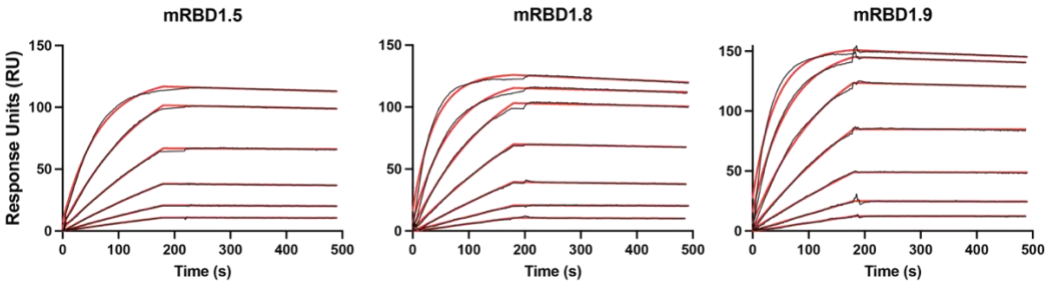

Figure 3.6 SPR kinetics of selected affinity matured RBD1 Fabs. SPR sensogram of selected Fabs: mRBD1.5, mRBD1.8, and mRBD1.9, showing the improved slow-dissociation rate. The concentration of the Fab was serially diluted 2-fold, starting at 25 nM. The affinities of all variants are presented in Table 3.1.

Fab	K_{on} (M^{-1} s^{-1})	K_{off} (s^{-1})	K_D (nM)
mRBD1.1	5.70×10^{5}	3.05×10^{-4}	0.54
mRBD1.2	9.62×10^{5}	2.69×10^{-4}	0.28
mRBD1.3	7.92×10^{5}	3.57×10^{-4}	0.45
mRBD1.4	8.90×10^{5}	2.29×10^{-4}	0.26
mRBD1.5	7.11×10^{5}	2.98×10^{-5}	0.04
mRBD1.6	3.91×10^{5}	1.33×10^{-4}	0.34
mRBD1.7	1.39×10^{6}	1.72×10^{-4}	0.12
mRBD1.8	6.47×10^{5}	7.23×10^{-5}	0.12
mRBD1.9	7.05×10^{5}	5.00×10^{-5}	0.07
mRBD1.10	1.38×10^{6}	2.75×10^{-4}	0.02
mRBD1.11	9.03×10^{5}	5.23×10^{-4}	0.56
mRBD1.12	9.49×10^{5}	2.92×10^{-4}	0.31
mRBD1.13	7.86×10^{5}	3.34×10^{-4}	0.46
mRBD1.14	5.21×10^{5}	3.62×10^{-4}	0.69
mRBD1.15	1.07×10^{6}	1.14×10^{-4}	0.11
mRBD1.16	1.12×10^{6}	2.47×10^{-4}	0.22
mRBD1.17	5.84×10^{5}	1.07×10^{-4}	0.18
mRBD1.18	1.26×10^{6}	3.54×10^{-4}	0.27
mRBD1.19	7.02×10^{5}	1.27×10^{-4}	0.18

Table 3.1 RBD1 affinity maturation results.

3.3.3. SARS-CoV-2 detection using GA1-Fab^{LRT} β-lactamase complementation-based assay.

Previously described in chapter 2, plug-and-play β-lactamase complementation assay was a suitable system for the POC application. SARS-CoV-2 Fabs mRBD1.5 and sRBD7 were grafted into Fab^{LRT} scaffold, which allowed us to generate the pair of RBD1-BLF2 and sRBD7-BLF1 by simply premixing them separately with appropriate GA1-BLF fragment to a final concentration of 250 nM. Since we had no firm idea about the Fabs' epitope positions on the RBD, I decided to use a 15 residue Gly-Ser (GGGGS)3 linker between the GA1 and BLF fragments (Figure 3.7A). The RBD concentration was systematically increased, resulting in a detectable fluorescent signal at 7 nM, which increased linearly with a maximum at 60 nM. The signal decreased with excess of RBD, presumably due to a hook effect at high concentration of antigen (Figure 3.7B).

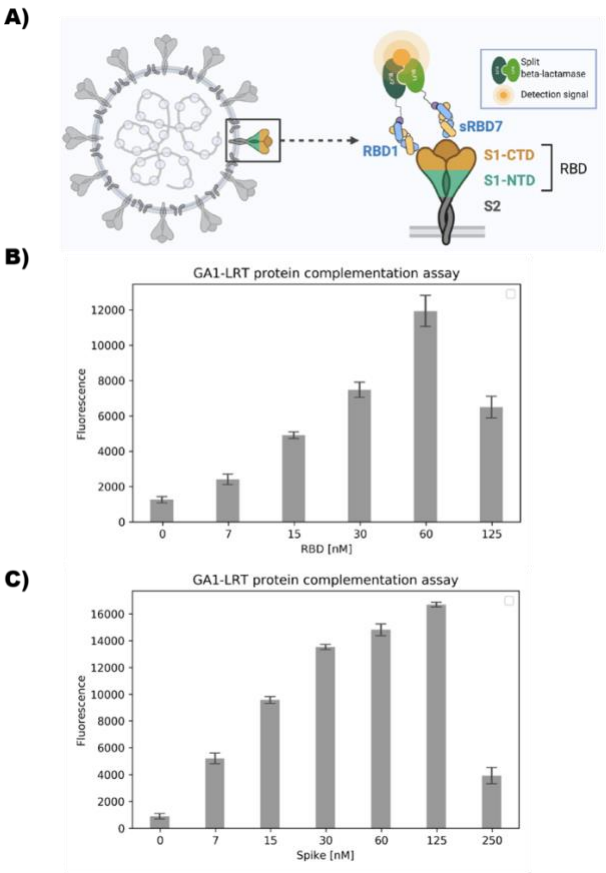

Figure 3.7 GA1-Fab^{LRT} complementation assay. (**A**) Model of SARS-Cov-2 detection using GA1-Fab^{LRT} β-lactamase complementation assay. Two fragments of β-lactamase enzyme are attached to two different Fabs via the plug-and-play GA1- Fab^{LRT} platform. BL activity is reconstituted when both Fabs bind to the RBD. (**B**) Detection of RBD at different concentrations using sRBD7/GA1-BLF2 and mRBD 1.5/GA1-BLF1 as complementary parts. The detectable signal was observed from 7 to 125 nM, with the characteristic hook effect occurring at the higher concentration. (**C**) Detection of SARS-CoV-2 in the context of full-length S-protein using complementary parts: sRBD7/GA1-BLF1 and RBD1/GA1-BLF2. The detectable signal was observed from 7 to 125 nM, identical to the RBD domain detection using affinity maturated mRBD 1.5 Fab. At higher concentrations, the hook effect was observed. The reaction was incubated for 20 minutes at room temperature. Error bars display the SD value from the mean.

The successful SARS-CoV-2 detection using our platform provided the proof of concept for developing a sensitive POC test. Such an assay requires the ability to preserve the functionality of the components upon reconstitution from a lyophilized form. To establish the viability of this

approach, the separate components of our assay, RBD1-BLF2, and sRBD7-BLF1, were freeze-dried at 500 nM concentration overnight. Upon reconstitution, the components' binding properties were unaffected. (Figure 3.8A). They performed equally well in the GA1-Fab^{LRT} β-lactamase complementation assay when they were supplemented with a protein carrier (BSA) as a part of the lyophilization procedure. The absence of BSA supplementation resulted in a 40% signal reduction (Figure 3.8B).

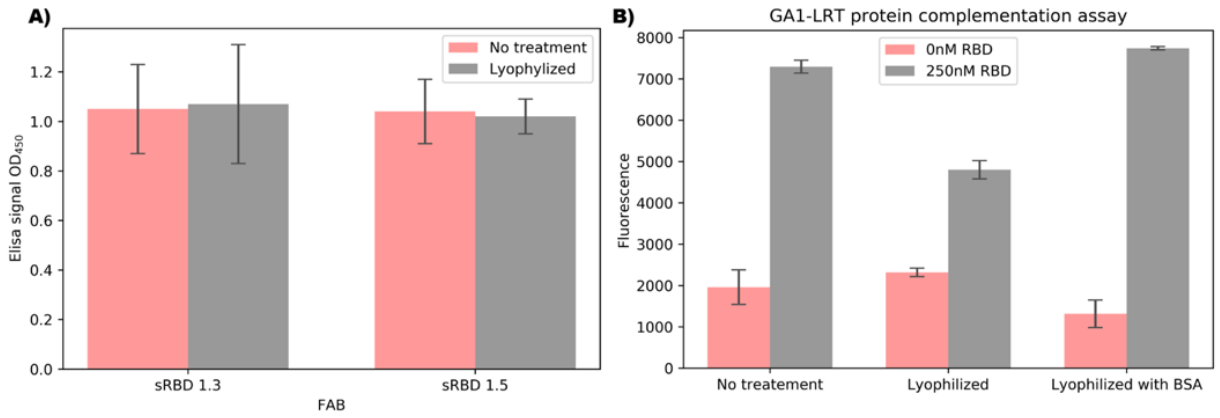

Figure 3.8 Post-lyophilization stability of a GA1-Fab^{LRT} *β*-lactamase complementation assay. (**A**) Single-point ELISA of Fabs after reconstitution from lyophilization. No difference in binding was observed. Error bars represent the SD value from the mean. (**B**) SARS-CoV-2 detection using GA1-Fab^{LRT} protein complementation assay after reconstitution from lyophilization. No difference was observed when lyophilization was done with BSA. 40% signal reduction was observed when samples were freeze-dried in PBS but without BSA. The reaction was incubated for 20 minutes at room temperature. Error bars represent the SD value from the mean.

3.3.4. Antibody mediated SARS-CoV-2 neutralization.

When this project was initiated, there was an urgent need to develop a potent anti-viral therapy. The high affinity of our antibodies and a long lifetime in the bloodstream makes them an excellent candidate to stop the virus's spread. To block the viral entry into the host cell, the antibody must recognize the identical surface area Spike protein uses to interact with the ACE2 receptor in human cells (Yan et al., 2020). I used a single-point ELISA to determine the direct epitope competition with ACE2. The 100 nM ACE2 competition challenged the antibody binding to RBD. As a result, I identified the shared binding site between RBD1 and ACE2. Unsurprisingly, sRBD7 possesses a different epitope that is unaffected by the ACE2 addition (Figure 3.9).

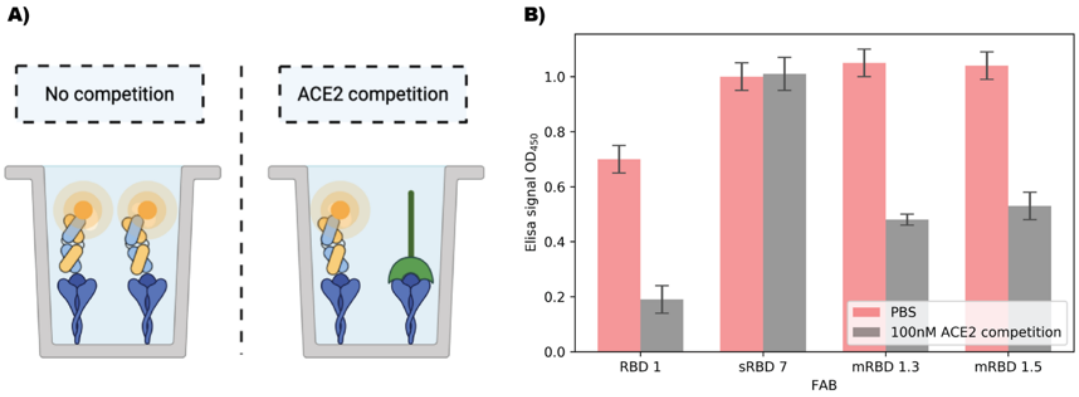

Figure 3.9 Single-point ELISA with ACE2 competition. RBD was immobilized on a high binding plate, and the Fabs' binding was evaluated with and without 100 nM ACE2 competition. The decrease in the detected signal confirms the overlapping epitope with the RBD-ACE2 interface. (**A**) ELISA competition model. (**B**) Single-point ELISA. Results show the competition for a binding site between RBD1 and ACE2. The level of ACE2 competition decreased for affinity-matured variants mRBD1.3 and mRBD1.5. Error bars represent the SD value from the mean.

To determine the potential in virus neutralization, I performed a plaque reduction assay that measured the human cell survival upon the Fab addition. This is a gold standard assay to determine the SARS-CoV-2 neutralization potency (Wu et al., 2020). Consistently with the previous results, RBD1 showed a dose-dependent virus neutralization with an IC_{50} of 4.8 nM, while sRBD7 showed no capability to block viral entry (Figure 3.10B). Moreover, the bivalency of full-length IgG should further increase the neutralization capacity of RBD1. To test that, I took an alternative approach to dimerize RBD1 by using GA1 dimer connected by a 52 Gly-Ser linker and two RBD1 grafted into Fab^{LRT}. This improved the viral neutralization by 2.5 times (IC_{50}= 1.9 nM) (Figure 3.10C). Finally, the affinity-matured variant mRBD1.15 had over ten times improved neutralization capabilities (IC50= 0.48 nM) in a monovalent form (Figure 3.10D).

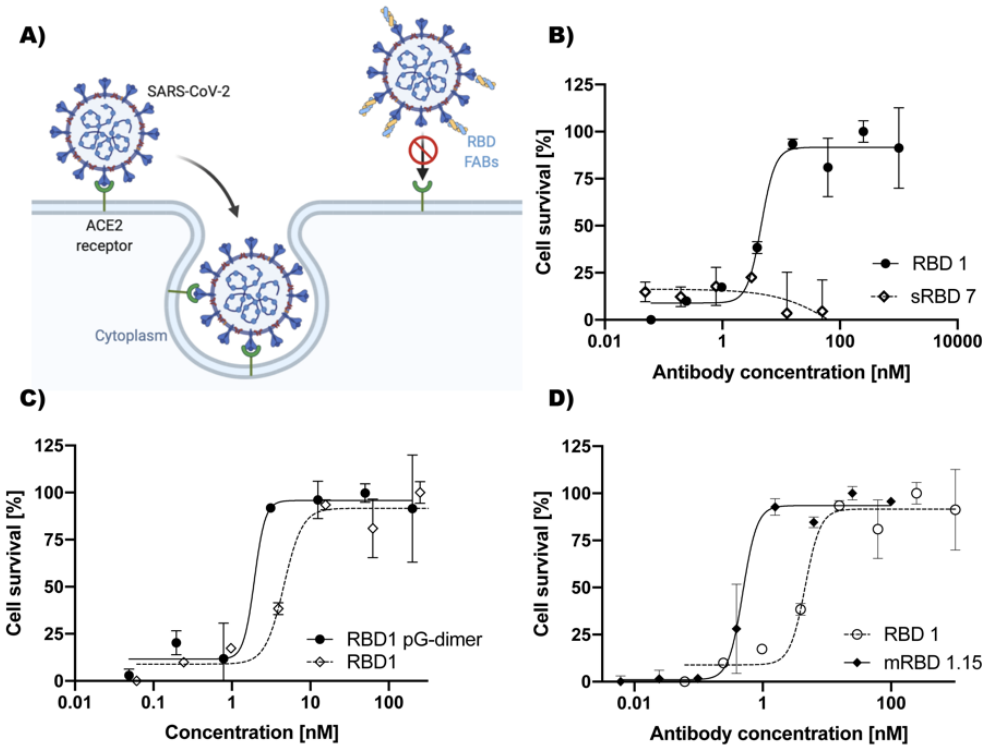

Figure 3.10 Antibody mediated SARS-CoV-2 neutralization. (**A**) Model of neutralization mechanism. RBD1 Fabs block the SARS-CoV-2 Spike protein interaction with human ACE2 receptors on the cell surface. (**B**) Different concentrations of the RBD1 and RBD7 Fabs achieve protection from cell death. The neutralization IC50 value for RBD1 is 4.8 nM. No efficient neutralization with RBD7 was observed. (**C**) Virus neutralization improved over 2.5-fold by RBD1 dimerization using the plug-and-play GA1-FabLRT platform. IC50 neutralization for the dimerized RBD1 is 1.9 nM. (**D**) Improvement in SARS-CoV-2 neutralization. IC50 of mRBD1.15 was 10-fold improved with a value of 0.48 nM.

3.4 Conclusions

The 2019 SARS-CoV-2 outbreak has caused a global pandemic, prompting research into developing antibodies against various SARS-CoV-2 proteins for effective treatment and diagnosis of viral infection. This article outlines the creation of a set of Fabs using phage display mutagenesis, which demonstrated the ability to block viral entry into human cells and can be applied in a sensitive SARS-CoV-2 detection assay. The receptor binding domain (RBD) of the

S1 subunit of the spike protein (S-protein) was targeted since it is mainly available on the virus surface as a homo-trimeric assembly, a hypothetically effective target for affinity reagents like antibodies. However, the extensive glycosylation of the S-protein poses a challenge in developing antibodies to the RBD. The phage display campaign resulted in antibodies binding to two non-overlapping epitopes. The first epitope was recognized by four Fabs, with RBD1 having superior properties and an affinity of ~ 3 nM. RBD1 was converted into a bivalent format, which improved its neutralization potency by 2.5-folds. Affinity maturation biopanning was performed to improve the affinity further, resulting in 19 unique RBD1 variants, with the best variant, mRBD 1.5, having over 100-fold affinity improvement over the original RBD1. A plaque reduction assay was performed with mRBD 1.15 to establish that higher affinity translates into more efficient neutralization. It showed a 10-fold improved inhibitory activity than the parental RBD1.

Finally, our primary goal was to develop a point-of-care assay that could help limit viral proliferation across populations. Such test and all its reagents must be stable upon packaging, shelf storage, and reconstitution upon rehydration. To accomplish this task, I tested the Fabs and GA1-BLF's stability and functionality upon lyophilization and rehydration. Results showed that components are not affected by the procedure and behave identically as their non-lyophilized counterparts, allowing for the production of an easy, stable, and readily usable kit.

CHAPTER 4: THE COLLABORATIVE PORTFOLIO OF ANTIBODY-BASED REAGENTS FOR BIOLOGICAL AND STRUCTURAL STUDIES

4.1 Summary

Antibody-based reagents have a broad spectrum of applications and can facilitate or improve structural studies by cryoEM and X-ray crystallography. These attributes make Fab an important tool that impacts the efforts and direction of many projects. Our expertise in antibody-Fab development using phage display resulted in my participation in numerous collaborations (Table 4.1). While each had a different scientific question in mind; however, all include the generation of reagents in Fab or IgG formats. My responsibilities depended on the project, but generally included target protein preparation, phage display biopanning, primary validation, cloning, and secondary validation, as described in chapter 1. These efforts resulted in the generation of 575 synthetic antibodies (sABs) against 45 targets (Table 4.1). Most of these projects are still in progress, and thus far, they have resulted in one publication (Rohaim et al., 2022) and two patent applications.

			Antigen concentration in subsequent sorting rounds (nM)					
	Antigen	**Collaborator (Lab)**	**1st**	**2nd**	**3rd**	**4th**	**5th**	**Unique sABs**
1	HLA-F	Adams	1000	500	200	50	20	12
2	pHLA-F	Adams	1000	500	200	50	20	15
3	HLA-B.73	Adams	500	250	100	50	10	11
4	3A1	Adams	500	200	50	20	10	2
5	2A1	Adams	1000	200	50	20	10	15
6	NT1	Adams	1000	200	50	20	10	6
7	NT3	Adams	500	200	50	20	10	6
8	MR1	Adams	500	200	50	20	10	5
9	pMR1	Adams	500	200	50	20	10	12
10	XNC4	Adams	1000	200	50	10	-	19
11	TCR_δ9Δ2	Adams	500	200	50	10	2	8
12	hGPR126+ss	Arac	500	200	100	50	20	7
13	hGPR126-ss	Arac	500	200	100	50	20	28
14	zfGPR126+ss	Arac	500	200	50	20	10	29
15	zfGPR126-ss	Arac	500	200	50	20	10	47
16	cDIP	Ozkan	1000	200	50	20	10	12
17	CV	Ozkan	1000	200	50	20	-	8
18	SOG	Ozkan	1000	200	50	20	-	27
19	Calprotectin	Dickinson	500	200	50	20	10	18
20	Bach1	Rosner	1000	200	50	20	10	1
21	Laminin	Hubbell	1000	200	50	20	10	35
22	LSECtin	Hubbell	1000	300	150	75	20	11

Table 4.1 Summary of collaborations.

23	RBD	Tay	1000	200	50	20	10	2
24	Artemin	Weichselbaum	500	200	200	100	50/20	4
25	NNMT	Lengyel	1000	200	50	10	5/2	8
26	SC-4	Crosson	1000	200	50	20	10	5
27	LovK	Crosson	1000	200	50	20	10	8
28	Bab2	Crosson	1000	200	50	20	10	8
29	KCSA	Roux	-	-	-	-	-	1
30	CUX1	McNerney	1000	200	50	20	10	17
31	SeHAS	Zimmer	1000	200	50	20	10	17
32	NSP1	Joachimiak	1000	200	50	20	10	10
33	RNAbd	Joachimiak	1000	200	50	20	10	10
34	ADRP	Joachimiak	1000	200	50	20	10	2
35	NSP8	Joachimiak	1000	200	50	20	10	11
36	HSCUDV53	Joachimiak	500	200	100	50	20	1
37	NSP12/NSP8	Joachimiak	1000	200	50	20	10	9
38	NSP13	Joachimiak	1000	200	50	20	10	4
39	NSP16	Joachimiak	1000	200	50	20	10	8
40	hHv1	Perozo	1000	200	50	20	-	4
41	Survivin 2B	Kossiakoff	500	250	125	60	30	65
42	Survivin dEx3	Kossiakoff	500	250	125	60	30	14
43	SNAP	Kossiakoff	1000	200	50	10	1	9
44	FRB	Kossiakoff	500	200	50	10	-	7
45	NC3Z	Guo	1000	200	50	20	10	11
46	SHP-2	Kern	1000	200	50	20	10	15
							Total	**584**

Table 4.1 continued.

CHAPTER 5: CLOSING REMARKS

My research focused on developing powerful plug-and-play reagents for multiple biological research applications. Using direct evolution approaches, I generated a cohort of synthetic proteins and antibody scaffolds that can be linked together to facilitate affinity-driven cargo delivery to a target of choice. An attribute of a plug-and-play protein G system is its universality and simplicity, allowing for its incorporation into many other applications. As such, I established and optimized a portfolio of potential system applications (Figure 6.1); for instance, a sensitive detection assay based on the protein complementation concept and a new method to target of CAR-T cells to cancer cells. In chapter 3, I demonstrated how the technology could be effectively applied to respond to a real-life threat such as the COVID pandemic. Due to its universality, my detection assay was quickly optimized for SARS-CoV-2 detection, even with the limited resources. This work showed the plug-and-play protein G system's potential to response to threats we may have to face in the future. In chapter 4, I listed all the collaborative projects I have spearheaded with faculty at the University of Chicago and other universities. This work most times involved multiple steps and a significant time commitment. The work includes, for example, antibody generation for various targets, primary and secondary validation of antibodies, and antibody cloning and production.

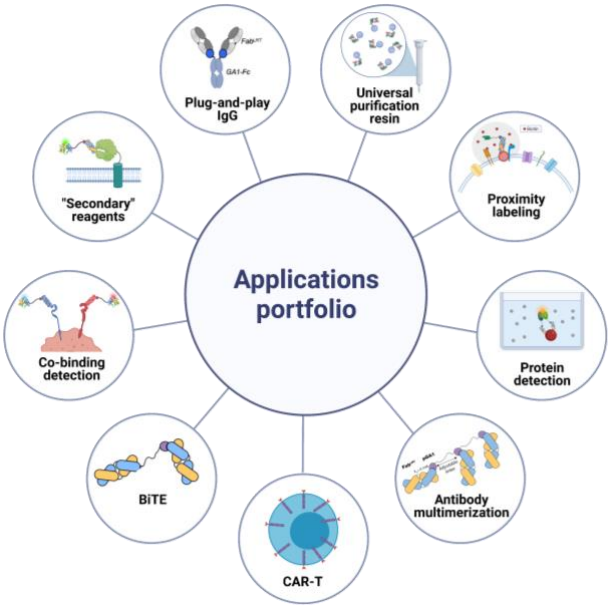

Figure 5.1 The summary of developed applications for a plug-and-play protein G-based system.

In conclusion, I developed a powerful set of biological tools that can be readily applied to help answer a broad range of scientific questions. Further, I created various applications that exploit this technology, and the portfolio is still expanding. More recently, the system was successfully applied for SARS-CoV-2 detection as a response to a identification and treatment of this global threat.

CHAPTER 6: MATERIAL AND METHODS

6.1 Protein cloning and production

6.1.1 Protein cloning

The open-reading frames (ORFs) encoding the C-terminal domain of Nucleoprotein (NP^{CT}) from Zaire (EBOV), Reston, full-size EBOV NP and Zika virus Methyltransferase (MT ZIKV) were cloned using Sma1 site into pEKD40 with the cleavable N-terminal SNAP-tag and the C-terminal 6x His tag, to serve as targets for phage selection. pEKD40 is a derivative of pSNAP-tag (T7)-2 vector (NEB) that was modified with the thrombin-cleavage site at the C-terminus of the SNAP-tag followed by Sma1 site and a C- terminal 6x His tag added for enabling of protein purification. Anti-silencing factor 1 (Asf1)(Schaefer et al., 2016), all protein G variants, and the proteins for the split enzyme proximity assay (BLF_GA1) were cloned into pHFT2 vector (Huang et al., 2008) using Xho1-BamH1 sites. BLF_GA1 fusion constructs comprised of one of two TEM-1 β-lactamase (BL) complementation fragments: BLF1, aa 26-196 bearing a M182T mutation (Galarneau et al., 2002) or BLF2, aa 198-290, connected to the N- or C-termini of GA1 by roughly 30 aa-long GS linkers. SNAP-SNAP-GA1 was cloned by PCR linearization of the GA1-SNAP vector to generate complementary ends for an insert containing SNAP. SNAP-SNAP-GLM was generated by site-directed mutagenesis using SNAP-SNAP-GA1 as a template. GA1-hFc was cloned into the pSCSTa vector containing a human IgG construct. First, the vector was linearized via PCR designed to remove the CH1 portion. GA1 was amplified by PCR to contain a C-terminal linker (GGGGGGSGGGGSGGGGSSSGSS) and was then cloned into the N-terminal portion of the CH2-CH3 construct remaining in the open vector. A gBlock (IDT) coding for a fusion of GA1-GGGGGGSGGGGSGGGGS-MurineFc (IgG2a CH2-CH3) was cloned into the pSCSTa vector

linearized by NotI-BamHI digestion. GLM-hFc and GLM-mFc were generated by site-directed mutagenesis using GA1-hFc and GA1-mFc as templates.

Selected Fabs were cloned from phage into Sph1 sites of pSFV4 expression vector using an Infusion HD cloning kit (Takara Bio) according to the recommended protocol. The Fab scaffolds were grafted into Fab light chain at aa positions 123-127 using quick change site-directed mutagenesis (Liu and Naismith, 2008). To obtained Her2, OKT3 and UCHT1 Fabs, their humanized CDR-containing regions (gBlocks, IDT) were cloned into pSFV4 using Nco1 and SgrA1 sites. To improve bacterial expression of the OKT3 Fab, the Cys in CDR H3 of OKT3 was substituted with Ser. Genetic fusion of GA1 to the C-terminus of Fab^H variants was achieved by cloning of GA1 containing an N-terminal 13 aa long linker into SgrA1 of pSFV4. In order to use Fab^H and Fab^L as a selection target, the avi-tag was cloned into pSFV4 vector.

6.1.2 Protein expression and purification

Protein Gs, ASF1, Zika protein and Ebola proteins were expressed in BL21 (DE3) cells grown overnight in 2xYT medium in 20°C post induction with 1 mM IPTG at OD_{600}= 0.6. Cells were sonicated in buffer A containing 50 mM Tris-HCl, pH 8.0, 150 mM NaCl and 10% glycerol. His-tagged protein was purified from the supernatant post centrifugation using Talon (TaKaRa) cobalt resin and eluted with 100 mM imidazole in buffer A. For the split enzyme assay, BLF-GA1 fusions constructs were expressed in BL21 (DE3) cells, as described above, however the sample purification required a refolding step. To that end, proteins were extracted from the insoluble fractions by 6H Gua-HCl in buffer A (50 mM Tris-HCl, pH 8.0, 150 mM NaCl, 5 mM BME) post sonication and centrifugation. The sample was then purified using TALON Metal affinity resin

(Clontech) with on-column renaturation procedure (6 washes of 2-fold 6M Gua-HCl dilutions in buffer A) followed by 100 mM imidazole elution.

Fabs and Fab_GA1 fusions were expressed in the periplasm of *E. coli* BL21 cells for 4 hours at 37°C post induction with 1 mM IPTG at OD_{600}= 0.8-1. The cells were harvested by sonication in Protein G-wash buffer (50 mM Phosphate buffer, 500 mM NaCl, pH 7.4). After centrifugation the supernatant was applied on the protein GF affinity column. Proteins were eluted from the column with 0.1 M glycine, pH 2.6, and neutralized with 1M Tris-HCl, pH 8.5.

Protein G fused to Fc domain were expressed in Expi293 cells by transient transfection using FectoPro transfection reagent (Polyplus), following the manufacturer recommendations. Briefly, 25mL of Expi 293 cells were seeded in 125 mL flask (Corning) at $2x10^6$ cells/mL, and transfected with 15 µg of plasmid, using Opti-MEM media (Gibco) and FectoPro transfection reagent (Polyplus). Four days after transfection the media was harvested by the centrifugation and the proteins were purified by protein A affinity chromatography (GenScript) and eluted with 0.1 M glycine, pH 2.6. Next, buffer was exchanged to 1xPBS and stored at -80°C.

6.2 Phage Display

6.2.1 Fab scaffold phage library preparation

Fab scaffold phage library was created using the strategy previously published (Fuh and Sidhu, 2000). To that end, the stop codon was introduced using quick change site-directed mutagenesis at position 125 prior to ssDNA isolation from phage. Five residues at position 123-127 (SQLKS) were randomized using hard randomization with the phosphorylated primer. The randomization strategy allowed for the introduction of all amino acids in the positions 123, 124,

126 and 127, while position 125 was limited to leucine or valine. Phosphorylated primers were used in Kunkel mutagenesis (Kunkel, 1985) and the next day the library was precipitated using 20% PEG/ 2.5M NaCl.

6.2.2 Protein G phage library preparation

The library generation strategy was designed using previously described approach (Bailey et al., 2014; Sidhu et al., 2000). Protein G was displayed on the surface of M13 phage by fusion to the minor coat protein pIII. After the inspection of the Fab- protein G crystal structures (1IGC and 6U8C) the 6 amino acids at the position 38-43 were identified to interact with the Fab constant light chain. These residues were randomized using hard randomization strategy (NNK) where all amino acids are possible. Stop codon was placed using quick change site-directed mutagenesis in the aa position 40 prior to ssDNA preparation from phage. Phosphorylated primers were used in Kunkel mutagenesis (Kunkel, 1985) and the next day the library was precipitated using 20% PEG/ 2.5M NaCl.

6.2.3 Phage display selection protocol

Prior to library sorting, the target proteins were biotinylated depending on the system. Purified SNAP-tagged target proteins were biotinylated via SNAP-tag at 20% excess of SNAP-Biotin (NEB) in the presence of 0.3 mM TCEP for 30 min at 37°C. RBD protein was biotinylated via glycoproteins with EZ-Link Hydrazide Biotin (Thermo Scientific) as recommended by the manufacturer. Fab^H and Fab^L were biotinylated via avi-tag, using the BirA enzyme (Avidity) with the protocol provided by the manufacturer. The efficiency of the biotinylation was evaluated using

SDS-PAGE gel with streptavidin (SA). Briefly, samples were incubated with streptavidin before adding and incubating with a non-reducing SDS. Then, without boiling, the samples were loaded on the stain-free SDS-PAGE gel (Mini-PROTEAN TGX Stain-Free, Biorad), and the protein migration was estimated.

In the first selection round, 1 μM (500 nM in RBD selection) of target protein was immobilized on 200 μl streptavidin magnetic beads (Promega) and incubated with 1 mL phage library for 1 hour at room temperature with gentle shaking. The beads were washed three times to remove nonspecific phage, added to log phase E. coli XL-1 blue cells (Stratagene), and incubated for 20 minutes at room temperature. Then, media containing 100 μg/mL ampicillin and 109 p.f.u./mL of M13K07 helper phage (NEB) was added for overnight phage amplification at 37°C. The amplified phage was precipitated in 20% PEG/2.5 M NaCl for 20 minutes on ice for subsequent rounds. Before each round, the phage pool was negatively selected against empty paramagnetic beads for 30 minutes with shaking to eliminate nonspecific binders. The final concentration of antigen was dropped gradually from 1 μM to 1 nM from the first to the fifth round (2nd round: 200 nM, third round: 50 nM, fourth round 10 nM, and fifth-round 1 nM) (500 nM to 1 nM in selection against RBS, with the subsequent rounds concentrations equal to the listed values). After phage binding, the beads were subjected to five washing rounds. The bound phages were eluted using 0.1 M glycine, pH 2.6, and neutralized with TRIS-HCl, pH 8.5. Then, the phage eluate was used for E. coli infection and phage amplification, as described above. After rounds, fourth and fifth phages were plated on ampicillin plates, and 96 single colonies were picked for single-point phage ELISA assays. The promising clones demonstrating high ELISA signal and low nonspecific binding were sequenced and reformatted into pSFV4 expressing vectors (Fabs) or pEKD40 expressing vectors (protein Gs) as described in Protein expression and purification.

Additional selection to generate a non-overlapping epitope with sRBD1 was performed. The selection protocol was as described above, adding 1 μM of sRBD1 in every step to ensure binding to a distinctive epitope. The final antigen concentration was dropped gradually from 200 to 1 nM from the first to the fifth round (2nd round: 50 nM, third round: 20 nM, fourth round 10 nM, and fifth-round 1 nM). After rounds, fourth and fifth phages were plated on ampicillin plates, and 96 single colonies were picked for single-point phage ELISA assays. The promising clones demonstrating high ELISA signal and low non-specific binding were sequenced and reformatted into a pSFV4 expressing vector as described in Protein expression and purification.

6.2.4 Affinity maturation of RBD1

Phage libraries for affinity maturation of RBD1 were generated using a previously published strategy (Sidhu et al., 2004). The strategy involved introducing a stop codon in CDR-H1 via quick-change mutagenesis, followed by the creation of two phage libraries using "hard" and "tailored" randomization strategies with phosphorylated oligos. The ssDNA containing the stop codon was isolated from the phage and subjected to Kunkel mutagenesis (Kunkel, 1985). The Kunkel reaction was purified, and the resulting DNA was electroporated into TG1 cells and cultured with helper phage. After precipitation, three rounds of biopanning were performed with varying target concentrations. The selection process included four consecutive 30-minute washing steps to ensure improvement in dissociation constant. Affinity improvement of the selected clones was evaluated using SPR.

6.3 Single point ELISA

Phage particles obtained from the fourth and fifth rounds were utilized to infect E. coli XL-1 cells. Subsequently, 96 individual phages per target were picked and cultured in 400 µl of 2xYT media supplemented with 50 µg/ml ampicillin and 10^9 pfu/ml of KO7 in a 96-deep-well block plate for 20 hours at 37 °C and 280 rpm. The bacterial cells were centrifuged, and the supernatants containing phage particles were diluted ten-fold in PBS buffer and utilized as an analyte for single-point phage ELISA assays. The target proteins were immobilized on high-binding experimental wells (Greiner Bio) at 50 nM concentration, followed by extensive blocking with BSA. After 15 minutes of incubation with phage, well were extensively washed three times and incubated with Protein L- HRP (Thermo Scientific, 1:5000 dilution in HBST) for 20 minutes. The plates were again washed and developed with TMB substrate (Thermo Scientific) and quenched with 10% H3PO4, followed by the absorbance at A450 determination.

6.4 Multipoint ELISA

High-binding experimental wells (Greiner Bio) were used to immobilize the target proteins at a concentration of 50 nM. The wells were extensively blocked with BSA. Twelve 2-fold serial dilutions were added and incubated for 20 minutes at room temperature for each construct being analyzed. The wells were then subjected to extensive washing before being incubated with HRP-conjugated anti-human (Fab)2 antibody (JacksonImmunoResearch) at a dilution of 1:5000 in PBST for 20 minutes at room temperature. After washing again, the wells were developed with TMB substrate (Thermo Scientific), and the reaction was quenched with 10% H3PO4. The absorbance at A450 was then determined.

6.5 Surface plasmon resonance analysis

All Surface plasmon resonance (SPR) analyses were performed on a MASS-1 (Bruker). All targets were immobilized via a 6x His-tag to a Ni-NTA sensor chip. Fabs in twofold dilutions were run as analytes at 30 µl/min flow rate at 20°C. Sensogram were corrected through double referencing, and a 1:1 binding model fit was done using Sierra Analyser (Bruker). For the epitope binning experiments, 100 nM of the first antibody was injected into a His-tagged target immobilized on the sensor surface to saturate the interaction epitope. Next, an equal molar mixture of another Fab was injected, and the Response Unit (RU) increase was observed.

6.6 Protein complexes purification and crystallization

6.6.1 Crystallization of Fab^{LRT}-GA1

Prior to the formation of the complex, the 10x His tag on GA1 was removed using TEV protease. The Fab^{LRT}-GA1 complex was obtained by incubating Fab^{LRT}11M with GA1 at a 1:1 molar ratio on ice for 3 hours. The complex was then purified using size-exclusion chromatography on a Superdex 200 Increase 10/300 GL column (Cytiva) equilibrated with 20 mM HEPES, 150 mM sodium chloride, pH 7.5, and the purity of the complex was confirmed by SDS-PAGE. Using the hanging-drop vapor-diffusion method, the Mosquito Crystal robot (TTP Labtech) was used to set up initial crystallization trials of the Fab^{LRT}-GA1 complex at room temperature. The protein complex at 17 mg/ml was mixed with a Protein Complex Suite (QIAGEN) screen solution. Promising crystals were observed in 0.1 M magnesium chloride, 0.1 M sodium acetate pH 5.0, and 15% (w/v) PEG 4000 at 19°C. To optimize the initial crystallization condition and improve crystal quality, hanging-drop crystallization trials were set up at room temperature by mixing 1 µL of

complex solution with 1 μL of reservoir solution. The seeding technique obtained good quality crystals in 0.1 M magnesium chloride, 0.1 M sodium acetate pH 5.0, and 20% (w/v) PEG 4000 at 19°C. The resulting crystals were soaked in mother liquor containing 20% glycerol and flash-frozen in liquid nitrogen for data collection.

The X-ray diffraction experiments were conducted at 100° K on beamline 23-ID-D at the GM/CA in Argonne National Laboratory. XDS (Kabsch, 2010) was used to index and integrate the data, which was then scaled with AIMLESS (Evans and Murshudov, 2013) in the CCP4 program suite (Winn et al., 2011). The data set was initially processed in the $P6_222$ space group, but the molecular replacement was unsuccessful due to split reflections at high resolution, indicating twinning. To investigate twinning, the data was reprocessed in $P6_1$, P321, and P312 point group symmetries, and the best structure solution with Rfactor = 33.5% and Rfree = 37.8% was obtained in the $P3_221$ space group by molecular replacement using BALBES (Long et al., 2008). BALBES generated a starting PDB model for the Fab^{LRT}-GA1 complex structure based on protein sequence similarity. Phenix.xtriage (Afonine et al., 2012) confirmed the crystal twinning with one twin operator (-h,-k, l) and estimated a twin fraction of 0.49. The structure was refined in PHENIX (Afonine et al., 2012) using the obtained twin law to Rwork = 19.2% and Rfree = 25%. Manual corrections were made in Coot (Emsley and Cowtan, 2004), and MolProbity (Chen et al., 2010) was used to determine atom contacts and validate the structure. The surface accessible solvent area between Fab^{LRT} and GA1 was calculated in AREAIMOL (Lee and Richards, 1971). The structure was aligned with the CCP4 support program LSKAB (Winn et al., 2011) and structural figures were created with ChimeraX (Goddard et al., 2018). The coordinates and structure factors have been deposited in the Protein Data Bank under entry 6U8C (Berman et al., 2000).

6.6.2 Crystallization of Fab^{H}-GF

Recombinant Fab^{H} E5, its target ASF1 (Bailey et al., 2018) and protein GF were produced and purified as described above. SNAP-tag was removed from the protein G by Thrombin cleavage at room temperature overnight and purified by IMAC on a Talon resin (TaKaRa). To obtain the ASF1-Fab^{H}-GF complex, the proteins were incubated in a 1:1 molar ratio. The complex was purified on size exclusion chromatography on a Sephadex 200 column, equilibrated with HBS. SDS-PAGE confirmed the purity of the complex. The complex was concentrated to 10mg/ml before initial crystallization trials set up at room temperature using the hanging-drop vapor-diffusion method utilizing the Mosquito Crystal robot (TTP Labtech). The ASF1-Fab^{H}E5-GF complex was crystallized by mixing 100 nL of protein complex solution with 100 nL of a Protein Complex Suite (NeXtal) screen solution. The most promising crystals were observed in 0.1 M Sodium Cacodylate pH 5.5, 0.1 M Calcium acetate hydrate, and 12 % PEG 8000. The condition optimization and seeding improved crystal quality. Hanging-drop crystallization was set up by mixing 1 µl of a complex with 1 µl of reservoir solution. The seeding technique (Luft and DeTitta, 1999) further improved quality in 0.1 M Sodium Cacodylate pH 6.0, 0.1 M Calcium acetate hydrate, and 10 % PEG 8000 at room temperature. The crystals were soaked in mother liquid containing 20 % PEG 400 as a cryoprotectant and flash-frozen in liquid nitrogen for data collection.

X-ray diffraction datasets were collected at the NECAT 24-ID-E beamline at the Advanced Photon Source. Data were indexed and integrated with iMOSFLM (Battye et al., 2011) and scaled using AIMLESS (Evans and Murshudov, 2013) in the CCP4 program suite. The data was processed in $P22_12_1$ space group, and the crystal structure was determined by molecular replacement method using the structures of the Fab-ASF1 complex (PDB: 6AYZ) and protein G

(PDB: 6U8C) using PHASER (McCoy et al., 2007). The structure was refined in PHENIX (Afonine et al., 2012) using the obtained twin law to Rwork = 23% and Rfree = 29%. The manual corrections were performed using Coot (Emsley and Cowtan, 2004). The structural figures were created with ChimeraX (Goddard et al., 2018).

6.6.3 Crystallization of Fab^{H}-GD

Recombinant Fab^{H} E5, its target ASF1 (Bailey et al., 2018) and protein GD were produced and purified as described above. SNAP-tag was removed from the protein G by Thrombin cleavage at room temperature overnight and purified by IMAC on a Talon resin (TaKaRa). To obtain the ASF1-Fab^{H}-GD complex, the proteins were incubated in a 1:1 molar ratio. The complex was purified on size exclusion chromatography on a Sephadex 200 column, equilibrated with HBS. SDS-PAGE confirmed the purity of the complex. The complex was concentrated to 10mg/ml before initial crystallization trials set up at room temperature using the hanging-drop vapor-diffusion method utilizing the Mosquito Crystal robot (TTP Labtech). The ASF1-Fab^{H}E5-GD complex was crystallized by mixing 100 nL of protein complex solution with 100 nL of a JCSG Top96 (Rigaku) screen solution. The most promising crystals were observed in 0.1 M Sodium cacodylate pH 6.5 and 1 M Sodium citrate tribasic. The condition optimization and seeding improved crystal quality. Hanging-drop crystallization was set up by mixing 1 µl of a complex with 1 µl of reservoir solution. The seeding technique (Luft and DeTitta, 1999) further improved quality in 0.1 M Sodium cacodylate pH 6.8 and 0.8 M Sodium citrate tribasic at room temperature. The crystals were soaked in mother liquid containing 20 % PEG 400 as a cryoprotectant and flash-frozen in liquid nitrogen for data collection.

X-ray diffraction datasets were collected at the NECAT 24-ID-E beamline at the Advanced Photon Source. Data were indexed and integrated with iMOSFLM (Battye et al., 2011) and scaled using AIMLESS (Evans and Murshudov, 2013) in the CCP4 program suite. The data was processed in $I4_122$ space group, and the crystal structure was determined by molecular replacement method using the structures of the Fab-ASF1 complex (PDB: 6AYZ) and protein G (PDB: 6U8C) using PHASER (McCoy et al., 2007). The structure was refined in PHENIX (Afonine et al., 2012) using the obtained twin law to Rwork = 19% and Rfree = 23%. The manual corrections were performed using Coot (Emsley and Cowtan, 2004). The structural figures were created with ChimeraX (Goddard et al., 2018).

6.7 GA1-Fab^{LRT} protein complementation assay

Before the experiment, 250 nM of each GA1-BLF fusion (GA1-BLF1 and GA1-BLF2) were premixed with corresponding Fabs, depending on a detected target (ASF1: Fabs E11 and E12, EBOV Zaire: Fabs MJ6 and MJ20, ZIKV MT: Fabs Z2C4 and Z2G6, RBD: RBD1 and sRBD7). Both BLF assemblies were combined in a black 96-well plate (FluoroNunc, Nunc) at a final volume of 100 uL, including 2 μM of a fluorogenic BL substrate (Fluorocillin Green 495/525, Life Technologies). Different concentrations of target proteins were added, and the fluorescence signal was monitored at room temperature using Safire2 Tecan Plate Reader (483 nm excitation, 525 nm emission). The background fluorescence of a substrate was subtracted, and the results were reproduced at least three times.

6.8 Protein GF resin preparation

Protein GF resin was generated as previously described (Bailey et al., 2014). Briefly, protein GF was cloned with a SUMO-tag, that contains a free cysteine to allow for covalent linkage to SulfoLink Coupling Resin (Thermo Scientific), and the resin was created following the manufacturer's protocol.

6.9 T-cell redirection cell-culture assay

SKBR3 cells (ATCC), a human breast cancer cell line that overexpresses the Her2 gene product on the cell surface, were cultured following ATCC protocols. CD3+ PBMC cells were isolated from patient blood samples (Vissers et al., 1988), and then stored in liquid nitrogen. The day before the experiment, SKBR3 cells were seeded into a 96-well plate at a density of 20,000 cells in 100 μL per well. Meanwhile, the PBMC cells were thawed and placed into a suspension culture at 2 million cells per milliliter. After 16 to 24 hours of incubation, the PBMC cells were washed and then transferred to the SKBR3 wells at an effector cell-to-target cell ratio of 10:1. The bi-specific components were added at a concentration of 50 nM, unless otherwise specified, in a final volume of 100 μL per well. After 24 hours of co-culturing, the medium in each plate was analyzed using commercially available kits for LDH presence (CytoTox96, Promega #G1781, positive control – complete cancer-cell lysis), as well as cytokine release (INFg, Cisbio #62HIFNGPEG) and (IL2, Cisbio #62HIL02PEG). The values obtained were then normalized using the protocols and standards provided in the kits. The experiment was repeated at least three times.

6.10 Flow cytometry

SNAP-GA1 and SNAP-GLM were conjugated with BG-Alexa Fluor 647 and BG-Alexa Fluor 488 (New England Biolabs), respectively, according to the manufacturer's protocol. The excess substrate was removed with PD MiniTrap G-25 (Cytiva) desalting columns.

6.10.1 Flow cytometry analysis of GA1-SNAP as a secondary detection reagent.

A human embryonic kidney (HEK) cell line stably transfected to express extracellular MBP anchored to a transmembrane domain and intracellular green fluorescent protein (HEKM-TM-G) was used for initial assessment of SNAP-GA1-A647 as a secondary detection reagent. HEKM-TM-G cells were cultured to ~70% confluency before detachment by trypsin digestion. Cells were washed once in PBS/1% BSA and added at a concentration of 500,000 cells per tube to Eppendorf tubes. Cells were incubated with no Fab, $7O^{LRT}$, $7O^{LRT}$ in 10 mM maltose, and $MJ6^{LRT}$ for 30 minutes at room temperature before washing two times in 1 mL PBS/1% BSA. Next, Alexa Fluor 647 AffiniPure Goat Anti-Human IgG F(ab')2 fragment specific (Jackson ImmunoResearch) and SNAP-GA1-A647 were added to samples for 20 minutes at room temperature. Cells were resuspended in 250 uL PBS/1% BSA after the final wash and subjected to analysis by a CytoFLEX flow cytometer (Beckman Coulter). The experiment was repeated as described above for the construct containing two SNAP-tags.

6.10.2 Flow cytometry analysis of co-binding detection using GA1-SNAP and GLM-SNAP.

The human breast cancer cell line SKBR3 (ATCC) was cultured to ~70% confluency before detachment by trypsin digestion. Cells were washed once in PBS/1% BSA and added at a concentration of 500,000 cells per well to a 96-well round bottom plate. SNAP-GLM-A488 and SNAP-GA1-A647 were incubated at equimolar concentrations with combinations of $MJ20^{H}$, $HER2^{H}$, $7O^{LRT}$, and $EGFR^{LRT}$ for 1 hour on ice before diluting to a final concentration of 250 nM for each component in PBS/1% BSA. Samples were incubated on cells for 30 minutes at room temperature before washing three times with 250 uL of PBS/1% BSA by centrifugation at 400 x g for 5 minutes. Cells were resuspended in 250 uL PBS/1% BSA after the final wash and subjected to analysis by a CytoFLEX flow cytometer (Beckman Coulter).

6.10.3 Flow cytometry analysis of Protein G-Fc fusions.

The MDA-MB-453 cell line was used to assess GA1-hFc and GLM-mFc constructs initially. Before the experiments, GA1-hFc and GLM-mFc were premixed modularly with HER2LRT, HER2H, S1LRT (isotype control), or MJ20H (isotype control), respectively. Flow cytometry analysis was performed as described above. Alexa Fluor 488-conjugated AffiniPure Goat Anti-Human IgG Fc Fragment Specific, Alexa Fluor 647-conjugated AffiniPure Goat Anti-Human IgG Fc Fragment Specific (Jackson ImmunoResearch), and Alexa Fluor 647-conjugated AffiniPure Goat Anti-Mouse IgG Fc Subclass 2a Specific (Jackson ImmunoResearch) were used as secondary detection agents.

6.10.4 Flow cytometry analysis of co-binding detection using Protein G-Fc fusions.

Co-staining detection of GA1-hFc and GLM-mFc with $HER2^{H}$ and $EGFR^{LRT}$ Fabs was performed with the HCC1954 cell line. PG-Fc fusions were pre-incubated with $HER2^{H}$, $EGFR^{LRT}$, $MJ20^{H}$ (isotype control), or $S1^{LRT}$ (isotype control) on ice for 30 minutes. The $EGFR^{LRT}$ + GA1-hFc assembly was first added to cells at 20 nM for 15 minutes on ice. Cells were washed three times with PBS/1% BSA before adding $HER2^{H}$ + GLM-mFc at 20 nM for 15 minutes on ice. Cells were washed three times before adding a mixture of Alexa Fluor 488-conjugated Anti-Human Fc (Jackson ImmunoResearch) and Alexa Fluor 647-conjugated Anti-Mouse Fc (Jackson ImmunoResearch) for 15 minutes on ice, followed by three washes.

6.11 CAR-T emergency stop switch

Human breast cancer cell line SKBR3 was cultured according to ATCC protocol. The day before the experiment, cells were seeded into a 96-well plate (10k cells per well). The next day, cells were washed, and the fresh medium containing 100k CAR-T and 100 nM Her2 Fab in different scaffolds was added to the final volume of 100 μL/well. After one, two, four, or eight hours, 5 μL of 20 μM RBD1 Isotype Fab (anti-SARS-CoV-2 RBD Fab) in the Fab^{LRT} scaffold was directly added to the well for the final concentration of 1 μM. The same Isotype Fab in the Fab^{H} scaffold was added as a negative control. After 24h of co-culturing, the cells were spun down, and the medium was transferred and analyzed with commercially available kits for the LDH presence (CytoTox-96, Promega) and cytokine release (INFg, Cisbio). The results were reproduced at least three times.

6.12 Plaque reduction neutralization assay

The plaque reduction neutralization assay was performed with some modifications to the previously described method (De Madrid and Porterfield, 1969). The Vero E6 cell line (ATCC) was infected with SARS-CoV-2 (nCoV/Washington/1/2020), which was kindly provided by the National Biocontainment Laboratory in Galveston, TX, under biosafety level 3 conditions. To conduct the neutralization assay, the Fabs were serially diluted 4-fold, mixed with 400 PFU of SARS-CoV-2, and incubated at 37 ºC for one hour. The mixture was then used to infect Vero E6 cells for three days. Following incubation, the cells were fixed with 3.7 % formalin and stained with 0.25 % crystal violet. The stained cells were quantified by measuring the absorbance at 595 nm using a Tecan m200 microplate reader. The 50 % neutralization titer was calculated using GraphPad Prism.

6.13 Model generation

Models were created using BioRender.com.

REFERENCES

Afonine, P.V., Grosse-Kunstleve, R.W., Echols, N., Headd, J.J., Moriarty, N.W., Mustyakimov, M., Terwilliger, T.C., Urzhumtsev, A., Zwart, P.H., and Adams, P.D. (2012). Towards automated crystallographic structure refinement with phenix.refine. Acta Crystallogr D Biol Crystallogr *68*, 352-367.

Agarwal, P., and Bertozzi, C.R. (2015). Site-specific antibody-drug conjugates: the nexus of bioorthogonal chemistry, protein engineering, and drug development. Bioconjug Chem *26*, 176-192.

Alfaleh, M.A., Jones, M.L., Howard, C.B., and Mahler, S.M. (2017). Strategies for Selecting Membrane Protein-Specific Antibodies using Phage Display with Cell-Based Panning. Antibodies (Basel) *6*.

Almen, M.S., Nordstrom, K.J., Fredriksson, R., and Schioth, H.B. (2009). Mapping the human membrane proteome: a majority of the human membrane proteins can be classified according to function and evolutionary origin. BMC Biol *7*, 50.

Armache, J.P., and Cheng, Y. (2019). Single-particle cryo-EM: beyond the resolution. Natl Sci Rev *6*, 864-866.

Arrigoni, C., Lolicato, M., Shaya, D., Rohaim, A., Findeisen, F., Fong, L.K., Colleran, C.M., Dominik, P., Kim, S.S., Schuermann, J.P., *et al.* (2022). Quaternary structure independent folding of voltage-gated ion channel pore domain subunits. Nat Struct Mol Biol *29*, 537-548.

Axup, J.Y., Bajjuri, K.M., Ritland, M., Hutchins, B.M., Kim, C.H., Kazane, S.A., Halder, R., Forsyth, J.S., Santidrian, A.F., Stafin, K., *et al.* (2012). Synthesis of site-specific antibody-drug conjugates using unnatural amino acids. Proc Natl Acad Sci U S A *109*, 16101-16106.

Bai, C., Zhong, Q., and Gao, G.F. (2022). Overview of SARS-CoV-2 genome-encoded proteins. Sci China Life Sci *65*, 280-294.

Bailey, L.J., Sheehy, K.M., Dominik, P.K., Liang, W.G., Rui, H., Clark, M., Jaskolowski, M., Kim, Y., Deneka, D., Tang, W.J., *et al.* (2018). Locking the Elbow: Improved Antibody Fab Fragments as Chaperones for Structure Determination. J Mol Biol *430*, 337-347.

Bailey, L.J., Sheehy, K.M., Hoey, R.J., Schaefer, Z.P., Ura, M., and Kossiakoff, A.A. (2014). Applications for an engineered Protein-G variant with a pH controllable affinity to antibody fragments. J Immunol Methods *415*, 24-30.

Bar, D.Z., Atkatsh, K., Tavarez, U., Erdos, M.R., Gruenbaum, Y., and Collins, F.S. (2018). Biotinylation by antibody recognition-a method for proximity labeling. Nat Methods *15*, 127-133.

Barbas, C.F., 3rd, Kang, A.S., Lerner, R.A., and Benkovic, S.J. (1991). Assembly of combinatorial antibody libraries on phage surfaces: the gene III site. Proc Natl Acad Sci U S A *88*, 7978-7982.
Barnkob, M.S., Simon, C., and Olsen, L.R. (2014). Characterizing the human hematopoietic CDome. Front Genet *5*, 331.

Bass, S., Greene, R., and Wells, J.A. (1990). Hormone phage: an enrichment method for variant proteins with altered binding properties. Proteins *8*, 309-314.

Battye, T.G., Kontogiannis, L., Johnson, O., Powell, H.R., and Leslie, A.G. (2011). iMOSFLM: a new graphical interface for diffraction-image processing with MOSFLM. Acta Crystallogr D Biol Crystallogr *67*, 271-281.

Benvenuti, M., and Mangani, S. (2007). Crystallization of soluble proteins in vapor diffusion for x-ray crystallography. Nat Protoc *2*, 1633-1651.

Berman, H.M., Westbrook, J., Feng, Z., Gilliland, G., Bhat, T.N., Weissig, H., Shindyalov, I.N., and Bourne, P.E. (2000). The Protein Data Bank. Nucleic Acids Res *28*, 235-242.

Binz, H.K., Amstutz, P., and Pluckthun, A. (2005). Engineering novel binding proteins from nonimmunoglobulin domains. Nat Biotechnol *23*, 1257-1268.

Bjorck, L., and Kronvall, G. (1984). Purification and some properties of streptococcal protein G, a novel IgG-binding reagent. J Immunol *133*, 969-974.

Boder, E.T., and Wittrup, K.D. (2000). Yeast surface display for directed evolution of protein expression, affinity, and stability. Methods Enzymol *328*, 430-444.

Bonifant, C.L., Jackson, H.J., Brentjens, R.J., and Curran, K.J. (2016). Toxicity and management in CAR T-cell therapy. Mol Ther Oncolytics *3*, 16011.

Bottger, V., and Bottger, A. (2009). Epitope mapping using phage display peptide libraries. Methods Mol Biol *524*, 181-201.

Bradbury, A.R., and Marks, J.D. (2004). Antibodies from phage antibody libraries. J Immunol Methods *290*, 29-49.

Bradbury, A.R., Sidhu, S., Dubel, S., and McCafferty, J. (2011). Beyond natural antibodies: the power of in vitro display technologies. Nat Biotechnol *29*, 245-254.

Brinkmann, U., and Kontermann, R.E. (2017). The making of bispecific antibodies. MAbs *9*, 182-212.

Brudno, J.N., and Kochenderfer, J.N. (2016). Toxicities of chimeric antigen receptor T cells: recognition and management. Blood *127*, 3321-3330.

Burns, G.F., Boyd, A.W., and Beverley, P.C. (1982). Two monoclonal anti-human T lymphocyte antibodies have similar biologic effects and recognize the same cell surface antigen. J Immunol *129*, 1451-1457.

Carter, P., Presta, L., Gorman, C.M., Ridgway, J.B., Henner, D., Wong, W.L., Rowland, A.M., Kotts, C., Carver, M.E., and Shepard, H.M. (1992). Humanization of an anti-p185HER2 antibody for human cancer therapy. Proc Natl Acad Sci U S A *89*, 4285-4289.

Cater, R.J., Chua, G.L., Erramilli, S.K., Keener, J.E., Choy, B.C., Tokarz, P., Chin, C.F., Quek, D.Q.Y., Kloss, B., Pepe, J.G., *et al.* (2021). Structural basis of omega-3 fatty acid transport across the blood-brain barrier. Nature *595*, 315-319.

Chames, P., and Baty, D. (2009). Bispecific antibodies for cancer therapy: the light at the end of the tunnel? MAbs *1*, 539-547.

Chen, V.B., Arendall, W.B., 3rd, Headd, J.J., Keedy, D.A., Immormino, R.M., Kapral, G.J., Murray, L.W., Richardson, J.S., and Richardson, D.C. (2010). MolProbity: all-atom structure validation for macromolecular crystallography. Acta Crystallogr D Biol Crystallogr *66*, 12-21.

Clarke, J.B. (2010). Mechanisms of adverse drug reactions to biologics. Handb Exp Pharmacol, 453-474.

Cwirla, S.E., Peters, E.A., Barrett, R.W., and Dower, W.J. (1990). Peptides on phage: a vast library of peptides for identifying ligands. Proc Natl Acad Sci U S A *87*, 6378-6382.

Dauter, Z. (1999). Data-collection strategies. Acta Crystallogr D Biol Crystallogr *55*, 1703-1717.
De Madrid, A.T., and Porterfield, J.S. (1969). A simple micro-culture method for the study of group B arboviruses. Bull World Health Organ *40*, 113-121.

Derrick, J.P., and Wigley, D.B. (1992). Crystal structure of a streptococcal protein G domain bound to an Fab fragment. Nature *359*, 752-754.

Dodd, R.B., Wilkinson, T., and Schofield, D.J. (2018). Therapeutic Monoclonal Antibodies to Complex Membrane Protein Targets: Antigen Generation and Antibody Discovery Strategies. BioDrugs *32*, 339-355.

Dominik, P.K., and Kossiakoff, A.A. (2015). Phage display selections for affinity reagents to membrane proteins in nanodiscs. Methods Enzymol *557*, 219-245.

Dostalek, M., Gardner, I., Gurbaxani, B.M., Rose, R.H., and Chetty, M. (2013). Pharmacokinetics, pharmacodynamics and physiologically-based pharmacokinetic modelling of monoclonal antibodies. Clin Pharmacokinet *52*, 83-124.

Ducancel, F., and Muller, B.H. (2012). Molecular engineering of antibodies for therapeutic and diagnostic purposes. MAbs *4*, 445-457.

Earp, L.J., Delos, S.E., Park, H.E., and White, J.M. (2005). The many mechanisms of viral membrane fusion proteins. Curr Top Microbiol Immunol *285*, 25-66.

Ecker, D.M., Jones, S.D., and Levine, H.L. (2015). The therapeutic monoclonal antibody market. MAbs *7*, 9-14.

Eigenbrot, C., Randal, M., Presta, L., Carter, P., and Kossiakoff, A.A. (1993). X-ray structures of the antigen-binding domains from three variants of humanized anti-p185HER2 antibody 4D5 and comparison with molecular modeling. J Mol Biol *229*, 969-995.

Emsley, P., and Cowtan, K. (2004). Coot: model-building tools for molecular graphics. Acta Crystallogr D Biol Crystallogr *60*, 2126-2132.

Evans, P.R., and Murshudov, G.N. (2013). How good are my data and what is the resolution? Acta Crystallogr D Biol Crystallogr *69*, 1204-1214.

Fellouse, F.A., Esaki, K., Birtalan, S., Raptis, D., Cancasci, V.J., Koide, A., Jhurani, P., Vasser, M., Wiesmann, C., Kossiakoff, A.A., *et al.* (2007). High-throughput generation of synthetic antibodies from highly functional minimalist phage-displayed libraries. J Mol Biol *373*, 924-940.

Fellouse, F.A., Wiesmann, C., and Sidhu, S.S. (2004). Synthetic antibodies from a four-amino-acid code: a dominant role for tyrosine in antigen recognition. Proc Natl Acad Sci U S A *101*, 12467-12472.

Feng, P., Wu, X., Erramilli, S.K., Paulo, J.A., Knejski, P., Gygi, S.P., Kossiakoff, A.A., and Rapoport, T.A. (2022). A peroxisomal ubiquitin ligase complex forms a retrotranslocation channel. Nature *607*, 374-380.

Fishman, J.B., and Berg, E.A. (2019). Protein A and Protein G Purification of Antibodies. Cold Spring Harb Protoc *2019*.

Forsgren, A., and Sjoquist, J. (1966). "Protein A" from S. aureus. I. Pseudo-immune reaction with human gamma-globulin. J Immunol *97*, 822-827.

Fuh, G., and Sidhu, S.S. (2000). Efficient phage display of polypeptides fused to the carboxy-terminus of the M13 gene-3 minor coat protein. FEBS Lett *480*, 231-234.

Galarneau, A., Primeau, M., Trudeau, L.E., and Michnick, S.W. (2002). Beta-lactamase protein fragment complementation assays as in vivo and in vitro sensors of protein protein interactions. Nat Biotechnol *20*, 619-622.

Galfre, G., Howe, S.C., Milstein, C., Butcher, G.W., and Howard, J.C. (1977). Antibodies to major histocompatibility antigens produced by hybrid cell lines. Nature *266*, 550-552.

Gao, J., Sidhu, S.S., and Wells, J.A. (2009). Two-state selection of conformation-specific antibodies. Proc Natl Acad Sci U S A *106*, 3071-3076.

Gebel, H.M., Lebeck, L.K., Jensik, S.C., Webster, K., and Bray, R.A. (1989). T cells from patients successfully treated with OKT3 do not react with the T-cell receptor antibody. Hum Immunol *26*, 123-129.

Goddard, T.D., Huang, C.C., Meng, E.C., Pettersen, E.F., Couch, G.S., Morris, J.H., and Ferrin, T.E. (2018). UCSF ChimeraX: Meeting modern challenges in visualization and analysis. Protein Sci *27*, 14-25.

Graille, M., Stura, E.A., Housden, N.G., Beckingham, J.A., Bottomley, S.P., Beale, D., Taussig, M.J., Sutton, B.J., Gore, M.G., and Charbonnier, J.B. (2001). Complex between Peptostreptococcus magnus protein L and a human antibody reveals structural convergence in the interaction modes of Fab binding proteins. Structure *9*, 679-687.

Groff, K., Allen, D., Casey, W., and Clippinger, A. (2020). Increasing the use of animal-free recombinant antibodies. ALTEX.

Groff, K., Brown, J., and Clippinger, A.J. (2015). Modern affinity reagents: Recombinant antibodies and aptamers. Biotechnol Adv *33*, 1787-1798.

Guilliams, T., El-Turk, F., Buell, A.K., O'Day, E.M., Aprile, F.A., Esbjorner, E.K., Vendruscolo, M., Cremades, N., Pardon, E., Wyns, L., *et al.* (2013). Nanobodies raised against monomeric alpha-synuclein distinguish between fibrils at different maturation stages. J Mol Biol *425*, 2397-2411.

Gulich, S., Linhult, M., Stahl, S., and Hober, S. (2002). Engineering streptococcal protein G for increased alkaline stability. Protein Eng *15*, 835-842.

Hornsby, M., Paduch, M., Miersch, S., Saaf, A., Matsuguchi, T., Lee, B., Wypisniak, K., Doak, A., King, D., Usatyuk, S., *et al.* (2015). A High Through-put Platform for Recombinant Antibodies to Folded Proteins. Mol Cell Proteomics *14*, 2833-2847.

Huang, J., Koide, A., Makabe, K., and Koide, S. (2008). Design of protein function leaps by directed domain interface evolution. Proc Natl Acad Sci U S A *105*, 6578-6583.

Huehls, A.M., Coupet, T.A., and Sentman, C.L. (2015). Bispecific T-cell engagers for cancer immunotherapy. Immunol Cell Biol *93*, 290-296.

Kabsch, W. (2010). Integration, scaling, space-group assignment and post-refinement. Acta Crystallogr D Biol Crystallogr *66*, 133-144.

Kohler, G., and Milstein, C. (1975). Continuous cultures of fused cells secreting antibody of predefined specificity. Nature *256*, 495-497.

Koldobskaya, Y., Duguid, E.M., Shechner, D.M., Suslov, N.B., Ye, J., Sidhu, S.S., Bartel, D.P., Koide, S., Kossiakoff, A.A., and Piccirilli, J.A. (2011). A portable RNA sequence whose recognition by a synthetic antibody facilitates structural determination. Nat Struct Mol Biol *18*, 100-106.

Krauss, J., Arndt, M.A., Martin, A.C., Liu, H., and Rybak, S.M. (2003). Specificity grafting of human antibody frameworks selected from a phage display library: generation of a highly stable humanized anti-CD22 single-chain Fv fragment. Protein Eng *16*, 753-759.

Kunkel, T.A. (1985). Rapid and efficient site-specific mutagenesis without phenotypic selection. Proc Natl Acad Sci U S A *82*, 488-492.

Landegren, U., Andersson, J., and Wigzell, H. (1984). Mechanism of T lymphocyte activation by OKT3 antibodies. A general model for T cell induction. Eur J Immunol *14*, 325-328.

Lazar, G.A., Dang, W., Karki, S., Vafa, O., Peng, J.S., Hyun, L., Chan, C., Chung, H.S., Eivazi, A., Yoder, S.C., *et al.* (2006). Engineered antibody Fc variants with enhanced effector function. Proc Natl Acad Sci U S A *103*, 4005-4010.

Lee, B., and Richards, F.M. (1971). The interpretation of protein structures: estimation of static accessibility. J Mol Biol *55*, 379-400.

Lee, C.M., Iorno, N., Sierro, F., and Christ, D. (2007). Selection of human antibody fragments by phage display. Nat Protoc *2*, 3001-3008.

Lee, C.V., Liang, W.C., Dennis, M.S., Eigenbrot, C., Sidhu, S.S., and Fuh, G. (2004). High-affinity human antibodies from phage-displayed synthetic Fab libraries with a single framework scaffold. J Mol Biol *340*, 1073-1093.

Lee, G.M., and Palsson, B.O. (1994). Monoclonal antibody production using free-suspended and entrapped hybridoma cells. Biotechnol Genet Eng Rev *12*, 509-533.

Letko, M., Marzi, A., and Munster, V. (2020). Functional assessment of cell entry and receptor usage for SARS-CoV-2 and other lineage B betacoronaviruses. Nat Microbiol *5*, 562-569.

Liu, H., and Naismith, J.H. (2008). An efficient one-step site-directed deletion, insertion, single and multiple-site plasmid mutagenesis protocol. BMC Biotechnol *8*, 91.

Long, F., Vagin, A.A., Young, P., and Murshudov, G.N. (2008). BALBES: a molecular-replacement pipeline. Acta Crystallogr D Biol Crystallogr *64*, 125-132.

Lu, R.M., Hwang, Y.C., Liu, I.J., Lee, C.C., Tsai, H.Z., Li, H.J., and Wu, H.C. (2020). Development of therapeutic antibodies for the treatment of diseases. J Biomed Sci *27*, 1.

Luft, J.R., and DeTitta, G.T. (1999). A method to produce microseed stock for use in the crystallization of biological macromolecules. Acta Crystallogr D Biol Crystallogr *55*, 988-993.

Luppa, P.B., Muller, C., Schlichtiger, A., and Schlebusch, H. (2011). Point-of-care testing (POCT): Current techniques and future perspectives. Trends Analyt Chem *30*, 887-898.

Mack, M., Riethmuller, G., and Kufer, P. (1995). A small bispecific antibody construct expressed as a functional single-chain molecule with high tumor cell cytotoxicity. Proc Natl Acad Sci U S A *92*, 7021-7025.

Majzner, R.G., and Mackall, C.L. (2018). Tumor Antigen Escape from CAR T-cell Therapy. Cancer Discov *8*, 1219-1226.

McCafferty, J., Griffiths, A.D., Winter, G., and Chiswell, D.J. (1990). Phage antibodies: filamentous phage displaying antibody variable domains. Nature *348*, 552-554.

McCoy, A.J., Grosse-Kunstleve, R.W., Adams, P.D., Winn, M.D., Storoni, L.C., and Read, R.J. (2007). Phaser crystallographic software. J Appl Crystallogr *40*, 658-674.

Miersch, S., Li, Z., Hanna, R., McLaughlin, M.E., Hornsby, M., Matsuguchi, T., Paduch, M., Saaf, A., Wells, J., Koide, S., *et al.* (2015). Scalable high throughput selection from phage-displayed synthetic antibody libraries. J Vis Exp, 51492.

Miller, K.R., Koide, A., Leung, B., Fitzsimmons, J., Yoder, B., Yuan, H., Jay, M., Sidhu, S.S., Koide, S., and Collins, E.J. (2012). T cell receptor-like recognition of tumor in vivo by synthetic antibody fragment. PLoS One *7*, e43746.

Mukherjee, S., Griffin, D.H., Horn, J.R., Rizk, S.S., Nocula-Lugowska, M., Malmqvist, M., Kim, S.S., and Kossiakoff, A.A. (2018). Engineered synthetic antibodies as probes to quantify the energetic contributions of ligand binding to conformational changes in proteins. J Biol Chem *293*, 2815-2828.

Neelapu, S.S., Tummala, S., Kebriaei, P., Wierda, W., Gutierrez, C., Locke, F.L., Komanduri, K.V., Lin, Y., Jain, N., Daver, N., *et al.* (2018). Chimeric antigen receptor T-cell therapy - assessment and management of toxicities. Nat Rev Clin Oncol *15*, 47-62.

Nilson, B.H., Solomon, A., Bjorck, L., and Akerstrom, B. (1992). Protein L from Peptostreptococcus magnus binds to the kappa light chain variable domain. J Biol Chem *267*, 2234-2239.

O'Neil, K.T., and Hoess, R.H. (1995). Phage display: protein engineering by directed evolution. Curr Opin Struct Biol *5*, 443-449.

O'Shannessy, D.J., Dobersen, M.J., and Quarles, R.H. (1984). A novel procedure for labeling immunoglobulins by conjugation to oligosaccharide moieties. Immunol Lett *8*, 273-277.

Omidfar, K., and Daneshpour, M. (2015). Advances in phage display technology for drug discovery. Expert Opin Drug Discov *10*, 651-669.

Ovacik, M., and Lin, K. (2018). Tutorial on Monoclonal Antibody Pharmacokinetics and Its Considerations in Early Development. Clin Transl Sci *11*, 540-552.

Overington, J.P., Al-Lazikani, B., and Hopkins, A.L. (2006). How many drug targets are there? Nat Rev Drug Discov *5*, 993-996.

Padlan, E.A. (1994). Anatomy of the antibody molecule. Mol Immunol *31*, 169-217.

Paduch, M., Koide, A., Uysal, S., Rizk, S.S., Koide, S., and Kossiakoff, A.A. (2013). Generating conformation-specific synthetic antibodies to trap proteins in selected functional states. Methods *60*, 3-14.

Paduch, M., and Kossiakoff, A.A. (2017). Generating Conformation and Complex-Specific Synthetic Antibodies. Methods Mol Biol *1575*, 93-119.

Park, J.H., Riviere, I., Gonen, M., Wang, X., Senechal, B., Curran, K.J., Sauter, C., Wang, Y., Santomasso, B., Mead, E., *et al.* (2018). Long-Term Follow-up of CD19 CAR Therapy in Acute Lymphoblastic Leukemia. N Engl J Med *378*, 449-459.

Poljak, R.J., Amzel, L.M., Avey, H.P., Chen, B.L., Phizackerley, R.P., and Saul, F. (1973). Three-dimensional structure of the Fab' fragment of a human immunoglobulin at 2,8-A resolution. Proc Natl Acad Sci U S A *70*, 3305-3310.

Pollock, S.B., Hu, A., Mou, Y., Martinko, A.J., Julien, O., Hornsby, M., Ploder, L., Adams, J.J., Geng, H., Muschen, M., *et al.* (2018). Highly multiplexed and quantitative cell-surface protein profiling using genetically barcoded antibodies. Proc Natl Acad Sci U S A *115*, 2836-2841.

Rizk, S.S., Paduch, M., Heithaus, J.H., Duguid, E.M., Sandstrom, A., and Kossiakoff, A.A. (2011). Allosteric control of ligand-binding affinity using engineered conformation-specific effector proteins. Nat Struct Mol Biol *18*, 437-442.

Rodgers, K.R., and Chou, R.C. (2016). Therapeutic monoclonal antibodies and derivatives: Historical perspectives and future directions. Biotechnol Adv *34*, 1149-1158.

Rohaim, A., Slezak, T., Koh, Y.H., Blachowicz, L., Kossiakoff, A.A., and Roux, B. (2022). Engineering of a synthetic antibody fragment for structural and functional studies of K+ channels. J Gen Physiol *154*.

Santos, R., Ursu, O., Gaulton, A., Bento, A.P., Donadi, R.S., Bologa, C.G., Karlsson, A., Al-Lazikani, B., Hersey, A., Oprea, T.I., *et al.* (2017). A comprehensive map of molecular drug targets. Nat Rev Drug Discov *16*, 19-34.

Sauer-Eriksson, A.E., Kleywegt, G.J., Uhlen, M., and Jones, T.A. (1995). Crystal structure of the C2 fragment of streptococcal protein G in complex with the Fc domain of human IgG. Structure *3*, 265-278.

Schaefer, Z.P., Bailey, L.J., and Kossiakoff, A.A. (2016). A polar ring endows improved specificity to an antibody fragment. Protein Sci *25*, 1290-1298.

Schiffer, C., Ultsch, M., Walsh, S., Somers, W., de Vos, A.M., and Kossiakoff, A. (2002). Structure of a phage display-derived variant of human growth hormone complexed to two copies of the extracellular domain of its receptor: evidence for strong structural coupling between receptor binding sites. J Mol Biol *316*, 277-289.

Sidhu, S.S., and Fellouse, F.A. (2006). Synthetic therapeutic antibodies. Nat Chem Biol *2*, 682-688.

Sidhu, S.S., Li, B., Chen, Y., Fellouse, F.A., Eigenbrot, C., and Fuh, G. (2004). Phage-displayed antibody libraries of synthetic heavy chain complementarity determining regions. J Mol Biol *338*, 299-310.

Sidhu, S.S., Lowman, H.B., Cunningham, B.C., and Wells, J.A. (2000). Phage display for selection of novel binding peptides. Methods Enzymol *328*, 333-363.

Slamon, D.J., Godolphin, W., Jones, L.A., Holt, J.A., Wong, S.G., Keith, D.E., Levin, W.J., Stuart, S.G., Udove, J., Ullrich, A., *et al.* (1989). Studies of the HER-2/neu proto-oncogene in human breast and ovarian cancer. Science *244*, 707-712.

Slezak, T., Bailey, L.J., Jaskolowski, M., Nahotko, D.A., Filippova, E.V., Davydova, E.K., and Kossiakoff, A.A. (2020). An engineered ultra-high affinity Fab-Protein G pair enables a modular antibody platform with multifunctional capability. Protein Sci *29*, 141-156.

Slezak, T., and Kossiakoff, A.A. (2021). Engineered Ultra-High Affinity Synthetic Antibodies for SARS-CoV-2 Neutralization and Detection. J Mol Biol *433*, 166956.

Smith, G.P. (2019). Phage Display: Simple Evolution in a Petri Dish (Nobel Lecture). Angew Chem Int Ed Engl *58*, 14428-14437.

Tian, F., Lu, Y., Manibusan, A., Sellers, A., Tran, H., Sun, Y., Phuong, T., Barnett, R., Hehli, B., Song, F., *et al.* (2014). A general approach to site-specific antibody drug conjugates. Proc Natl Acad Sci U S A *111*, 1766-1771.

Tsuchiya, Y., and Mizuguchi, K. (2016). The diversity of H3 loops determines the antigen-binding tendencies of antibody CDR loops. Protein Sci *25*, 815-825.

Uysal, S., Vasquez, V., Tereshko, V., Esaki, K., Fellouse, F.A., Sidhu, S.S., Koide, S., Perozo, E., and Kossiakoff, A. (2009). Crystal structure of full-length KcsA in its closed conformation. Proc Natl Acad Sci U S A *106*, 6644-6649.

Vissers, M.C., Jester, S.A., and Fantone, J.C. (1988). Rapid purification of human peripheral blood monocytes by centrifugation through Ficoll-Hypaque and Sepracell-MN. J Immunol Methods *110*, 203-207.

Viti, F., Nilsson, F., Demartis, S., Huber, A., and Neri, D. (2000). Design and use of phage display libraries for the selection of antibodies and enzymes. Methods Enzymol *326*, 480-505.

Wallin, E., and von Heijne, G. (1998). Genome-wide analysis of integral membrane proteins from eubacterial, archaean, and eukaryotic organisms. Protein Sci *7*, 1029-1038.

Walsh, R.M., Jr., Roh, S.H., Gharpure, A., Morales-Perez, C.L., Teng, J., and Hibbs, R.E. (2018). Structural principles of distinct assemblies of the human alpha4beta2 nicotinic receptor. Nature *557*, 261-265.

Wang, L., Amphlett, G., Blattler, W.A., Lambert, J.M., and Zhang, W. (2005). Structural characterization of the maytansinoid-monoclonal antibody immunoconjugate, huN901-DM1, by mass spectrometry. Protein Sci *14*, 2436-2446.

Wang, L., Wang, Y., Ye, D., and Liu, Q. (2020). Review of the 2019 novel coronavirus (SARS-CoV-2) based on current evidence. Int J Antimicrob Agents *55*, 105948.

Watanabe, Y., Allen, J.D., Wrapp, D., McLellan, J.S., and Crispin, M. (2020). Site-specific glycan analysis of the SARS-CoV-2 spike. Science *369*, 330-333.

Williams, A.F., and Barclay, A.N. (1988). The immunoglobulin superfamily--domains for cell surface recognition. Annu Rev Immunol *6*, 381-405.

Winn, M.D., Ballard, C.C., Cowtan, K.D., Dodson, E.J., Emsley, P., Evans, P.R., Keegan, R.M., Krissinel, E.B., Leslie, A.G., McCoy, A., *et al.* (2011). Overview of the CCP4 suite and current developments. Acta Crystallogr D Biol Crystallogr *67*, 235-242.

Winter, G. (2019). Harnessing Evolution to Make Medicines (Nobel Lecture). Angew Chem Int Ed Engl *58*, 14438-14445.

Wrapp, D., Wang, N., Corbett, K.S., Goldsmith, J.A., Hsieh, C.L., Abiona, O., Graham, B.S., and McLellan, J.S. (2020). Cryo-EM structure of the 2019-nCoV spike in the prefusion conformation. Science *367*, 1260-1263.

Wu, S., Avila-Sakar, A., Kim, J., Booth, D.S., Greenberg, C.H., Rossi, A., Liao, M., Li, X., Alian, A., Griner, S.L., *et al.* (2012). Fabs enable single particle cryoEM studies of small proteins. Structure *20*, 582-592.

Wu, Y., Wang, F., Shen, C., Peng, W., Li, D., Zhao, C., Li, Z., Li, S., Bi, Y., Yang, Y., *et al.* (2020). A noncompeting pair of human neutralizing antibodies block COVID-19 virus binding to its receptor ACE2. Science *368*, 1274-1278.

Yan, R., Zhang, Y., Li, Y., Xia, L., Guo, Y., and Zhou, Q. (2020). Structural basis for the recognition of SARS-CoV-2 by full-length human ACE2. Science *367*, 1444-1448.

Ye, J.D., Tereshko, V., Frederiksen, J.K., Koide, A., Fellouse, F.A., Sidhu, S.S., Koide, S., Kossiakoff, A.A., and Piccirilli, J.A. (2008). Synthetic antibodies for specific recognition and crystallization of structured RNA. Proc Natl Acad Sci U S A *105*, 82-87.

Zhu, N., Zhang, D., Wang, W., Li, X., Yang, B., Song, J., Zhao, X., Huang, B., Shi, W., Lu, R., *et al.* (2020). A Novel Coronavirus from Patients with Pneumonia in China, 2019. N Engl J Med *382*, 727-733.